

LINEAMENT EXTRACTION FROM DIGITAL TERRAIN MODELS

Case Study San Antonio del Sur Area, South-Eastern Cuba

Manuel Alejandro Arenas Abarca
March 2006

Lineament Extraction from Digital Terrain Models

Case Study San Antonio del Sur Area, South-Eastern Cuba

by

Manuel Alejandro Arenas Abarca

Thesis submitted to the International Institute for Geo-information Science and Earth Observation in partial fulfilment of the requirements for the degree of Master of Science in Geo-information Science and Earth Observation, Specialisation: Natural Hazards Studies

Supervisors:

MSc. C.A. Hecker

Dr. B.H.P. Maathuis

Thesis Assessment Board:

Prof. Dr. F.D. van der Meer (Chair)

Dr. V.G. Jetten (External)

MSc. C.A. Hecker (First supervisor)

Dr. B.H.P. Maathuis (Second supervisor)

Observer:

Dr. P.M. van Dijk (Programme Director)



**INTERNATIONAL INSTITUTE FOR GEO-INFORMATION SCIENCE AND EARTH OBSERVATION
ENSCHEDA, THE NETHERLANDS**

Disclaimer

This document describes work undertaken as part of a programme of study at the International Institute for Geo-information Science and Earth Observation. All views and opinions expressed therein remain the sole responsibility of the author, and do not necessarily represent those of the institute.

...A mis amadas emes

Abstract

Tectonic and structural studies are the starting issues to deal with the construction of an earthquake source model. Morphological analysis of topographic features, by means of aerial photographs, satellite images and most recently digital elevations models have been long applied for these kind of studies. These morphological analysis, however, are mainly based on visual interpretation of images.

The scope of this thesis is help to avoid the bias related to visual interpretation of lineaments and to increase the speed of data processing by means of a semi-automatic methodology for linear feature extraction. Hence, the main objective is to develop a procedure, based on quantified terrain parameters, to extract lineaments from grid-based digital elevation models.

The study area is located in the Oriente Province, south-eastern Cuba. It comprises an area of 600 square kilometres with different landforms from the coast to the north due to climatic, tectonic and lithological factors. The geology of the area includes ophiolite complex, volcanic rocks, terrigenous and carbonate sedimentary rocks ranging in age from Mesozoic till the present.

Processing to obtain lineament maps from digital terrain models can be separated into 4 main stages:

- DEM construction from topographic contour lines and subsequent calculation of DTM's (slope gradient, profile curvature and shaded relief maps). Algorithms for interpolation and terrain derivative calculations and the level of DEM generalization prior to the latter procedure are clue issues in this step.
- Pre-processing procedures for lineament enhancement and thresholding. Selection of enhancement methods and number of candidate pixels (i.e., threshold value) to be presented to the extraction algorithm are the most important factors to be considered in this stage.
- Automatic extraction of lineaments. Hough Transform (HT) was selected to carry out this research because its usefulness for shape recognition and lineament extraction. Selection of the two user required parameters is the critical point in this step.
- Post-processing procedures for conversion of lineaments from raster to vector, and for cleaning and generalization of these lines. Raster to vector algorithm is one of the critical issues in this stage.

Assessment of lineament outputs was made in two steps. The first validation was made with respect to visual interpretation of input binary maps in order to fix the parameters required by the HT algorithm and to assess the extraction procedure performance. After having fixed the HT parameters and processing procedures, the second accuracy assessment was done with respect to a geological lineament map. That was done to find the optimal amount of candidate pixels (threshold value), validate the overall extraction method with respect to an independent truth and select the DTM with better performance. Finally, the stated procedure (after final selection and fixing of all variables, processing and DTM) was evaluated at larger grid sizes to assess the influence of the latter in the extraction performance.

The results show that lineaments extracted from slope gradient map better resembles the geological map of the study area with higher accuracies than shaded relief and profile curvature maps. Despite of the fact that methodology gives accuracies relatively low (16%) to be considered as completely successful, the procedure was able to delineate the main structural trends in the study area, which also coincide with the regional main orientations.

Acknowledgements

I want to start these words expressing my sincere gratitude to the people who made possible my attendance to this MSc. course in ITC: Sven Renner from BGR (Germany) who provided me the financial support and Jorge Muñoz who support me when I was trying to come to Holland. Muchas gracias a ambos.

It's difficult to remember and name all the people I have met here. Students, administrative staff, people from every where, to all of you my endless grateful.

I'm very grateful with all the lecturers who gave us during one and a half year the basement to construct this building called thesis. I want to express specially my gratitude to the persons who played a role in the development of my research: to my first supervisor MSc Chris Hecker for all the guidance and advices during the research. I really appreciate your critical comments and all the discussions that always encourage me to improve the work. Thanks a lot. To Dr. Ben Maathuis, my second supervisor, who always was available to advice and put me in the right way. To Dr. Paul van Dijk for his understanding and support in difficult moments. I'm greatly grateful to Harald van der Werff who brought me when I was completely lost to the Linux Center where he directly connected me to the HT code. Thanks a lot for the script and all. To all lecturers and staff members who provided me with a very enlighten discussion during the midterm: Dr. B. (Balduino) de Smeth, Dr. David Rossiter, Prof. Dr. F.D.van der Meer, Dr. Mark van der Meijde, and of course my supervisors. To B. van Leeuwen who gave me the clue for the implementation of automatic thresholding method in an ILWIS script. The very earliest discussions that guide me to this thesis research are mainly owed to Enrique Castellanos who also provided the whole data set used in this study. *Gracias Chico!!* (léase con acento cubano). I want to extent the gratitude as well to Dr. Cees van Westen for the earlier guidance and provided material. To Drs. Robert Voskuil and Dr. T. Woldai who gave me part of their precious time to discuss and sliced the pencil on a hillshading image. To all of them and those who have been forgotten my sincere and great gratitude.

I cannot forget to my EREG fellow students: Zul, Gimmee, Tommy, Sheila, Kun, Li, Samuel, Fekerte, Dennis, Mwale, Chen, Edgard, Shekahr and others. I will never forget all the moments we spent together. My best wishes for all of you.

A mis amigos latinos: Isabella, Jaime, Jenny, Jessica, Johana, Laura, Lily, Sebastian, Rafael y muy especialmente a mi amigo Alex por todos los inolvidables momentos juntos y el apoyo brindado. A los new arrived Paco, Sebastian, Javier, Martin, Maria y los demas my best wishes of success in ITC. To my friends Esther, Petra, Christie, Olga, Jamshid, Dan, Carlos, Ricardo, Enrique, Jeovani, Boiki, Belinda and the forgotten who provided me a very nice environment inside, but also outside ITC: thanks for all of you.

Finally a mis adoradas emes, Marcela, Muriel, Marco y Martin por todo el effort y sacrificio de estar separados largos 12 months. Sin su fuerza y apoyo todo esto no hubiese sido possible...

Table of contents

1. Introduction	9
1.1. Research Motivation	9
1.2. Research Problem.....	9
1.3. Objectives.....	10
1.3.1. General	10
1.3.2. Specifics	10
1.4. Research questions.....	10
1.5. Hypothesis	10
2. Literature Review.....	11
3. Study Area and Data Set	14
3.1. Study Area.....	14
3.2. Data Set.....	16
4. Methodology	18
4.1. Overview	18
4.2. Digital Terrain Modelling	19
4.2.1. DEM construction	19
4.2.2. Terrain parameter and Shaded Relief maps	21
4.3. Pre-processing.....	21
4.3.1. Lineament enhancement.....	21
4.3.2. Threshold value selection and pre-thinning method	22
4.4. Automatic Extraction of Lineaments	23
4.5. Post-processing.....	24
4.6. Validation.....	24
4.6.1. Extracted lineaments with Visual Truth.....	25
4.6.2. Extracted lineaments with Geological Truth.....	26
5. Results and Discussion.....	27
5.1. Digital Terrain Modelling	27
5.1.1. Construction of DEM from 1:25,000 topographic map	27
5.1.2. Terrain parameters and hill shading calculation	30
5.2. Pre-processing	31
5.2.1. Lineament enhancement.....	31
5.2.2. Threshold value selection and pre-thinning method	33
5.3. Automatic lineament extraction	33
5.4. Post-HT processing, vectorizing and cleaning steps.....	39
5.5. Validation stages	41
5.5.1. Validation with Visual Truth	41
5.5.2. Validation with Geological Truth	43
5.6. Results for DEM's with larger grid sizes	50
5.7. Final Discussion	55
6. Conclusions	57
7. Recommendations	59
8. References	60

9.	Appendices	63
9.1.	Appendix 1: Tables	63
9.2.	Appendix 2: Scripts.....	68
9.2.1.	Evans and Young method for terrain derivative calculation.....	68
9.2.2.	Method for construction of shaded relief binary maps for lineament extraction.....	70
9.2.3.	Threshold method for enhanced shaded relief maps.....	72
9.2.4.	Threshold method for profile curvature maps.....	73
9.2.5.	Sobel enhancement and threshold method for slope gradient maps	74
9.2.6.	Laplacian enhancement and threshold method for slope gradient maps.....	75
9.2.7.	General threshold method used with slope gradient maps.....	75
9.2.8.	Post-processing steps for HT output lineament maps	76
9.2.9.	Method for extraction of medial axes	77
9.2.10.	Method for importing lineament into ILWIS and calculations for rose diagrams construction	78
9.2.11.	Method for selection of correctly extracted lineaments.....	79
9.2.12.	Converter TIFF to RW Format for Hough Transform Calculation.....	80

List of figures

Figure 3-1. Location of study area and main geomorphological features.....	14
Figure 3-2. Tectono-stratigraphic units.....	15
Figure 3-3. Tectonic setting of Cuba.....	16
Figure 4-1. General flowchart showing the different steps to find the most suitable DEM, parameters and pre and post-processing procedures.	20
Figure 5-1. Elevation frequency distribution of interpolated DEM's.....	28
Figure 5-2. Three-color shaded-relief maps constructed from three different interpolated DEM's.....	29
Figure 5-3. Aspect maps from the three different interpolated algorithms.....	29
Figure 5-4. Frequency and cumulative frequency distributions for ANUDEM interpolated DEM	30
Figure 5-5. Resulting cross maps between the binary images obtained with two different smoothing values.....	31
Figure 5-6. Resulting cross maps between the binary images obtained with two different edge enhancement methods	32
Figure 5-7. Slope gradient binary maps with different threshold values	34
Figure 5-8. Enhanced and binary maps for slope gradient and profile curvature	35
Figure 5-9. Original, enhanced and binary maps for two shaded relief maps.....	36
Figure 5-10. Extracted lineaments from slope gradient binary map (5%).....	37
Figure 5-11. HT output maps for most accurate thinned and not-thinned slope gradient binary maps.....	38
Figure 5-12. Selected area showing the output of HT for slope gradient binary map (5%) using the combination of HT parameters $n=30$ and $k=4$	40
Figure 5-13. Total, position and length accuracy graphs for slope gradient lineaments compared with longer-lines visual interpretation map and with short-detailed-lines visual interpretation map.....	42
Figure 5-14. Total, position and length accuracy graphs for pre-thinned slope gradient lineaments compared with longer-lines visual interpretation map.....	43
Figure 5-15. Graphs for total, positional and length accuracies for slope gradient, shaded relief and profile curvature lineament maps using the best HT combination $n=30$ $k=4$ and different threshold values.....	45
Figure 5-16. Rose diagrams for different extracted lineament maps, visual interpretations, and geological and morpholineament truth maps	46
Figure 5-17. Slope gradient map stretched with histogram equalization into 20 intervals and displayed with a gradual greyscale from white (lower values) to black (higher values)	47
Figure 5-18. Slope gradient map (25k) stretched with histogram equalization into 20 intervals and displayed with a gradual greyscale from white (lower values) to black (higher values).....	48
Figure 5-19. Binary slope gradient map (15%) overlain by the most accurate lineament map extracted from this image.....	49
Figure 5-20. Histograms and cumulative frequency distributions of elevation for ANUDEM 50k and SRTM DEM's in the study area.....	51
Figure 5-21. Histograms and cumulative frequency distribution of slope gradient for ANUDEM 50k and SRTM DEM's	52
Figure 5-22. Histograms and cumulative frequency distribution of elevation and slope gradient for regional SRTM DEM.....	52

Figure 5-23. Slope gradient map (50k) stretched with histogram equalization into 20 intervals and displayed with a gradual greyscale from white (lower values) to black (higher values).....53
Figure 5-24. Lineaments maps from SRTM and regional SRTM using the stated optimal procedure..54

List of tables

Table 1. Number of isolated pixels in two different maps.....	63
Table 2. Total, position and length accuracy for lineaments extracted from slope gradient binary map (5% threshold value) compared to long visual interpreted lines.....	63
Table 3. Total, position and length accuracy for lineaments extracted from slope gradient binary map (5% threshold value) compared to short-detailed visual interpreted lines.....	64
Table 4. Total, position and length accuracy for pre-thinned slope gradient map 5% threshold value compared to long visual interpreted lines.	65
Table 5. Total, position and length accuracy for slope gradient map, shaded relief and profile curvature lineament maps using the best HT parameter combination $n=30$ $k=4$ and different threshold values.....	66
Table 6. Total, position and length accuracy for slope gradient map from 50k, SRTM and regional SRTM using the HT parameter combination $n=30$ $k=4$ and the optimal threshold value 15%.....	67
Table 7. Rao's Test for extracted lineament maps, geological and morpholineaments truth maps.....	67

1. Introduction

1.1. Research Motivation

One of the basic elements in modern seismic hazard assessment is the determination of an earthquake source model (Giardini, 1999). This model describes the spatio-temporal distribution of seismic activity and requires integration of data from different sources (Slemmons and Depolo, 1986) (geology, geomorphology, seismology, geophysics and others). Knowledge about tectonic setting and active fault locations, are the starting issues to deal with the construction of such a model (Muir-Wood, 1993).

Morphological analysis of topographic features has been long applied for tectonic and structural studies. Aerial photographs, satellite images and, most recently, digital elevations models (DEM's) have been extensively used for these tasks (Heddi et al., 1999; Jordan et al., 2005; Koike et al., 1998; Murphy, 1993; Szykaruk et al., 2004; Woldai, 1995).

In the case of DEM's, shaded relief images and terrain derivative maps (gradient, aspect and curvatures) have largely demonstrated their usefulness for lineaments and fault extraction (Florinsky, 1996; Ganas et al., 2005; Jordan, 2003a; Jordan, 2003b; Oguchi et al., 2003; Onorati et al., 1992). However, most of the analyses are based on visual interpretation of images.

The scope of this thesis is help to avoid the bias related to visual interpretation of lineament extraction and to increase the speed of data processing by means of a (semi) automatic methodology for linear feature extraction.

1.2. Research Problem

The use of digital elevation data to map features related to tectonic activity and, particularly, lineaments, is in most of the cases restricted to visual interpretation of hill-shaded images. Although terrain derivative maps (gradient, aspect, curvatures) have been used to recognize features, again visual interpretation is the most used analysis approach.

The main criticism for this approach is related to probable biasing induced by the skills of interpreters and by the visualization techniques used. The application of both, lineament models based on quantified terrain parameters and a methodological procedure for extraction could lead to avoid interpretation bias related to the mentioned above.

Some DEM sources are free of charge and near global coverage, e.g. SRTM (Rabus et al., 2003), but with grid resolutions that only allow regional analyses. Contour maps are still the main sources for construction of more detailed digital elevation models (Wise, 1998). Nowadays, contours can easily be obtained digitising elevation data from topographic maps. Surface interpolation and topographical analysis tools available in many GIS and image analysis packages allow easy handling of these data.

1.3. Objectives

1.3.1. General

- To develop a methodological procedure to extract lineaments from grid-based digital elevation models.

1.3.2. Specifics

To carry out the main objective the following specifics tasks have been stated:

- To extract lineaments (semi) automatically from different digital terrain models.
- To validate the results by comparing with independent source data, establishing the combination of terrain model and processing methods with the best extraction performance.
- To assess the established best procedure on DEM's with coarser grid resolutions extending also the analysis to regional scale.

1.4. Research questions

- Is it possible to extract lineaments from terrain parameter and shaded relief maps in an automatic way?
- What kind of image processing is necessary to carry out this task?
- What are the spatial correlation and direction similarity between extracted features and independent lineament data?
- Which combination of DTM's and processing steps is the most suitable for lineament extraction?
- How does DEM resolution affect the established procedure?

1.5. Hypothesis

Due to the fractal nature of landscape, different detail of lineament features could be revealed by different DEM resolutions (Wood, 1996). Finer grid resolution gives more detailed lineament maps than coarser grid resolutions and therefore could be more accurate. However, regional orientation trends should be similar and show more or less the same pattern independent of scale of analysis (Burbank and Anderson, 2001; Tchalenko, 1970).

Assuming that the ability of human brain to integrated information from an image and to extract linear features is better than automatic computational extraction, the established procedure should be less accurate than experienced visual interpreters with adequate visualization techniques (Smith and Clark, 2005). Moreover, automatic lineament extraction methods are *blind* because they cannot discriminate between tectonic and non-tectonic features, and therefore, always require ancillary data to get the final tectonic lineament map.

Despite of these constraints, the procedure could be useful to assist subsequent visual interpretation extracting the general structural trend within the study area faster and without interpreter bias.

2. Literature Review

Lineaments are more or less rectilinear alignments that can be seen on satellite images, aerial photographs and digital elevation models (Ollier, 1981; Panizza et al., 1987). These linear features may represent natural morphological alignments or those of anthropogenic nature (roads, aqueducts, crops, etc.). Structural discontinuities of rocks and other features related to tectonic activity often results in morphological lineaments (fault scarps, joints, fold axis, etc.; (Ramsay and Huber, 1987). These lineaments can be expressed as linear valleys, linear slope breaks or linear ridgelines (Jordan et al., 2005).

There are many specific landforms associated with faults which allow the fault type recognition (Burbank and Anderson, 2001; Keller and Pinter, 1996). Fault scarps are the most clear fault features (Ollier, 1981). They are very steep slopes with the same aspect parallel to the fault trace. The size of fault scarps could vary between a few meters up to hundred of kilometres of length (Burbank and Anderson, 2001) and between fraction of meter and hundred of meters of height. As normal and strike slip faults usually present high dip angle they are not affected by topography and tend to be a straight line in plan view, although they may be curved or sinuous (Burbank and Anderson, 2001; Ollier, 1981). Thrust and reverse faults have low dip angles and in this way they present more complex topographic expressions and they are more difficult to recognize in remote sensed images (Burbank and Anderson, 2001; Ollier, 1981).

However, not only fractures and faults have linear topographic expressions. Lithological contacts, intersection of bedding and topography, some wind erosion and glacial features could also appear as lineaments in images (Jordan et al., 2005; Smith and Clark, 2005). In this way, discrimination between tectonic and non-tectonic features can only be stated using geological and other ancillary information.

Tectonic geomorphologic studies and river network analysis are nowadays being analysed in a fast and easier way by means of digital elevation data and geographical information systems (Jamieson et al., 2004; Jordan, 2003a; Koike et al., 1998; Korup et al., 2005; Mayer, 2000; Moore et al., 1994; Oguchi et al., 2003; Szykaruk et al., 2004).

Evans defined an integrated system of basic terrain parameters, extracted from digital elevation data, to characterize land surface forms (Evans, 1980; Evans, 1998). These are elevation itself and the results of its first and second derivatives, slope and convexity (curvature) respectively. Slope is defined as a plane tangent to the surface at a certain elevation point while curvature is defined as the rate of change of this plane. Gradient, the maximum rate of change of altitude, and aspect, the compass direction of this maximum, are the two components of the slope vector. Profile and plan convexity are respectively the rate of change of this two slope components, defining concavity by convention with negative values (Evans, 1980).

Fault and linear features can be morphologically expressed and quantified in terms of these parameters. For example, fault scarps present abrupt changes in slope gradient that could be expressed as lineaments in these parameter maps (Ganas et al., 2005; Jordan et al., 2005). The planar surface of fault traces can be expressed for elongated areas with uniform slope aspect and gradient. The linear boundaries of these areas can be used to place the fault trace (Jordan, 2003a). These lineaments might be detected enhancing the abrupt changes in slope gradient associated with these boundaries. Curvatures, planar and profile, have been used by Florinsky (1996) to identify and characterize

normal and strike-slip faults at regional scales. The analysis is based on morphology characterization of faults in terms of profile and planar curvature values, spatial distribution of homogeneous areas. Jordan *et al.*(2003a) applied a predefined threshold value to profile curvature maps to recognize slope breaks. Histogram and cumulative frequency analysis of terrain parameters have been largely used for tectonic studies for example in Riley and Moore (1993), Jordan *et al.*(2003a), Szynekruk *et al.*(2004). Jordan (2003b) classified the slope gradient map according to the break points in the cumulative frequency of this parameter. The sliced map shows the areas of uniform geometric attribute (slope gradient) and was used to analyse the shapes, distribution and continuity of these zones. Other morphotectonic indexes and techniques as profile measurements are also used for tectonic studies (Heddi *et al.*, 1999; Mayer, 1986; Szynekruk *et al.*, 2004). Jordan *et al.* (2005) have stated a method with simple and advanced analysis techniques for tectono-geomorphologic studies.

Shaded relief maps have been largely used to identify faults and lineaments from digital elevation data (Ganas *et al.*, 2005; Hooper *et al.*, 2003; Oguchi *et al.*, 2003; Onorati *et al.*, 1992). Onorati *et al.* (1992) compared geological data with two visual interpretations of shaded relief maps. Both of them used orthogonal illumination with respect to the known tectonic trends. They defined the accuracy in terms of detectability, length and displacement of features with respect to the truth.

DEM's are stored in different data structures: regular grid networks (mainly square grids), irregular grids preferably triangulated irregular networks (TIN) and contour based networks (Moore *et al.*, 1994). Because of simplicity of data and easy computation with GIS operations (Burrough and McDonnell, 1998) and despite of some TIN data structures advantages, raster format (square grids) is the most efficient DEM structure for topographic attribute extraction. There are a great variety of interpolation methods to construct a grid based digital elevation model. Ranging from nearest point to kriging techniques (Wise, 2000) there is not an interpolation technique appropriate for all applications (Hengl *et al.*, 2003). Wise (1998; 2000) prefers ANUDEM algorithm while Mitas and Mitasova (1999; cited in Hengl *et al.*, 2003) recommend the regular spline with tension as an optimal interpolator. Kienzle (2004) considers both algorithms as good interpolators.

As well as for interpolation, there are different algorithms for terrain parameters calculation. Skidmore (1989), Florinsky (1998) and Shary *et al.* (2002) preferred the method developed by Evans and Young, while Kienzle (2004) preferred the Horn and the Zeubergeren-Thorne algorithms. As curvatures are more sensitive to errors in elevation and algorithm methods (Evans, 1998) , some smoothing of elevation values is advisable prior to convexity calculation. However, Wise (1998; 2000) showed that quality of almost all the parameters is improved with a previous elevation smoothing.

Image processing for enhancement of features can be done in the spatial domain, frequency domain or other domains (*e.x.* Fourier, Hough). In the first domain the values of pixels are modified according to their original value (local or point processes) or combined with the immediately neighbour pixels (neighbourhood operations) to calculate the new value (Russ, 1999; page 227). Histogram manipulations processes and filter operations are examples of these methods respectively. Edge enhancement can be performed with both types of processes; however neighbourhood operations are preferred because these are most suitable to increase local contrast at boundaries. Filters as the non-directional Laplace operator or Sobel and Roberts'Cross directional operators are the most used for edge enhancement purposes (Russ, 1999).

The Hough Transform (Hough, 1962; cited in Low, 1991) describes features of interest in an image using a parameter space (Hough domain). For example a line can be defined in the Hough domain using parameters that can be defined as well in the image space (angle and perpendicular

distance to the origin). In similar ways other shapes can be parameterised and extracted using the Hough Transform (Low, 1991). The technique is based on a voting process where every point in the image votes for all the possible shapes, in this case lines, passing through these given points. An accumulator array stores the votes and the line with the maximum amount of votes is extracted as a real feature in the image. Modifications and improvements of the technique have been extensively reported and they are being used in different fields of work (Bonnet, 2002; van der Werff et al., ; Wang and Howarth, 1990). Wang and Howarth (1990) used the method to detect lineaments in satellite images. Fitton and Cox (1998) adapted the Hough Transform to extract lineaments from geoscientific images. They tested the algorithm using a satellite image and a photograph of a veined outcrop. The algorithm showed to be able to extract lineaments at different scales although not all linear features were recognized.

3. Study Area and Data Set

3.1. Study Area

The San Antonio del Sur area is located in the Oriente Province, southeastern Cuba between the approximate coordinates $19^{\circ}59'46''\text{N}$ - $20^{\circ}17'13''\text{N}$ and $74^{\circ}43'22''\text{W}$ - $74^{\circ}55'36''\text{W}$ (Figure 3-1). It comprises an area of 600 square kilometers with different landforms from the coast to the north due to climatic, tectonic and lithological factors (Castellanos, 2000). In general the relief is hilly and mountainous (Sierra de Caujeri and Sierra de Puriales) with a central depression (Caujeri valley) and an intermountain valley parallel to the coast (San Antonio valley). The geology of the area includes a Mesozoic ophiolite complex, Cretaceous volcanic rocks, Paleocene-middle Eocene volcanic rocks, middle to latest Eocene terrigenous and carbonate rocks deposited in a piggyback basin (Nuñez, 2000) all of these included in the so called Foldbelt main geological unit. Sedimentary rocks (terrigenous and calcareous) belonging to the Neoautochthon main geological unit were deposited during three Transgression-Regression cycles from latest Eocene till the present (Castellanos, 2000; Figure 3-2).

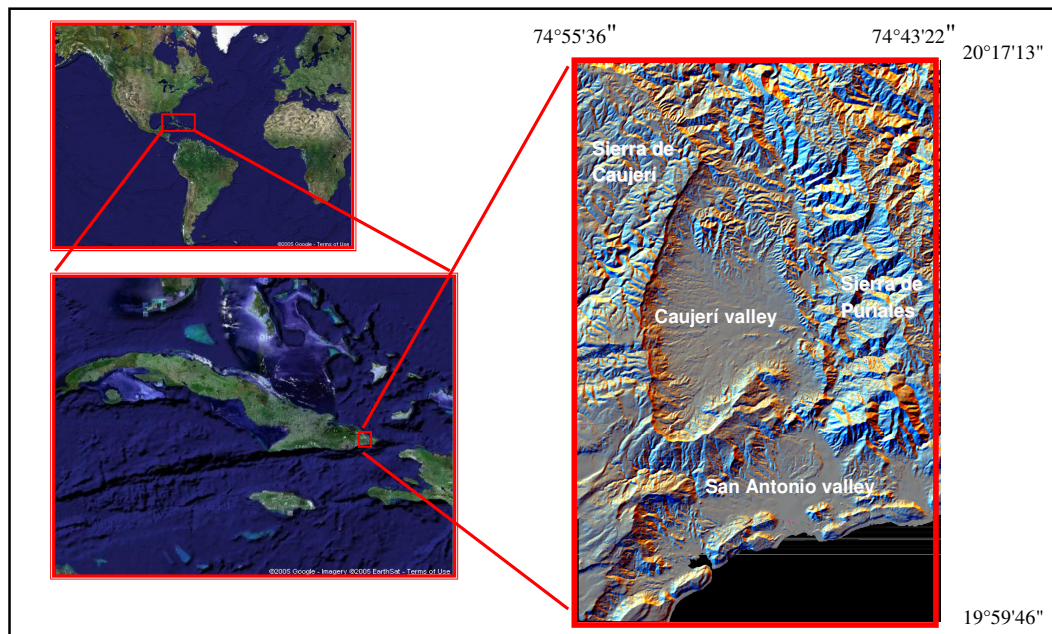


Figure 3-1. Location of study area and main geomorphological features.

Núñez (2000) divided the study area into 4 structural domains coinciding more or less with the tectono-stratigraphic units. The *Puriales-Convento* unit is the most complex due to the thrusting of Ophiolite complex. It's the oldest unit and appears strongly deformed and faulted, recording the whole structural history of the area. The *Sierra de Caujeri* domain contains the tectonically emplaced allocthonous Paleogene sequences that dip gently to the south and southeast. This unit was affected by continuous transgressions and regressions from the latest Eocene to Late Miocene. The *Caujeri Valley* is a tectonic depression where Miocene rocks were eroded and the Quaternary sediments were accumulated later. Some faults can be seen in this valley and they present NE direction. The sediments are in general dipping horizontally but in some places a gently dipping to the north can be observed indicating a differential uplift of valley bottom. The *Coastal Valley* structural domain shows evidence of three successive transgression and regression cycles, the first one from the latest Eocene to Oligocene, the second one during the Lower Miocene and the latter from Pliocene to the recent. Coastal terraces evidence tectonic uplift up to 200 m above the present sea level.

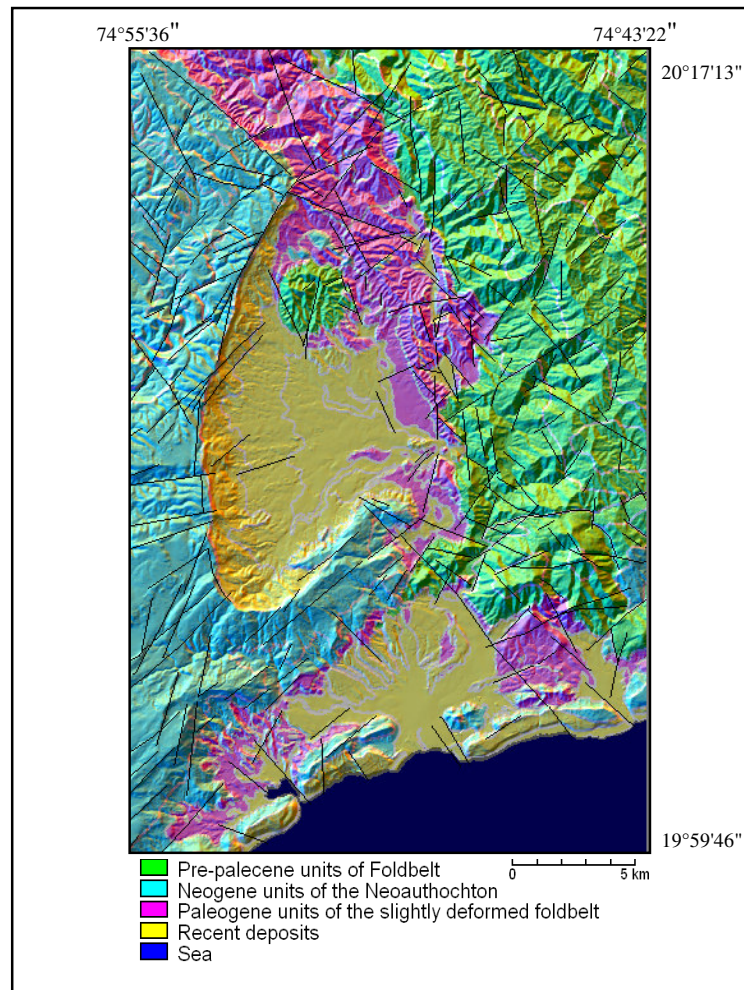


Figure 3-2. Tectono-stratigraphic units after Núñez (2000). Colors in map appear slightly different in the legend because a three-color shaded relief appears as background to give a more realistic impression of terrain. Black lines correspond to lineaments and faults in the geological map.

Cuba is located in the North American plate just to the north of the boundary with the Caribbean plate (Figure 3-3). From the Miocene the movement between these plates is approximately sinistral along the Oriente Transform Fault (Rojas-Agramonte et al., 2005). This is responsible of the high seismic activity of southern Cuba (García et al., 2003) and it has induced characteristic strike-slip brittle deformation fractures and reactivation of older faults within the study area (Nuñez, 2000). The main lineament system present the following preferred orientation: NE-SW, NW-SE, NNE-SSW, NNW-SSE (Nuñez, 2000). According to Nuñez (2000) four different stages have controlled the evolution of the area: during the Cretaceous period with volcanic activity and volcano-sedimentary rocks deposition deformed during a first stage of deformation after the end of the volcanism; Paleocene to early middle Eocene the deformed cretaceous volcanic arc was overthrust by ophiolite complex provoking the second deformation stage; middle to late Eocene with formation of an island arc that was in some places overthrust over the sediments of a back-arc basin; and the last stage from the Miocene until the Recent with transpressional-transtensional tectonic movements along the Oriente Transform Fault.

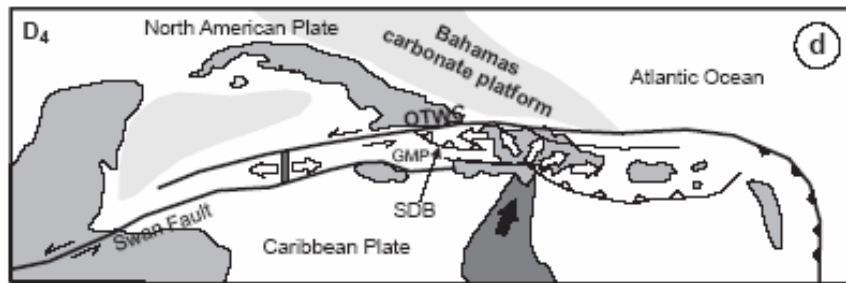


Figure 3-3. Tectonic setting of Cuba (from Rojas-Agramonte et al. (2005)).

3.2. Data Set

The data to carry out this thesis includes contour lines at 1:25,000 and 1:50,000 scales, SRTM processed data and a digital geological map from previous work (Nuñez, 2000).

The 1:25,000 contour lines were scanned and semiautomatic digitised from the corresponding topographic maps (Grupo de Atención Integral de la Montaña, 2000). Contours were digitised every 10 m and in some places every 5 m. No other data was provided for this contour map. The spotheights were obtained from the same source map and were added to contours to improve the interpolation results.

The 1:50,000 contour lines were semi automatically digitised and then cleaned and processed by Castellanos (2000). The processing includes manual drawing of contours for later digitising, scanning in pieces and later gluing of these pieces. A thinning procedure was developed to present one-pixel width lines to the semiautomatic tracer of contours. Finally the contours were georeferenced (using and spline interpolation in CARIS GIS package) cleaned and smoothed. The shape file was created from a DXF file format created in CARIS.

The SRTM data for the whole Cuba territory was also processed by Castellanos (2005). To eliminate the voids he used an average filter with 13 iterations to remove all the missing data. A RMSE accuracy of ± 10 m and ± 5.86 m were reported after the processing for absolute and relative

vertical accuracy respectively. A submap of this data set was created in ILWIS to fit the study area and extract the lineaments.

The digital geological map (Nuñez, 2000) contains linear features in two categories: *lineaments* (669 segments, 535,2 km) that were interpreted from aerial photographs (scale 1:37000), satellite images (Landsat TM, 30 m resolution; Spot panchromatic, 10 m resolution) and digital elevation model (shaded relief from the same DEM of Castellanos (2000); and *faults* (79 segments, 51,7 km), including observed and inferred features.

The morpholineament map (Tropical, 1994) to be used as truth for validation of regional SRTM extracted lines was constructed at 1:100000 scale from different sources (geology, geophysics, geomorphology). It includes river valleys, escarpments, lineal fluvial terraces and other linear landforms (432 segments, 709.7 km).

4. Methodology

4.1. Overview

The main scope of this thesis is the development of an automatic procedure to extract lineaments from digital terrain models (slope gradient, profile curvature and shaded relief maps).

In this way, the first task is related to the construction of a digital elevation model from topographic contour lines and the subsequent calculation of terrain derivatives and shaded relief maps. Algorithms for interpolation and terrain derivative calculations are crucial issues in this step. Level of DEM generalization prior to terrain parameter extraction is also important.

The main tasks during the following pre-processing stage deal with enhancement of lineaments and thresholding of the DTM's. These are done in order to get binary images required by the chosen automatic line extraction method. The most important issues in this step are the selection of lineaments enhancement methods and number of candidate pixels (i.e., threshold value) to be presented to the extraction algorithm.

Hough Transform has proved largely its usefulness for shape recognition and lineament extraction. Because of this it was selected to carry out this research. Since the used algorithm requires from the user the selection of two parameters that influence the outcome considerably these need to be selected carefully.

After automatic extraction, post-processing procedures are required for conversion of lineaments from raster to vector (R2V), and for cleaning and generalization of these vector lines. R2V algorithms and their required parameters are some critical points in this step.

Assessment of outputs was made in two steps. The first validation was made with respect to visual interpretation of input binary maps in order to fix the parameters required by the HT algorithm and to assess the extraction procedure performance. This allows answering the first research question dealing with the possibility to extract automatically lines from DTM's.

After fixing the parameters and processing procedures, the second outcome assessment was done with respect to a geological lineament map. That was done to find the optimal amount of candidate pixels (threshold value) to be used during the HT application, validate the overall extraction method with respect to an independent truth source and select the DTM with better performance. This is in relation with the answering of the second and third research questions.

Finally, the stated procedure (after final selection and fixing of variables and processing) and the most accurate DTM were evaluated at larger grid sizes to assess the influence of the latter in the extraction performance allowing the finding of answer to the fourth and last research question.

As the amount of variables involved in the whole procedure is large and due to thesis time constraint, it was decided to vary only certain parameters in every step and fix the rest of them. Further researches could be done to evaluate the procedures sensitivity to changes in all a priori fixed variables. In some cases the selection of parameters in earlier stages requires the results of later steps in the procedure. Hence, the description of the methodology will often make reference to earlier

and/or later steps. The following paragraphs explain the different criteria and methods. Methodology is also summarized in figure 4-1.

4.2. Digital Terrain Modelling

4.2.1. DEM construction

As interpolation method is one of the critical points in generation of digital elevation models, three different interpolation algorithms were tested (Figure 4-1): linear interpolation as implemented in ILWIS[®] software (ITC, 2001), and spline with tension and ANUDEM algorithms as implemented in ArcGIS[®] package (ESRI, 2004). The latter two algorithms were selected because they have been stated by different authors as *good* interpolators (Kienzle, 2004; Mitas and Mitasova, 1999; Wise, 1998; 2000), while linear interpolator creates less smoother surfaces than the former ones (Hengl et al., 2003). The DEM's quality was assessed by inspection of frequency distribution of elevation and visual inspection of aspect and shaded relief images (Jamieson et al., 2004) to look for systematic interpolation errors and artefacts respectively. In the former case increased frequencies at regularly spaced elevation values, usually related to values of contour lines, indicates a poor interpolation performance. Usual artefacts are “stepped” surfaces and flat hilltops. The former ones can be detected by visual inspection of shaded relief images, while aspect maps were used for detecting flat hilltops. These are artefacts produced where a neighbourhood is enclosed by the same contour value leading to areas of equal altitudes and null gradient (Hengl et al., 2004).

The algorithm that shows fewer artefacts in histograms and images (ANUDEM) was used for the interpolation of 1:25,000 as well as 1:50,000 topographic contour maps for the remainder of this work. The parameters used for the interpolation were the default values of the tool. The result of interpolation gave 0.1% of the area with negative values of elevation. As the amount is not significant the interpolated DEM was exported to tiff format using the exporting tool of ArcCatalog[®]. Then the tiff image was imported to ILWIS using the GeoGateway method (ITC, 2001). After that, the ocean was masked and negative values of elevation were replaced using the values of the linear interpolated DEM, the second better-evaluated algorithm.

For the initial analysis the map with the larger scale was used (1:25,000). This map gives the most detailed topographic and lineament information, although might be noisy for a regional analysis. Spot heights were added to contour data prior to interpolation in order to avoid some artefacts (e.g. flat hilltops). The grid size values were determined from the total length of contours (Hengl et al., 2003). According to these, the grid resolution should be at least half the average spacing between the contours. This is calculated as:

$$p = \frac{A}{2 * \sum l}$$

where p is the pixel size, A is the total study area and $\sum l$ is the total length of the contours within the area. In the case of 1:25,000 scale map the result of this calculation was 14.57 m and a value of 15 m was selected for the interpolation. For contour lines from 1:50,000 scale map $p=36.3$ and was approximated to 35 m for interpolation grid size.

For SRTM data it was necessary to change the georeference in order to fit the used for the other maps. Also a submap was created to get the local study area.

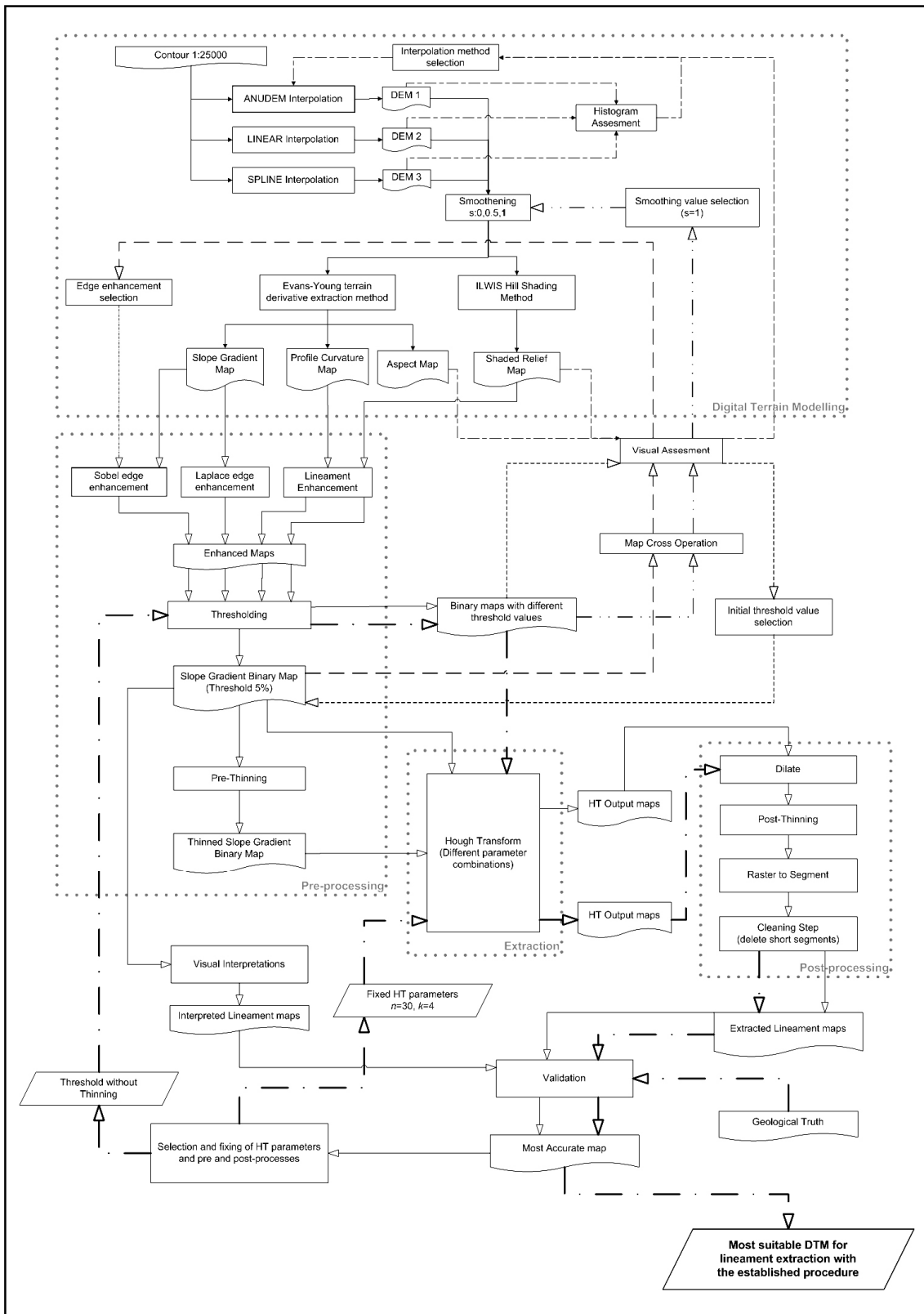


Figure 4-1. General flowchart showing the different steps to find the most suitable DTM, parameters and pre and post-processing procedures. The different patterns in line arrow intended to highlight the different iterations followed during the procedure.

4.2.2. Terrain parameter and Shaded Relief maps

The critical points at this step are the selection of the algorithm to calculate the derivatives and the level of DEM generalization (or smoothing) prior to that calculation. In this case study it was decided to test different levels smoothing while keeping the algorithm and smoothing methods fixed. It is thought that results of different interpolation methods influence the extraction methodology far less than, for example, the automatic extraction parameters. In this way only the influence of smoothing on the binary image results was tested. Different authors have mentioned the Evans-Young method as a good algorithm and because of this it was selected for the calculation of terrain derivatives in this study. Detailed explanation of this method can be found in Shary *et al.* (2002) and Hengl *et al.* (2003). For the application in ILWIS the script created by the latter authors was modified (included in the appendices of this thesis).

Smoothing of elevation data is useful to reduce noise and errors in derivative parameters (Wise, 1998). However this could lead to mask some features due to generalization. The elevation smoothing method proposed by Evans and Cox (cited in Hengl *et al.*, 2003) was applied prior to the calculation of all terrain derivatives (included in the script, Appendix 2). Three different smoothing values were used to construct slope gradient maps, the minimum (no smoothing), intermediate and maximum smoothing factors (0, 0.5 and 1). As the idea is to assess the influence of smoothing on binary image results, Sobel enhancement method and threshold value of 5% (to choose the highest values in cumulative histogram) were used to get binary images. These were visually tested using a map cross operation. The smoothing value that leads to less noisy images and more continuous and homogeneous areas (smoothing value 1) was chosen for the remaining steps.

Hillshading maps were calculated using the smoothing DEM and the shadow filter implement in ILWIS (ITC, 2001). This is a linear convolution filter consisting of a kernel of size 3x3. The nine values of the matrix are multiplied with nine pixel values of the input map and then summed to assign the resulting number to the central pixel. The standard filters in ILWIS simulated illumination from northwest, north and west. To obtain shadow filters with illumination from other 5 directions, the values in the kernel were rotated accordingly. In this way shaded relief with illumination from the 8 main compass directions were obtained.

As lineaments were defined in terms of abrupt change of slope gradient (see next section) only slope gradient, profile curvature and shaded relief maps were used in this research. Aspect maps can also be used for extraction of faults and lineaments but these require a different approach for enhancement due to the angular nature of this data. In order to work with a similar concept in all the maps only the mentioned maps were used.

4.3. Pre-processing

4.3.1. Lineament enhancement

Linear features as fault scarps, river valleys or ridgelines can be defined in terms of terrain parameters. Enhancement of these lineaments requires different approaches in each DTM. The following paragraphs refer to the different applied methods in the different terrain derivatives and hillshading maps.

Fault scarps and ridgelines can be identified as zones of abrupt change of slope gradient, the former mainly at the base and top of the escarpment. Edge detection filters were used as a way to

enhance these zones in slope gradient maps. Two edge enhancement methods were tested in this study:

a) Laplacian operator as implemented in ILWIS is based in the application of a non-directional Laplace filter. The resulting values are then subtracted from the original input values (ITC, 2001).

b) The Sobel operator is based in the calculation of gradient in x direction and y direction (Russ, 1999). The derivative gradient filters in vertical and horizontal direction were used as implemented in ILWIS (ITC, 2001). Both edge enhancement methodologies were implemented in scripts (Appendix 2).

A similar visual assessment approach as in smoothing factor selection was applied for choosing the slope gradient enhancement method. Therefore binary images were used for a map cross operation. As before, threshold value was fixed at 5% while smoothing values was fixed at 1 according to the previous result. The enhancement method that gives the most linear and thinner homogeneous areas (Sobel method) was selected to continue the research.

Profile curvature represents the change in slope angle (curvature in normal plane section in gradient direction). River valleys are often associated with high negative values of profile curvature while ridges are associated with high positive values. Abrupt changes in slope gradient were highlighted taking the values above and below given thresholds value in the profile curvature cumulative histogram, selecting in this way the large positive and negative numbers (most convex and concave values).

Lineaments in shaded relief images are associated to variations in sun illumination, which are related to changes in slope gradient or aspect angle. Ridges and fault scarps can be revealed for these changes in shadows. In this case a gradient filter perpendicular to the illumination azimuth can be applied for enhancement of abrupt changes in that direction. For the west and east illuminations the gradient in x direction (DFDX as implemented in ILWIS) was applied. In a similar way it was applied to gradients for north and south (gradient in y direction DFDY) and for diagonal illuminations (DFDDN, DFDUP filters; ITC, 2001).

4.3.2. Threshold value selection and pre-thinning method

Extraction procedure outcomes are considerably influence by the amount of candidate pixels (given by the threshold value) in the input image. Because of that threshold selection is one of the critical points in the extraction methodology. In this study binary maps were constructed selecting the pixels above (or below in some cases) a threshold value in the cumulative frequency curve of enhanced terrain maps.

In order to find the suitable pre-processing procedures, automatic extraction parameters and post-processing steps, it was necessary to keep the threshold value constant during the first stages. Prior to all pre-processing steps, binary maps were visually assessed. Different threshold values were used for construction of slope gradient, profile curvature and shaded relief maps using various smoothing values and enhancement methods. The binary maps that shows lineament information without too much noise was selected to start the research (5%).

Slope gradient and shaded relief enhanced maps were thresholded for the highest values in the respective cumulative frequency curve. For curvature maps the highest and lowest values were taken in account because they correspond to the maximum convexity and concavity that could represent, for example, ridges and river valleys respectively. In order to obtain a similar number of pixels as in the other two maps, the cumulative frequency values above and below the half threshold value were used for the selection of profile curvature candidate pixels (see scripts in Appendix 2).

In order to avoid azimuth biasing in shaded relief maps, after enhancement of lineaments and thresholding, binary images constructed from the 8 directions were aggregated in one map using a sum operation. As binary images are compounds of pixels with value 0 and 1, all shadow binary images were added and pixels with sum equal or higher than 1 were classified as 1. In this way every candidate pixel chosen in every shadow map is considered in the final map. Because of this joining and to get similar number of pixels as in slope and profile curvature binary images, the threshold value for individual shaded relief must be lower than those used for the other maps. Shaded relief map construction, enhancement of lines, thresholding and joining steps were implemented in the same ILWIS script (Appendix 2)

As a thinning process could improve the lineament extraction success, binary images were thinned using a medial axes extraction algorithm to obtain connected one-pixel thick skeletons. The thinning method used in this study is based on distance calculation and was developed by Pilouk and Tempfli (in (Hengl et al., 2004). That was implemented in a script based on one created by the latter authors (Appendix 2). Thinned and non-thinned binary images were used for lineament extraction and comparison of results (Figure 4-1).

After fixing the pre-processing procedures, extraction parameters and post processes, the optimal threshold value was selected during the last validation step (Figure 4-1). The idea is to select an optimal threshold that gives the best features extraction without too much noise. Threshold values 2.5%, 5%, 7.5%, 10%, 12.5%, 15%, 17.5%, 20%, 22.5% and 25% were tested in the final stage.

4.4. Automatic Extraction of Lineaments

The Hough Transform (HT) was chosen for automatic extraction of linear features from the enhanced images ((Hough, 1962); cited in (Fitton and Cox, 1998)). It has the ability to extract shapes from isolated pixels or short segments that are truly aligned and forming a line. Therefore it is suitable for extracting geologic lineaments, which are often visible in short, non-continuous segments. Before using the selected algorithm, the Hough Transform implemented in IDL of ENVI[®] package was tested (Research Systems, 2005). Although it extracts some lineaments it is not able to find the end of segments and these cross the image from edge to edge. More computational programming it is necessary to improve the performance of HT in IDL but this is out of the scope of this thesis.

Fitton and Cox (1998) developed the HT algorithm used in this study. They optimised the algorithm for extraction of lineaments from geoscientific images allowing for example, linear features to be detected at different scales. That allows extraction of longer regional lineaments and also segments related to considerably shorter or fragmented lines. The code is written in C++ language and can be downloaded from www.iamg.org. The algorithm requires only two parameters from the user. The first, called n , is related to the minimum number of pixels included in a line. This parameter is defined as percentage of number of pixels included in the longest extracted line (detected as maximum peak by the algorithm). The algorithm extracts lines in iterative steps, eliminating the line with maximum number of pixels (peak) and extracting lines again consecutively until the selected maximum (n) is reached. A higher n value results in fewer extracted features. The second parameter, k , is related to a normalization factor implemented in the algorithm to give the same weight to central lines with higher chances to be longer than off-centred lines. Value 0 for this parameter means no softening of normalization, given the same weight to the mentioned features. Higher values reduce the normalization factor given as result fewer extracted features (for more detailed explanation on how the algorithm works the reader is referred to the original source). The HT algorithm needs binary

images in RAW format as inputs to extract features. Binary images, constructed as was explained in the previous sections, were imported from ILWIS to TIFF format using the GeoGateway option. A script was written to transform from TIFF to RAW format, run the HT process, and write the output file again in TIFF format for further calculations after importing into ILWIS (Appendix 2).

Since the selection of the parameters n and k influence the outcome of the HT considerably, they need to be chosen carefully. The *best* combination of HT parameters was selected by varying both parameters and comparing the outputs with lines extracted visually from input binary image as is explained further below. The parameters used for the extraction of lines range from 15% to 35% in the case of cut-off value n (minimum number of pixels included in the line) and from 0 to 4 in the case of normalization factor k (softening of normalization factor).

4.5. Post-processing

Post-processing procedures are mainly necessary to generalize extracted lineaments and convert them to vector format for further validation steps. One of the most critical parts in this step is the method selected for conversion of lines from raster to vector format.

Prior to this conversion, binary filter operations and thinning process were used to generalize the HT output lineaments. An 8 connected dilate filter (as implemented in ILWIS) was applied in two steps to close lines next to each other. In order to get one-pixel thick lines, the medial axes extraction method mentioned above (section 1.3) was used to thin the previously dilated lineaments. Raster to vector algorithms (R2V) as implemented in ArcGIS® package (ESRI, 2004) and ERDAS® software (LeicaGeosystems, 2003) were visually tested in order to find the best converter procedure. That was done overlying the extracted vectors over the raster HT output images to evaluate the amount and characteristics of extracted artefacts. The algorithm with better performance (fewer artefacts) was selected (ERDAS® algorithm).

The resulting vector lineaments were later split into segments of two nodes for further direction calculation. The splitting procedure was made with the *Split line at vertices* tool implemented in the *Data Management toolbox* in ArcGIS® (ESRI, 2004). Calculation of segments directions was made using a script downloaded from the ESRI Support Center website (Zazula, 2005). The algorithm calculates arithmetic and geographic angles for every linear segment compounds of two nodes. After checking its correct performance, calculations were made for every extracted and visually interpreted vector map.

The last post-processing was the elimination of short segments in order to clean some artefacts (skeletal legs) created during the thinning and raster to vector conversion processes. Segments shorter than 6 times pixel size were eliminated in all the extracted lineament maps. To do that segments longer than 90 m (6 times pixel size) were selected by a simple SQL statement.

4.6. Validation

The products of the extraction procedure were assessed in two different steps. The first validation was made with respect to visual interpretation of input binary maps in order to fix the parameters required by the HT algorithm and to assess the extraction procedure performance. After fixing the parameters and processing procedures, the second assessment was done with respect to a geological map. That was done to find the optimal amount of candidate pixels to be used during the HT application, validate the overall extraction method with respect to an independent truth source, and to get the DTM with better performance.

4.6.1. Extracted lineaments with Visual Truth

To find the optimal HT parameters the final vector maps were compared with lines extracted visually from input binary images. The idea is supported in the assumption that human visual interpretation is equally good or better than automatic extraction. Hence, detection success for fixing parameters should be in comparison to the maximum possible, which is the visual interpretation of the input maps to HT. Lineaments visually interpreted are considered the *truth*, and all lineaments not appearing in this map are considered false lineaments or artefacts. Two visual interpretations of binary slope gradient map were screen digitised using ILWIS. One of them was digitised more detailed with a combination of short and relatively large segments. The other one was interpreted with less detail and with larger lines, trying to resemble what an expert image interpreter usually does by combining fragmented lines into long, coherent ones. To avoid bias interpretation only one map was interpreted based in the fact that the three maps have a similar general aspect. The interpretations were exported from ILWIS to shapefile format for later line segmentation and orientation calculation.

A vector line compound of two nodes is completely described by its length, position and angle with respect to a reference (geographic in this case). In this study more than try to measure the extraction accuracy for every individual line it was stated a general accuracy based in the length of all correctly extracted features. The latter were defined as lineaments with angle deviation lower than 15° and not far from the truth lines than 5 pixels, considering in this way the other vector characteristics (position and angle). All other extracted lineaments were accounted as false. The selection of correctly extracted features was carried out using a single buffer zone around the interpreted truth lines intersected later with the extraction output maps. Posterior table calculation of angle differences (see script in Appendices) allowed the final selection of segments close enough (within the buffer) and similar orientation (angle difference <15°)

Therefore length accuracy (LA in %), as a measure of extraction effectiveness was defined as the ratio between the length sum of all correctly extracted lines (CE) and the length sum of all the truth visually interpreted true lines (TL):

$$LA[\%] = \frac{CE}{TL} \times 100 \quad (1)$$

A large sum of correctly recognized features implies a higher accuracy and a better extraction performance. In an ideal situation, all existing lines are correctly extracted, giving a LA=100%. However, it is also necessary to measure the amount of falsely extracted lines. This measure is defined as the ratio between correctly extracted features, in terms of length, and all extracted lines. A positional accuracy expressed in percentage was defined in this way as:

$$PA[\%] = \frac{CE}{AE} \times 100 \quad (2)$$

where *CE* is the length sum of all correctly extracted features and *AE* the length sum of all extracted lineaments. It is necessary to notice that the term position accuracy in this case is not dealing with how far or close the extracted lines are with respect to the truth lines. It is just a measured of the amount of false lines in the images. The more correctly recognized lines within the buffer, i.e. in a

correct position, the higher the position accuracy. In the other hand, a higher amount of lines outside the buffer (false lines) leads to lower accuracy.

Both stated accuracy estimations were combined to get a total accuracy (TA). As the measures involved are ratios, the geometric mean it is the most suitable method for averaging the defined accuracies and get the final value. In this way the total accuracy is defined as:

$$TA[\%] = \sqrt{LA * PA} \quad (3)$$

The maximum total accuracy indicates the best combination of HT parameters, given the selected pre and post procedures, for extracting lineaments as compared to the visual interpretation. Having determined the *best* combination of HT parameters and the other procedures, these were applied to different slope gradient, profile curvature and shade relief binary maps to find the optimal threshold value and the best performing terrain model for lineament extraction.

4.6.2. Extracted lineaments with Geological Truth

At the end of the first stages all the parameters and processing steps of the extraction method have been fixed except the threshold value. The established extraction methodology was applied to all selected terrain models varying only the threshold value to find the optimal. An independent geological map was used in this case to validate the results. The methodology used for validation was the same as above. However, now it is also important to know the orientation trends of all extracted lineaments to evaluate the orientation matching with respect to the truth.

Rose diagrams were constructed from extracted, visually interpreted and geological lineament maps. In these ones, the length of the petals is proportional to the square of relative frequency to ensure equal area histograms. The rose diagrams were calculated using the EZ-ROSE 1.0 software implemented as Microsoft Excel® workbook (Baas, 2000).

Rao's spacing test of goodness-of-fit (Batschelet, 1981) was used to evaluate uniformity in extracted lines orientations. Because this technique is not restricted to alternative unimodal distributions is most suitable for data in which polymodal distributions can be anticipated (Bergin, 1991) as is common in geologic structural data. However this test does not indicate the number of populations and their means. The test is used here to evaluate whether or not the extraction methodology is giving a uniform distribution of line orientations. In circular statistics uniform distribution are equivalent to random distributions in common statistics. If lines are not uniformly orientated (reject the null hypothesis) the preferred orientations in rose diagrams can be considered more confident. The Rao's spacing test as implemented in the circular library of R software (Chambers and Others, 2006) was used in this research.

The established lineament extraction procedure applied to slope gradient led to the lineament map with the highest total accuracy and with a rose diagram similar as the geological truth. To test if the obtained results at 1:25,000 scale can yield similar results on smaller scale (larger grid size) DEM's, the established procedure was applied to slope gradient maps from 1:50,000 and SRTM elevation data. Validation of results was made with the geological truth in the local study area, and with the morpholineament map for the larger SRTM regional area.

5. Results and Discussion

5.1. Digital Terrain Modelling

5.1.1. Construction of DEM from 1:25,000 topographic map

To choose the DEM to be used in the research 3 different interpolation algorithms were tested: the linear interpolation as is implemented in the ILWIS software (ITC, 2001) and the spline with tension and *Topo to Raster* algorithms implemented in ArcGIS® package (ESRI, 2004). The three created DEM's were tested qualitatively by checking the elevation frequency distribution and three-coloured shaded relief and aspect maps to look for systematic errors and artefacts.

Although the values for mean, standard deviation and median are almost the same, the shapes of the histograms are different (Figure 5-1). Both, spline and linear algorithms show systematic peaks at each contour elevation while ANUDEM algorithm lacks these artefacts or at least reduces the problem considerably. The zoom on the interval 300 to 340 m elevation (E, F and G in figure 5-1) show the differences in the histogram with ANUDEM looking more homogeneous than the other two. Moreover some artefacts, such as *stepped* surface and flat hilltops, are visible in shaded relief and aspect maps respectively (Figures 5-2 and 5-3). The spline with tension is the algorithm that shows most artefacts while ANUDEM algorithm is almost lacking these. Despite the inserted artefacts, the replacement of negative values in ANUDEM interpolated DEM for those of linearly interpolated DEM, does not visibly change the histogram. Moreover, the values of mean, standard deviation and median do not show significantly differences with the original values. The relative large frequencies between 0-40 m and 120-250 m correspond roughly to the San Antonio Valley and Caujerí Valley respectively.

Hence, ANUDEM algorithm as implemented in the *Topo to Raster* tool in ArcGIS® was selected to continue the research. The selection was based in the fact that this DEM presents fewer artefacts compares to the other two DEM's. Although the selected interpolation method creates a DEM with fewer artefacts than the other interpolation algorithms, the created topographic surface looks very smooth. It is not known at this moment how this smoothing affects the lineament extraction. However, is probable that smoothing affects the extraction in zones with lower relief more than in those with higher relief.

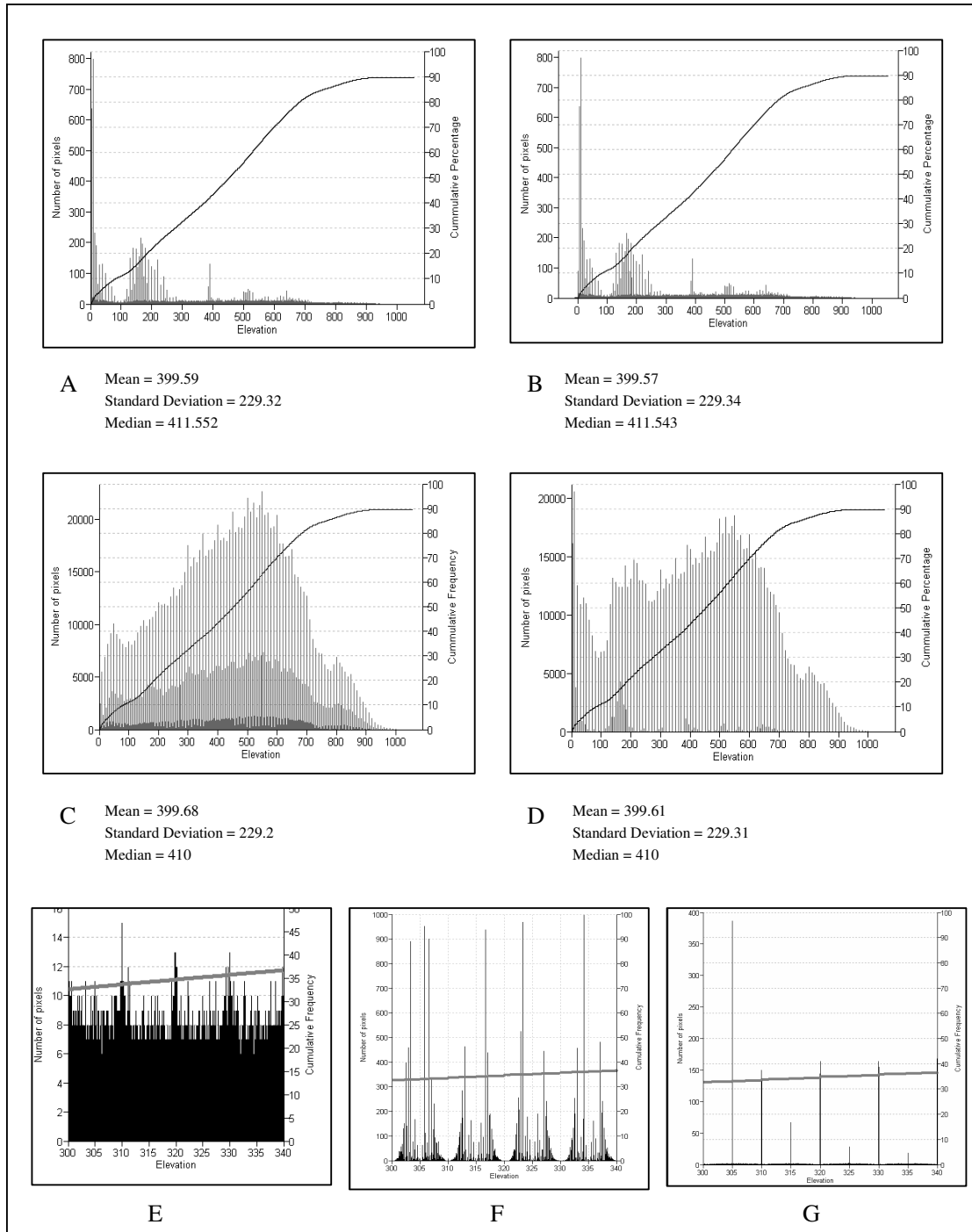


Figure 5-1. Elevation frequency distribution of interpolated DEM's. A: histogram corresponding to the final 15 m resolution DEM used in the research, interpolated with ANUDEM algorithm and negative values replaced with those obtained with the linear interpolation, B: ANUDEM algorithm histogram, C: linear interpolation histogram, D: spline with tension algorithm histogram. E: zoom on interval 300 m to 340 m elevation for final ANUDEM, F: zoom on the same interval for linearly interpolated DEM. G: same interval for spline interpolated DEM. The thin black lines correspond to cumulative frequency distribution of elevation (thick gray in the last three graphs).

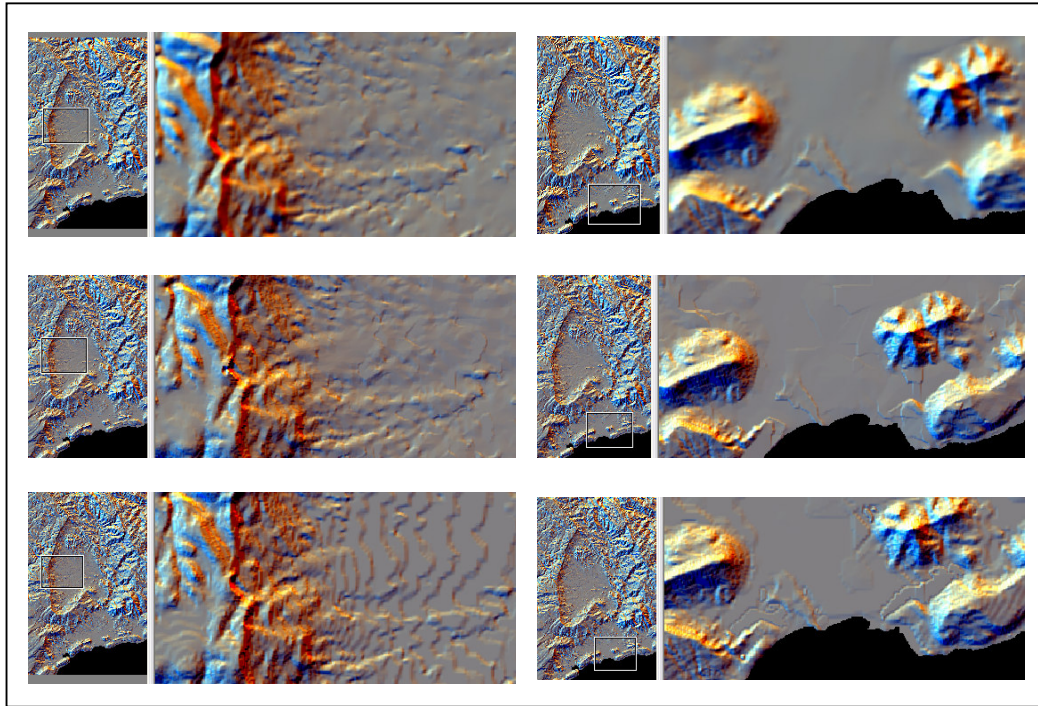


Figure 5-2. Three-color shaded-relief maps constructed from three different interpolated DEM's. The upper images correspond to the ANUDEM interpolated DEM showing the smoothest surface without great artifacts. The center images show the same areas for the linearly interpolated DEM. Here the artifacts are starting to appear, mainly in the right image. In the bottom, the spline with tension interpolated DEM shows the most prominent artifacts visible in both images.

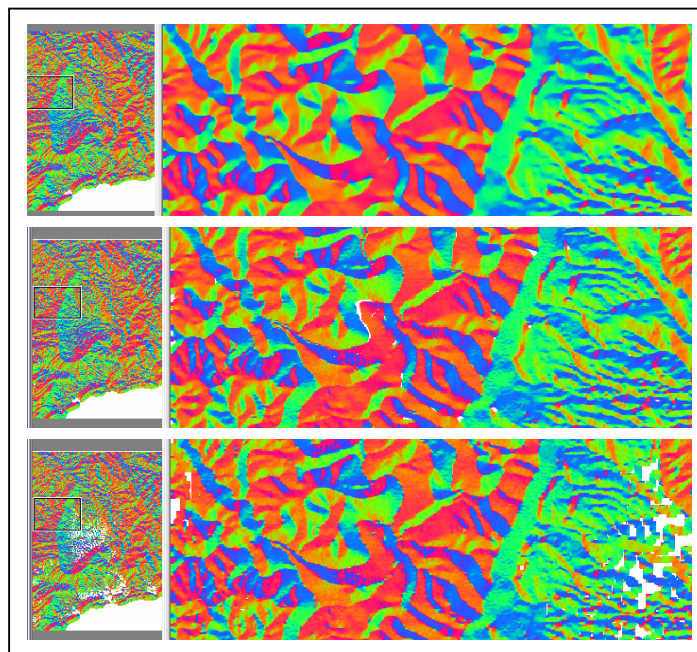


Figure 5-3. Aspect maps from the three different interpolated algorithms. Flat zones, corresponding mainly to created artifacts (flat hilltops), are shown as white zones (undefined values in the aspect map). The upper one

correspond to the ANUDEM method lacking flat zones, while the image of the center constructed from the linear interpolated DEM is showing some flat hilltops. The bottom image (spline with tension algorithm) shows bigger areas of artifacts.

5.1.2. Terrain parameters and hill shading calculation

Evans-young method was used for calculation of slope gradient and profile curvature derivative maps. In order to choose the level of DEM smoothing used for derivative calculation, three different smoothing values were applied to get three sets of terrain derivative maps. After enhancement and thresholding, the resulting binary maps were visually compared by means of a map cross operation. Shaded relief maps were created using the ILWIS method. Hillshading maps were created with illumination from the 8 compass directions allowed by a 3x3 kernel size. The shaded relief maps for northwest and northeast illuminations are shown as an example in figure 5-9.

The slope gradient maps are statistically summarized in Figure 5-4. As the smoothing factor increases the statistical parameters decrease, but not significantly to change the cumulative frequency curves. For plan curvature mean and median decrease as smoothing factor increases while standard deviation increases (Figure 5-4). Minimum and maximum values are slightly erratic but stable. In the case of profile curvature, mean and median almost remain the same values while standard deviation, minimum and maximum values decrease.

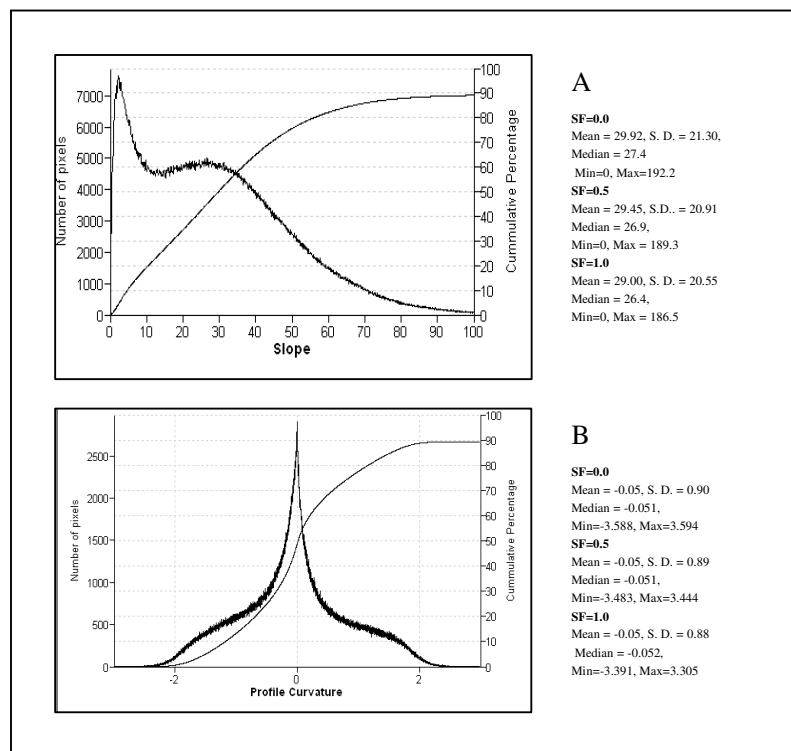


Figure 5-4. Frequency and cumulative frequency distributions for ANUDEM interpolated DEM (thin black line). A: slope gradient, B: profile curvature maps. As the shapes of the curves remain very similar only the graphs for smoothing factor 1 are shown.

For selecting DEM smoothing value a visual comparison approach of binary maps was used. Three different smoothing values (0, 0.5 and 1) were used to construct slope gradient, profile curvature and hill shaded relief maps. After enhancement and thresholding, the resulting binary

images were crossed for visual comparison (Figure 5-5). In general, a higher smoothing value leads to more continuous and homogeneous areas with less isolated pixels (maps are less noisy). Table 1 (Appendix 1) shows the number of isolated pixels for two different maps.

Because of the continuity and homogeneity the highest smoothing value was chosen for further calculations. However this might lead to the loss of some linear features due to elimination of isolated pixels that are in fact depicting a line. As with interpolation methods, the selection of high smoothing value leads to a high level of generalization, which might cause information lose in zones of lower relief. The evaluation of how much information is lost should be evaluated extracting lineaments from DTM's constructed with different smoothing values.

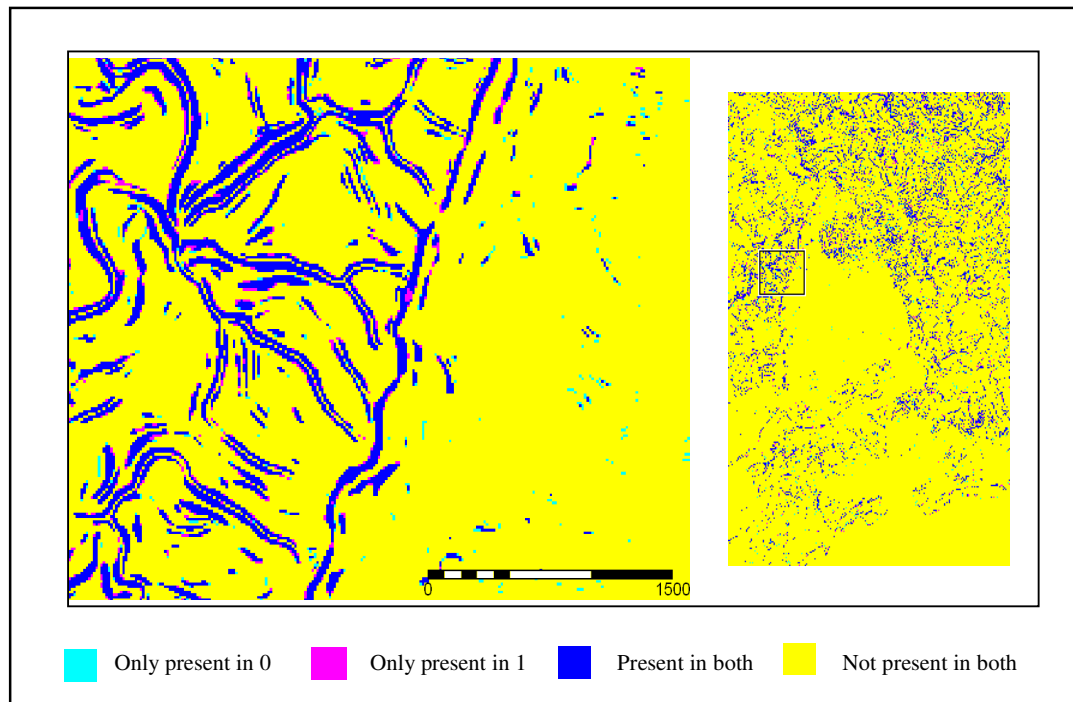


Figure 5-5. Resulting cross maps between the binary images obtained with two different smoothing values. The threshold value corresponds to the highest 5% values in edge maps. The case for smoothing factors 0 and 1 is illustrated in this case.

5.2. Pre-processing

5.2.1. Lineament enhancement

In this research lineaments have been defined in terms of abrupt change of slope gradient that can be expressed in shaded relief, profile curvature and slope gradient maps as it was explained previously. For each terrain map different enhancement processes were designed. In the case of slope gradient map, two different edge enhancement operators were evaluated.

Laplace and Sobel methods were applied to highlight lineaments in slope gradient maps. The highest 5% values in the cumulative frequency curve (see section 5.1.4) of enhanced maps were used to construct binary maps that were crossed with one of each other for visual testing and comparison. In Figure 5-6 it is noticeable how low the degree of overlapping is between the highest value pixels in

the two images. High value pixels in Sobel also often form the periphery of those in Laplace, showing in this way two lines where Laplace only gives one. However, Sobel operator often results in thinner and more linear homogeneous areas than Laplace. Hence because of the linearity and thinner properties of lines given by Sobel operator this method was selected for further operations.

Lineaments in profile curvature map were highlighted selecting the pixels with the highest convexity and concavity values. That was done selecting pixels above and below a threshold value in the cumulative frequency curve. To enhance lineaments in shaded relief images gradient filters perpendicular to the azimuth illumination were applied. That was done for the 8 illumination directions allowed by the applied method. Figures 5-8 and 5-9 show some results for the different enhancement methods applied in this study.

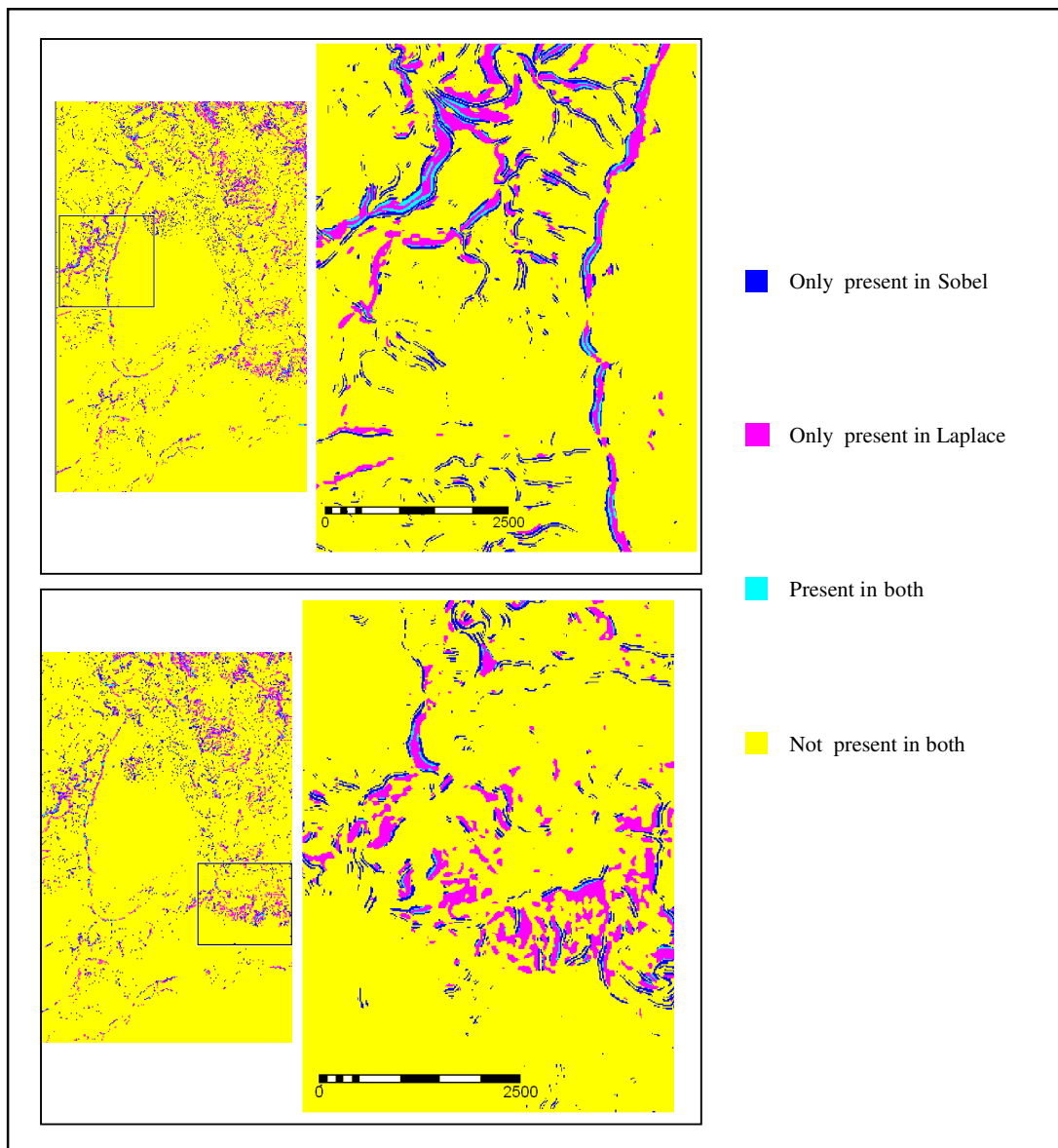


Figure 5-6. Resulting cross maps between the binary images obtained with two different edge enhancement methods. The threshold value corresponds to the highest 5% values in edge maps. Smoothing factor 1% is illustrated in this case.

5.2.2. Threshold value selection and pre-thinning method

Extraction procedure outcomes are considerably influence by the amount of candidate pixels (given by the threshold value) in the input image. Because of this it was designed a procedure to carefully choose the best threshold value. Results of this selection are given in the final validation (section 5.4.2). However during the first stages it was necessary to remain constant the threshold value in order to select and fix the other involved parameters.

After visual inspection of different binary maps constructed with different threshold values 5% was selected to work in the first stages. The decision was taken because this map shows more continuous lineaments and they are not too much noisy in comparison with extreme 1% and 10% tested binary maps. Figure 5-7 shows two different areas of slope gradient map for all visually checked threshold values. For slope gradient map were selected 134878 pixels (4.46%), for profile curvature map 134843 (4.46%) and for hill shading 162712 pixels (5.39%). For the latter the used threshold value was 1% for the 8 illuminated images, becoming more or less 5% after the joining all hill-shaded binary maps. The threshold processes were implemented in scripts to facilitate the processing (see Appendix 2). Figures 5-8 and 5-9 show some results of enhancement and threshold processes. It is possible to see that slope gradient and shaded relief binary maps look similar and show more continuous and clear defined lines than profile curvature map.

The result of applying pre-thinning procedure to binary images led to elimination of some isolated group of pixels. The final evaluation of medial axes extraction was done after lineament extraction. According to this pre-thinning procedure reduce considerably the amount of extracted lines, leading however to similar accuracy values than non-thinned binary images. Nevertheless, the methods led to the creation of artefacts that change the main trend orientations (see Figure 5-17). Because of the latter, non-thinned images were preferred for the remaining of this work.

5.3. Automatic lineament extraction

As it was stated before, the Hough Transform (HT) was selected to carry out this task. The previous pre-processing steps led to the construction of binary images that were used as inputs in the extraction procedure. Final lineament maps in vector format were obtained after post-processing procedures explained in the next section.

The resulting lineament maps have in general short and parallel segment lines. Parallel lines can be explained due to the presence of relatively thick areas in the binary images that were extracted in this way for the HT. In the case of slope gradient map the presence of parallel groups of pixels in the original binary images led to the same characteristics after lineament extraction. These lines were partially closed during the post-processing procedures.

As was expected the lower cut-off values (n) extracted more features than higher cut-off but the length of lines are longer (Figure 5-10). For normalization values k occur the same, higher values extracted fewer and in general shorter linear features than lower normalization factors. One remarkable thing is that the algorithm is able to extract lines longer than they appear in the threshold maps. This is maybe related to the multi-scale method used for recognition of lines at different sizes. In this way the lines length is probably determined by the minimum tile size used by the algorithm.

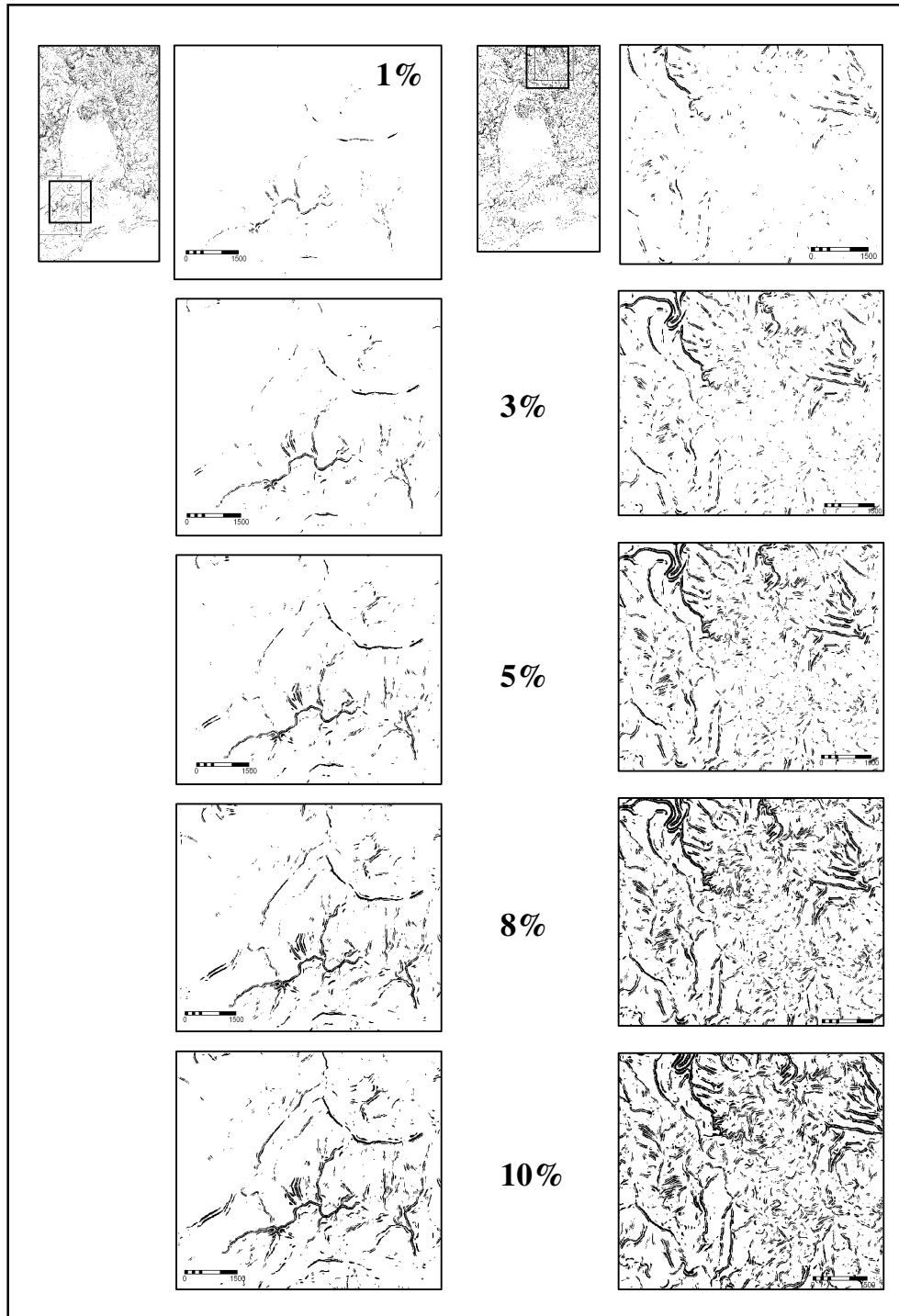


Figure 5-7. Slope gradient binary maps with different threshold values. From top to bottom 1%, 3%, 5%, 8% and 10% threshold values. The left images represent a terrain with lower relief than the right ones.

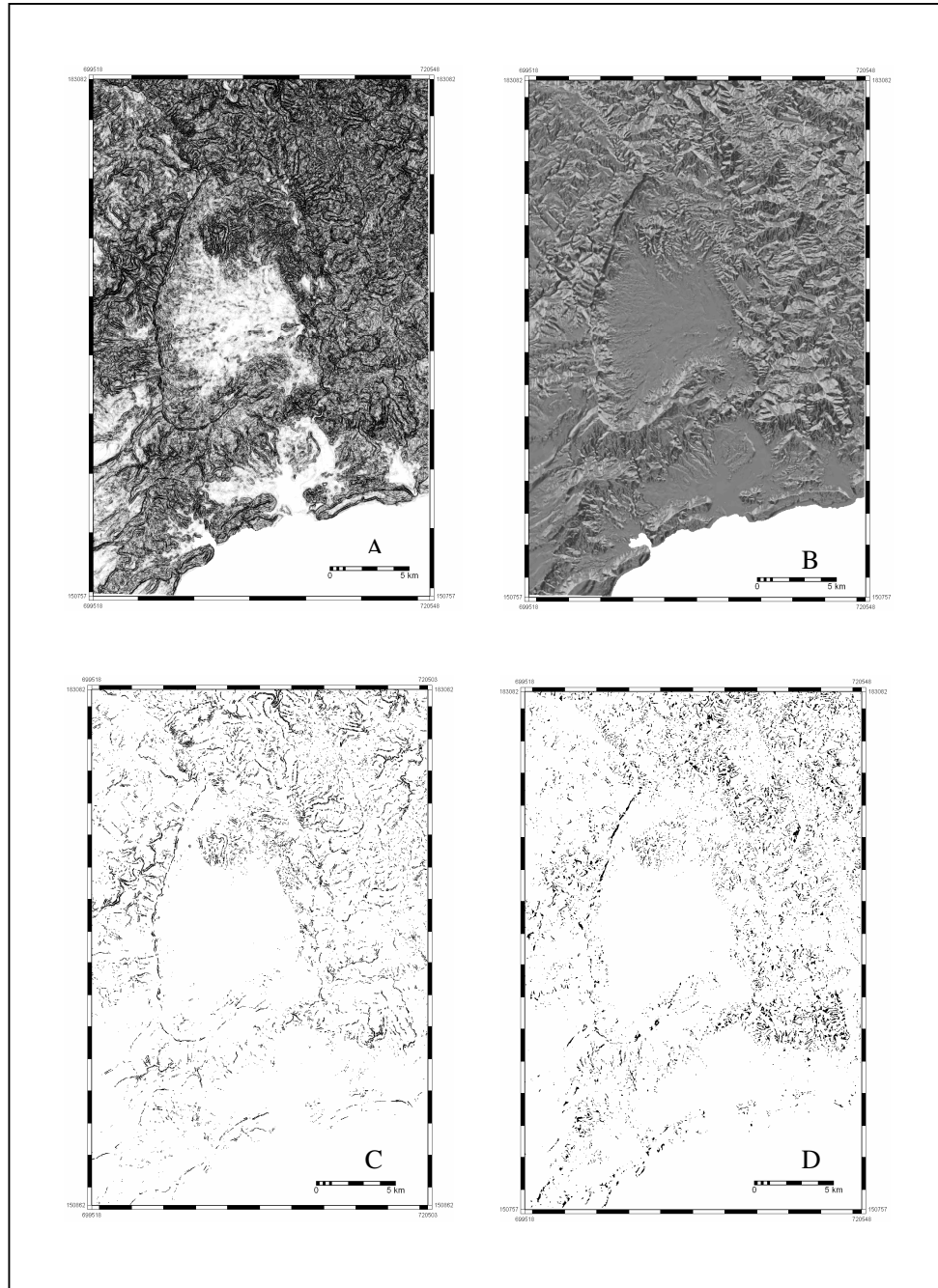


Figure 5-8. Enhanced and binary maps from slope gradient and profile curvature maps. A: enhanced slope gradient map stretched with and histogram equalization with 20 intervals and displayed with a gradual greyscale from white (lower values) to black (higher values). B: profile curvature map stretched with histogram equalization with 20 intervals and displayed with a gradual greyscale from black (lower values, concavity) to white (higher values, convexity). C: highest 5% values of edge enhanced slope gradient map. D: highest 2.5% and lowest 2.5% values of profile curvature map.

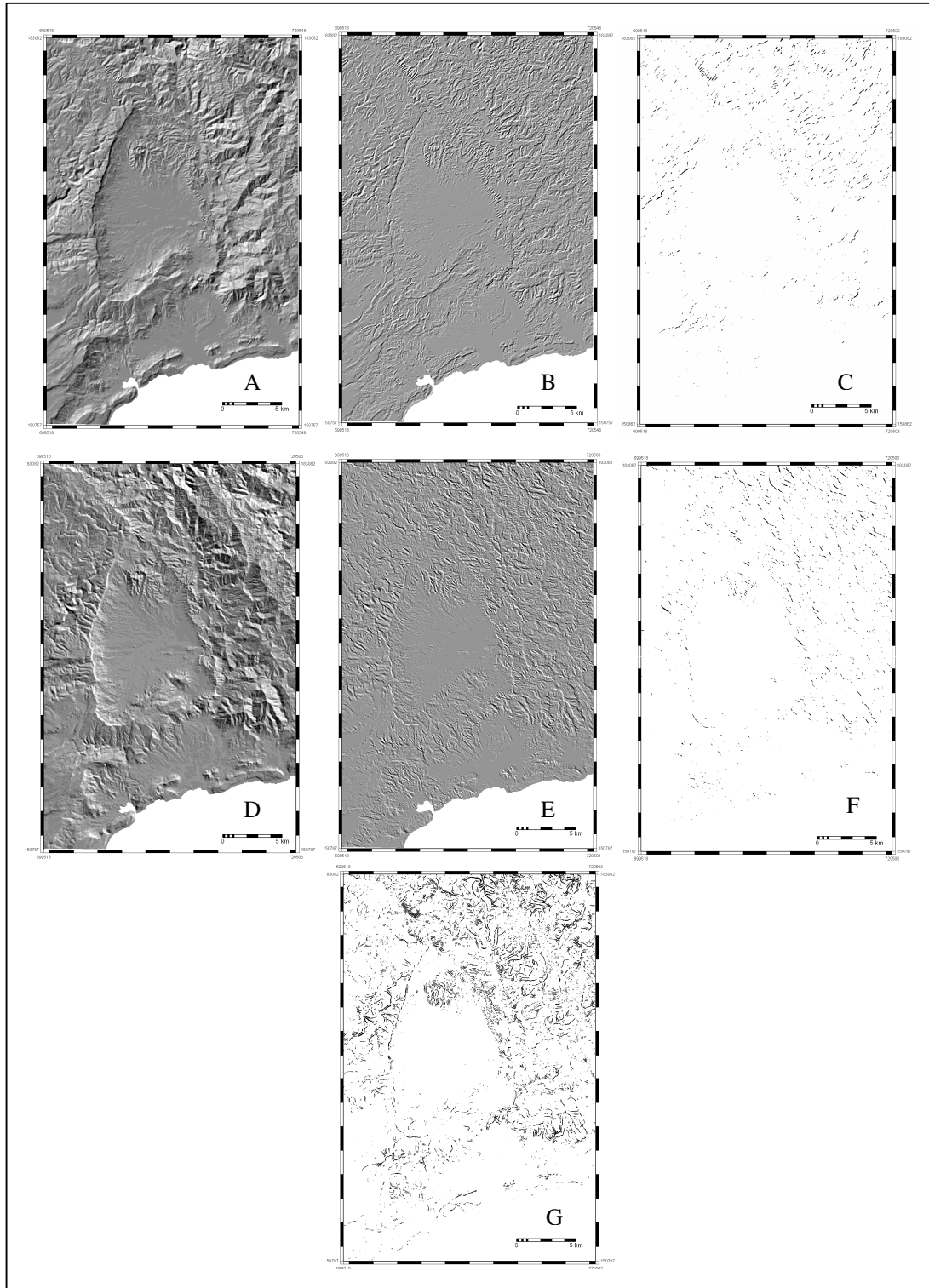


Figure 5-9. Original, enhanced and binary maps for two shaded relief maps. A: northwest illuminated shaded relief map. B: enhanced edge map after gradient filter application (DFDDN filter in ILWIS, see script in Appendix 2). C: highest 1% values in cumulative frequency curve of previous map. D: northeast illuminated shaded relief map. E: enhanced edge map after gradient filter application (DFDUP filter in ILWIS). F: highest 1% values in cumulative frequency curve of previous map. G: combined binary maps from the 8 enhanced shaded relief maps illuminated from the main azimuth direction.

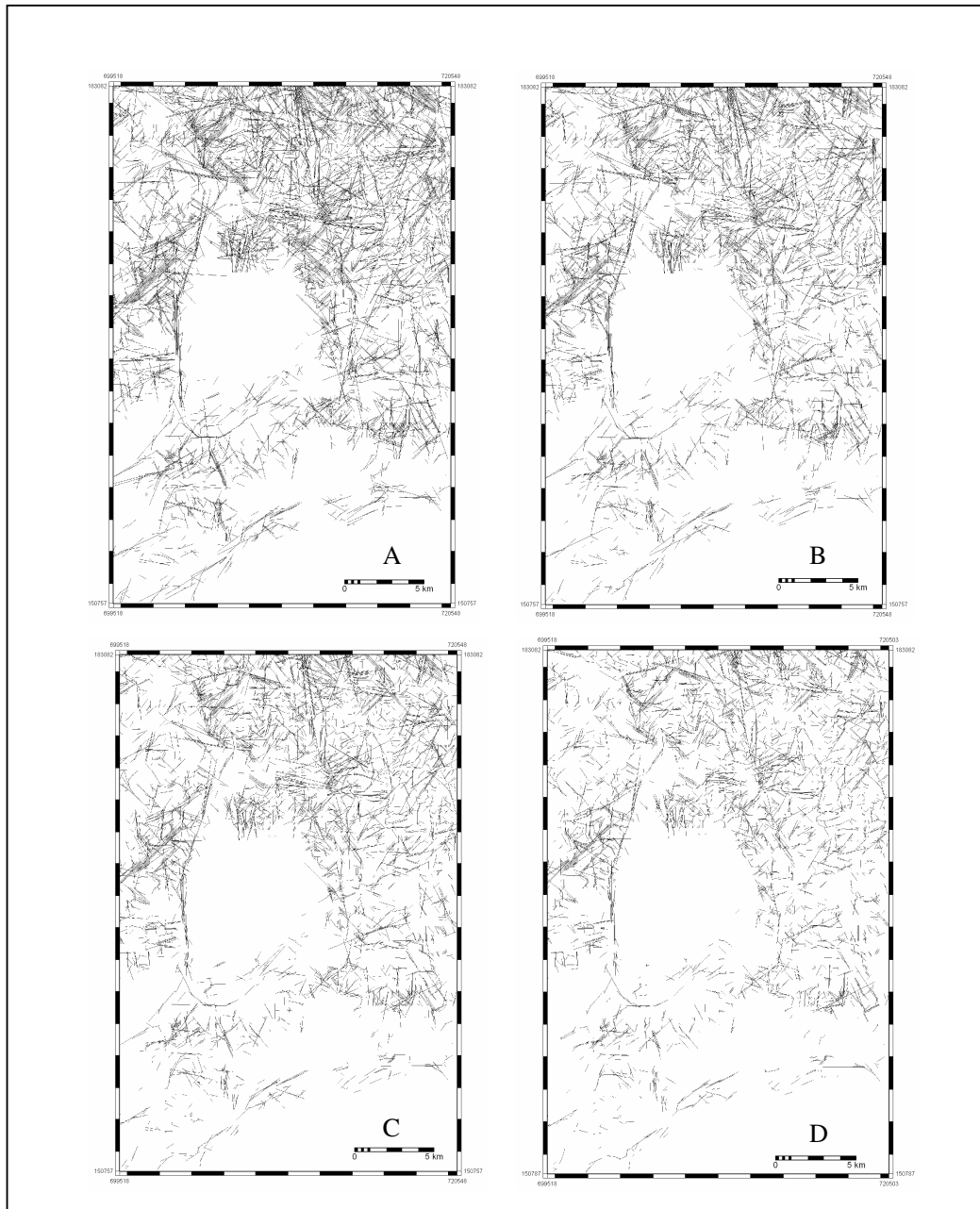


Figure 5-10. Extracted lineaments from slope gradient binary map (5%). A: lineaments extracted using cut-off value $n=15$ and normalization factor $k=0$. B: extracted linear features using $n=20$ and $k=0$. C: lines recognized using $n=25$ and $k=0$. D: lineaments extracted using $n=30$ and $k=0$.

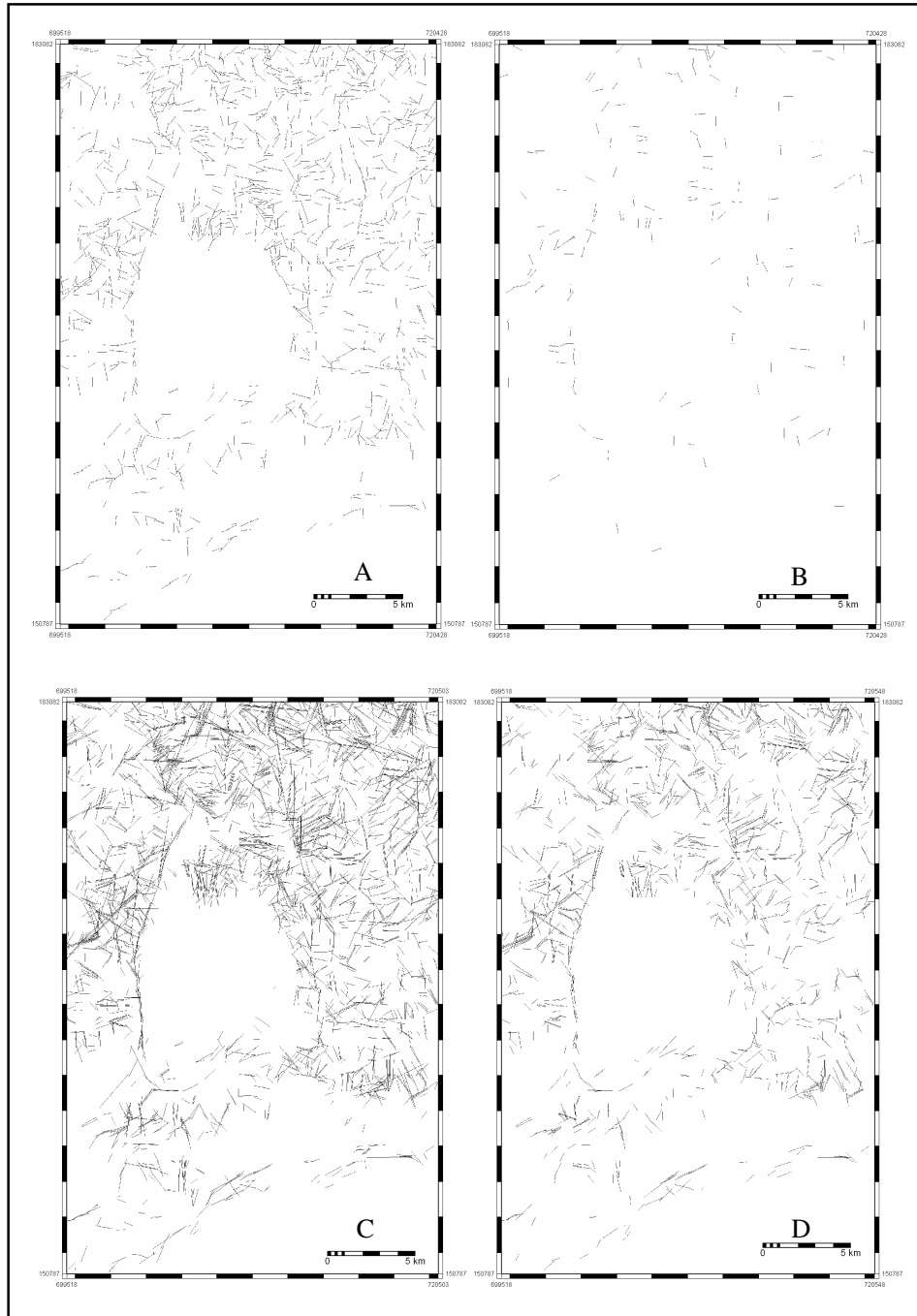


Figure 5-11. HT output maps for most accurate thinned and not-thinned slope gradient binary maps. A: thinned with HT parameters $n=20$ $k=3$, B: thinned with HT parameters $n=30$ $k=4$, C: non-thinned with HT parameters $n=20$ $k=3$, D: non-thinned with HT parameters $n=30$ $k=4$.

Pre-thinned and non-thinned images show some differences in relation to the length and the amount of extracted lines. The thinning procedure reduces the length and final number of lines when compared to non-thinned images (Figure 5-11). The reason for this is found in the fact that medial axis algorithm eliminate groups of isolated pixels leading to extraction of fewer and shorter lines. Nevertheless, these cleaner images are not useful because thinning creates linear artefacts that change considerably the orientation patterns (see section 5.4.1).

Comparison of the extraction performance with respect to the results obtained by Fitton and Cox (1998) shows that these are more or less similar. They also obtained some lines longer than they appear in the input binary images. Parallel lines are also shown in their results but mainly related to parallel group of pixels in the binary input image. With respect to how well are extracted the lineaments, they only did a visual assessment. In similar way as the results obtained in this research, the best extraction performance stated by the authors is not able to extract all the lineaments seen in the input binary images.

5.4. Post-HT processing, vectorizing and cleaning steps

Post-processing procedures are mainly necessary to generalize extracted lineaments and convert them to vector format for further validation steps.

As the results of HT transformation show parallel lines, most probably representing the same lineament (see Figure 5-10, 5-11 and 5-12 as examples) these need to be jointed by a closing procedure. That was made in raster format prior to vector conversion applying a dilate filter in two steps. That was followed by medial axes extraction in order to present one-pixel thick lines to the conversion algorithm.

Raster to vector (R2V) algorithms as implemented in ArcGIS[®] and ERDAS[®] packages were visually tested to choose one of them. After trying different parameters combination it was possible to see that in general the ArcGIS[®] tool creates more artefacts than ERDAS[®] tool. That was visually checked overlying the extracted vectors over the raster HT output images. The thinning procedure included in ERDAS[®] *Raster to Vector* tool (Leica Geosystems, 2003) was tested as an alternative to medial axes extraction, but the results show so many artefacts that are not useful for further calculations. Nevertheless and despite of previous thinning, selecting the thin option in ERDAS[®] R2V tool gives better results (fewer artefacts) than without choosing this option. The following are the chosen parameters for raster to vector conversion in ERDAS[®] tool: maximum thickness as default (10 times pixel size = 150 m), dangle length equals to 60 m (4 times pixel size) and weed tolerance equals to 45 m (3 times pixel size). Explanation of these parameters can be found in ERDAS user guide (Leica Geosystems, 2003). The selected values allow vector features resemble very well with raster format and also facilitate posterior cleaning of small segments.

Although the creation of some artefacts and loss of lines the combination of dilate filter, medial axes thinning and R2V processes performed very well. Artefacts correspond mainly to relatively short skeletal legs that appear in the end of the dilated areas. Incomplete joining of parallel lineaments and thick areas in dilate image also lead to some artefacts creation (Figure 5-12). Cleaning step allows the elimination of the shortest artefacts. However, cleaning also deleted correctly extracted linear features, being this most dramatic in lineament maps extracted with lower cut-off and normalization HT parameter values. Figure 5-12 show some results of vector to raster conversion overlain on binary input, HT output, dilate HT output map and post-thinned images.

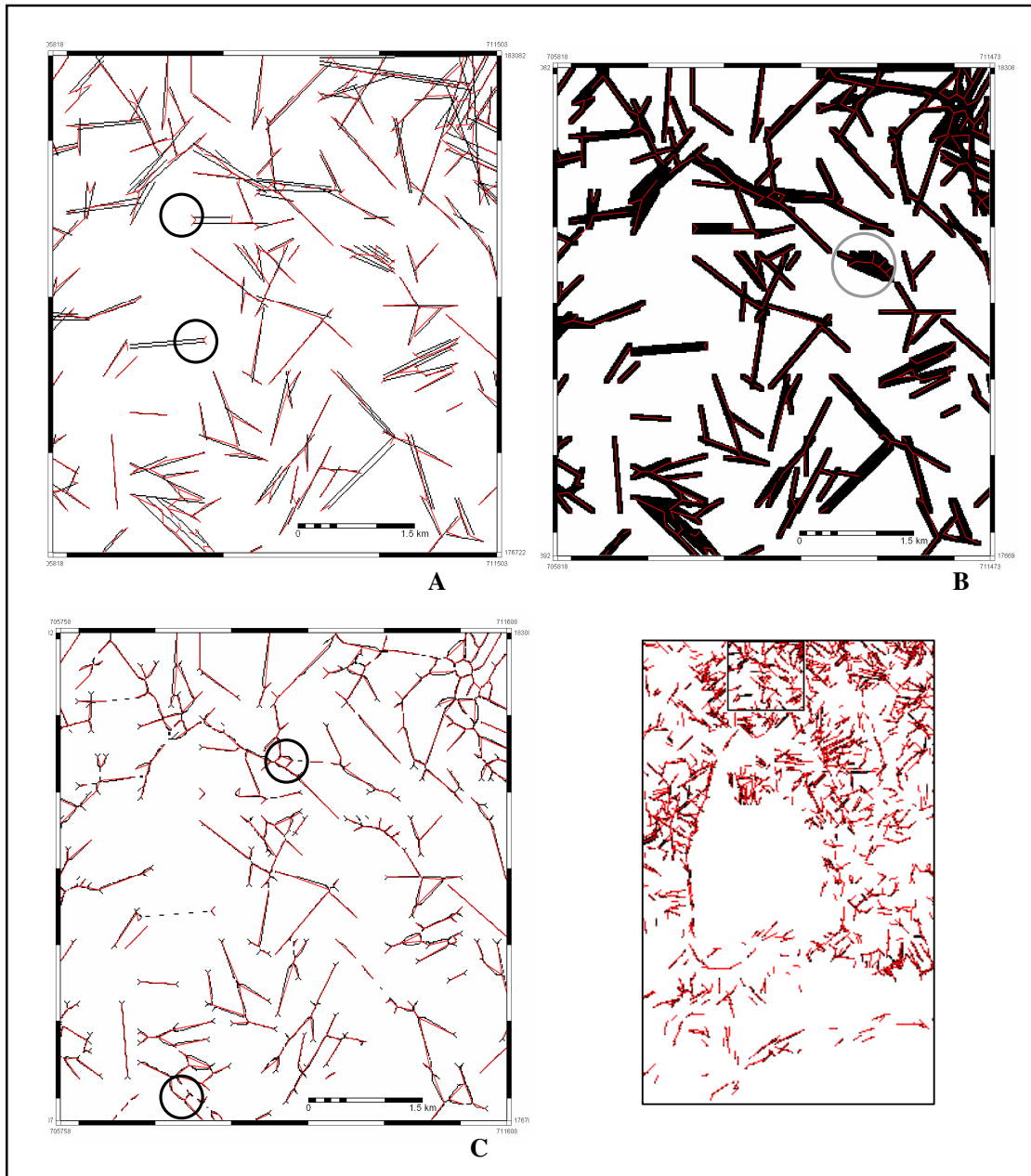


Figure 5-12. Selected area showing the output of HT for slope gradient binary map (5%) using the combination of HT parameters $n=30$ and $k=4$ (A) and the results of subsequent dilating (B) and thinning (C) procedures for the same area (upper and bottom right). Extracted lineament vectors (red lines) are plotted on the images to show the performance of raster to vector algorithm with respect to all images. Skeletal legs (encircle in A) appear as small v shaped lines in the end of some lines. Artifacts related to thick areas in dilate image (encircle in B) and those related to incomplete joining of lines (encircle in C) are also shown. The deleting side effect of extracted lines can also be observed in these images.

5.5. Validation stages

Extraction procedure outcomes were assessed in two different steps. The first validation was made with respect to visual interpretation of input binary maps in order to fix the parameters required by the HT algorithm and to assess the extraction procedure performance. After fixing the parameters and processing procedures, the second assessment was done with respect to a geological map. That was done to find the optimal amount of candidate pixels to be used during the HT application, validate the overall extraction method with respect to an independent truth source, and to get the DTM with better performance.

5.5.1. Validation with Visual Truth

In this step lineaments extracted from non-thinned and thinned binary slope gradient maps were compared to those visually interpreted in non-thinned binary slope gradient map. The results are summarized in Tables 2, 3 and 4 (Appendix 1) and Figures 5-13 to 5-15.

Lineaments extracted from non-thinned binary images give higher accuracies when compared to detailed visual interpretation (shorter and more interpreted lineaments) than compared to long and fewer lines interpretation (Figure 5-13). Maximum total accuracies of 47% and 28% are reported respectively (A and D in Figure 5-13). Nevertheless and despite of differences in the maximum accuracy values the combination of HT parameters for that maximums are very similar ($n=30, k=2$; $n=30, k=4$ respectively).

In general, total accuracies for lineaments extracted from thinned binary images are similar to non-thinned binary images compared to long-interpreted lines (Figures 5-13 and 5-14). However, positional accuracies tend to be higher and length accuracies relatively lower. This can be explained with the reduced amount and length of extracted lines from thinned images compared to non-thinned binary maps (see results in section 5.2). Fewer lines imply fewer artefacts (higher position accuracy) while reduced length imply short segments (lower length accuracy). The maximum total accuracy in this case is given by the HT parameter combination of $n=20$ and $k=3$ (Figure 5-14). In Figure 5-11 is possible to see that extracted features in the latter case and non-thinned image with combination $n=30, k=4$ (maximum in this case) are slightly similar. Despite of these similarities between thinned and non-thinned results, the former was ruled out for the next steps because the orientation trends are strongly changed with respect to those in visual interpretations and those seen in the geological truth (Figure 5-16, H).

In general, accuracy curves follow expected trends. Position accuracy increases when cut-off value and normalization factor are increased as well. In the case of length accuracy, higher cut-off values give higher accuracies. The same occurs as well for lower normalization factors. In other words these means that fewer extracted lines increased the position accuracy because fewer artefacts are extracted, while length accuracy decreases because fewer correct lines are extracted as well.

Deviation of these trends in length accuracy (Figure 5-13, C) might be explained with the cleaning step. During this process lines shorter than 90 m (6 pixels) were eliminated. Lower cut-off values extract more lines and also more artefacts are created. This artefacts cross correctly extracted lines what induced splitting them in shorter segments during segmentation process. In this way more correctly extracted lines were deleted during cleaning step leading to lower length accuracies for lower cut-off. This effect is considerably reduced when cut-off value increases because fewer lines

and artefacts are extracted and segmentation is not playing an important role (see for example Figure 5-10). Another explanation is related to artefacts creation during the post-processing steps. Lower cut-off and lower k values lead to extraction of more lines and in this way, closing step creates larger homogeneous areas (Figure 5-12, B). That leads to create more artefacts during medial axes extraction that could lead to reduce the amount of correctly extracted lines in these areas.

Despite of the lower accuracies, the combination of HT parameters that better resemble a map with long lines, as a visual expert usually extracts, was selected to continue the research. In this case parameters $n=30$ and $k=4$ give the highest total accuracy and therefore were selected for the next steps. Nevertheless, this combination does not correspond to a local maximum which remains open the question if higher normalization factors could lead to higher accuracies.

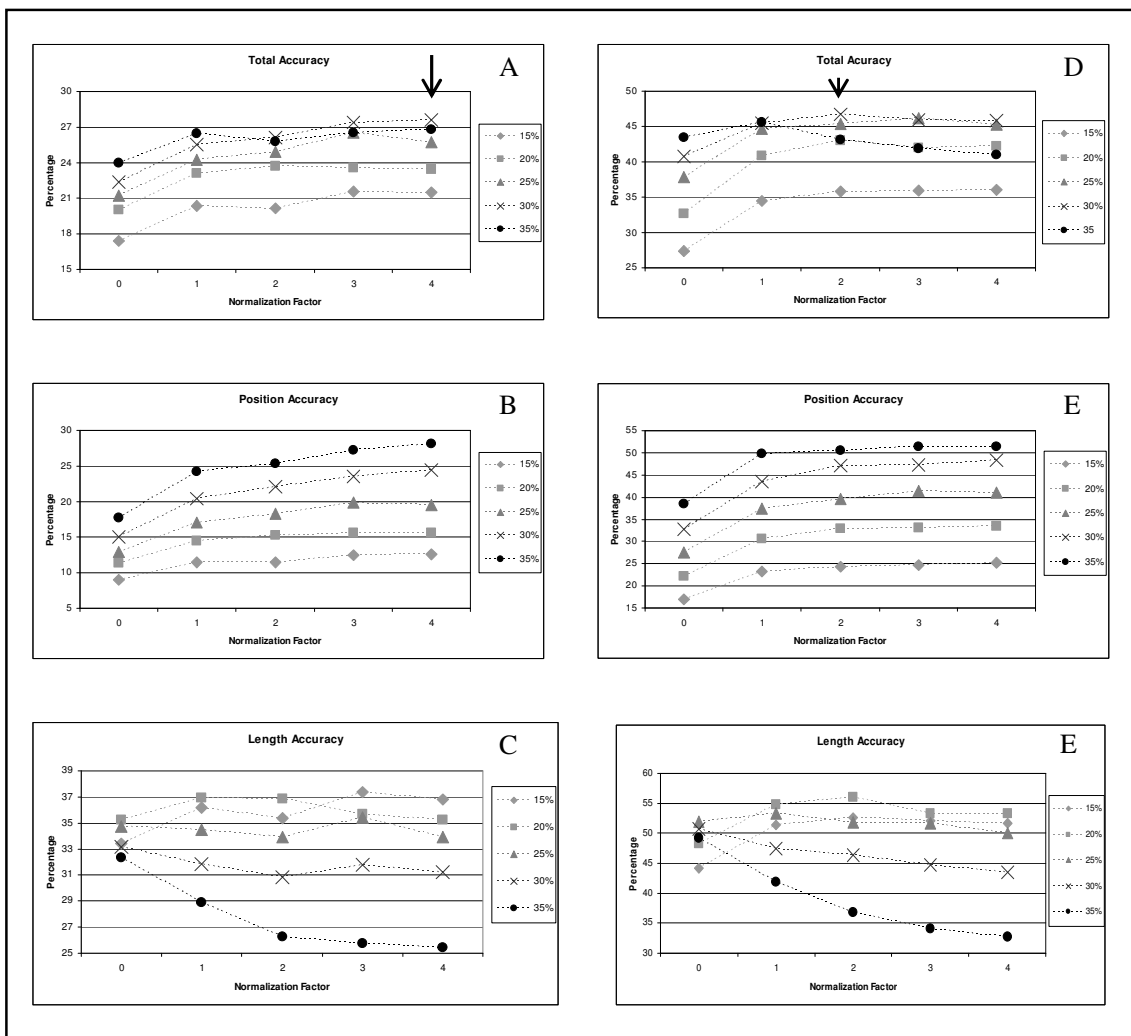


Figure 5-13. Total, position and length accuracy graphs for slope gradient lineaments compared with longer-lines visual interpretation map (A, B C) and with short-detailed-lines visual interpretation map (D, E, F). Higher total accuracy values are pointed with black arrows. The legend to the right of graphs refers to cut-off HT parameter.

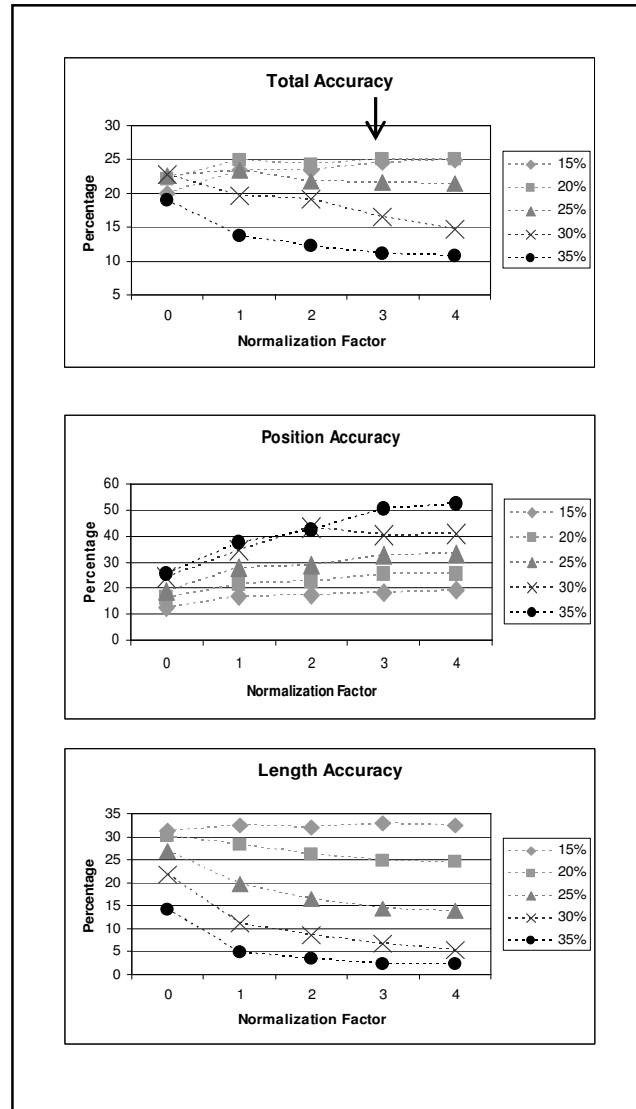


Figure 5-14. Total, position and length accuracy graphs for pre-thinned slope gradient lineaments compared with longer-lines visual interpretation map. Higher total accuracy value is pointed with a black arrow. The legend to the right of graphs refers to cut-off HT parameter.

5.5.2. Validation with Geological Truth

At the end of the previously explained stages, all the extraction method parameters and processing steps have been fixed except the threshold value. In this stage the established extraction methodology was applied to all selected terrain models varying only the threshold value to find the optimal. An independent geological map was used in this case to validate the results. The methodology used for validation was the same as above. However, now it is also important to know the orientation trends of all extracted lineaments to evaluate the orientation matching with respect to the truth.

The following threshold values were tested: 2.5%, 5%, 7.5%, 10%, 12.5%, 15%, 17.5%, 20%, 22.5% and 25%. Higher cut-off values give lineament maps with unacceptable amount of artefacts and because of these there were not tested. The geological truth corresponds to lineaments and faults appearing in the 1:50,000 geological map (Nuñez, 2000).

Total, positional and length accuracies for lineaments extracted from slope gradient, profile curvature and shaded relief maps are summarized in Figure 5-15 and Table 5 (Appendix). For position accuracy the increments in threshold values led to a decreasing accuracy. This reflects the increasing amount of artefacts when threshold value increases. Slope gradient map shows higher accuracies for all threshold values except for the two higher thresholds where shaded relief became the most accurate map. In the case of length accuracy values are higher when threshold increases up to a certain value where a maximum is reached and then the curve started decreasing. This is very clear for the slope gradient and curvature maps, while the shaded relief map present two local maximums. The presence of maximums could be explained by the creation of artefacts and the cleaning processes. Higher threshold values extract more lines and more artefacts. More artefacts in the HT output mean thicker homogenous areas created during closing step. This leads to more artefacts creation during medial axes extraction and raster to vector processes, reducing in this way correctly extracted features now replaced by artefacts.

The total accuracy graphs show similar shapes as length accuracy, with more or less increasing trend till the maximum is reached and then a decreasing trend starts. Again, this is very clear for slope gradient and profile curvature maps while shaded relief shows a dip between two local maximums. Slope gradient map shows the higher total accuracies for most threshold values. The maximum total accuracy is 16.3% and results from the combination of 28.4% length accuracy and 9.41% position accuracy. The low position accuracy, related to the amount of falsely extracted lineaments, was an expected result because here a more detailed map was used (1:25,000) compared to the maps used for preparing the geological map (1:50,000) and more lineaments can be recognized.

Figure 5-16 shows the rose diagrams for the most accurate lineaments extracted from the slope gradient, profile curvature and shaded relief maps. Visual interpretation of slope gradient binary map and the geological truth are also shown. Rao's statistical test applied to the extracted lineament maps (Table 7, Appendix) shows that these are not uniform distributed. This implies that the extraction methodology is not detecting lineaments in all directions and preferential orientations can be inferred in rose diagrams with more confidence. Although the rose diagrams for extracted lineaments are not exactly the same as the geological truth, it is possible to infer at least two main structural trends in the study area: the NE-SW and NW-SE. Nuñez (2000) did not mention the N-S minor trend appearing in the rose diagram of geological truth and that it is also appearing in lineaments from slope gradient and profile curvature maps at scale 1:25,000. The minor WNW-ESE trend is not seen in any extracted lineament map.

Rose diagram for the most accurate lineament map extracted from pre-thinned slope gradient binary map is also shown in Figure 5-16 (H). The main trends observed in the geological truth map and non-thinned lineaments cannot be recognized in this diagram, showing slightly major trends in N-S, E-W and NE-SW. This means that the thinning method creates artefacts in such way that affect strongly the line orientations, being in this way not suitable for application in this extraction methodology.

The overlay of the most accurate lineament map (slope gradient) on the geological truth shows that most of the truth lineaments are extracted to some degree. However, there are lineaments that are not detected at all. Overlying the best lineament map on the original slope gradient map

(Figure 5-17) it is possible to see that most of the extracted lineaments correspond to actual lines in the slope map, but with many lines that are actually artefacts created during the extraction procedure.

According to the obtained results slope gradient map produces the best lineament map. This was obtained using the Evans-Young method with prior DEM smoothing, using the method of Evans and Cox, and a smoothing value equal to 1. Lineaments were enhanced with a Sobel edge operator and transformed to a binary map using the highest 15% enhanced values in the respective cumulative frequency curve. The best performing HT parameters were $n=30$ and $k=4$. Lines in the output map were generalized using a dilate filter, applied in two steps, and a medial axes extraction processing to get one-pixel thick lines. After conversion from raster to vector using ERDAS R2V algorithm, lineaments were cleaned eliminating all the lines shorter than 90 m. Figure 5-17 shows the slope gradient map that gives the most accurate lineament map. In Figures 5-18 and 5-19 this lineament map is shown overlying on slope gradient map and slope gradient binary input map respectively.

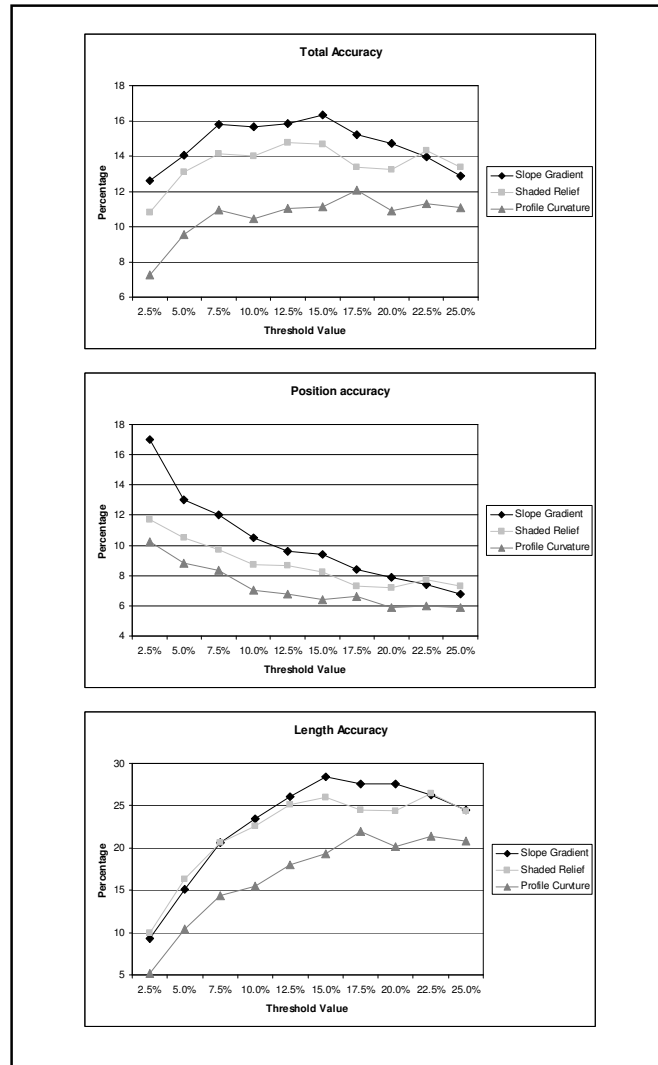


Figure 5-15. Graphs for total, positional and length accuracies for slope gradient, shaded relief and profile curvature lineament maps using the best HT combination $n=30$ $k=4$ and different threshold values.

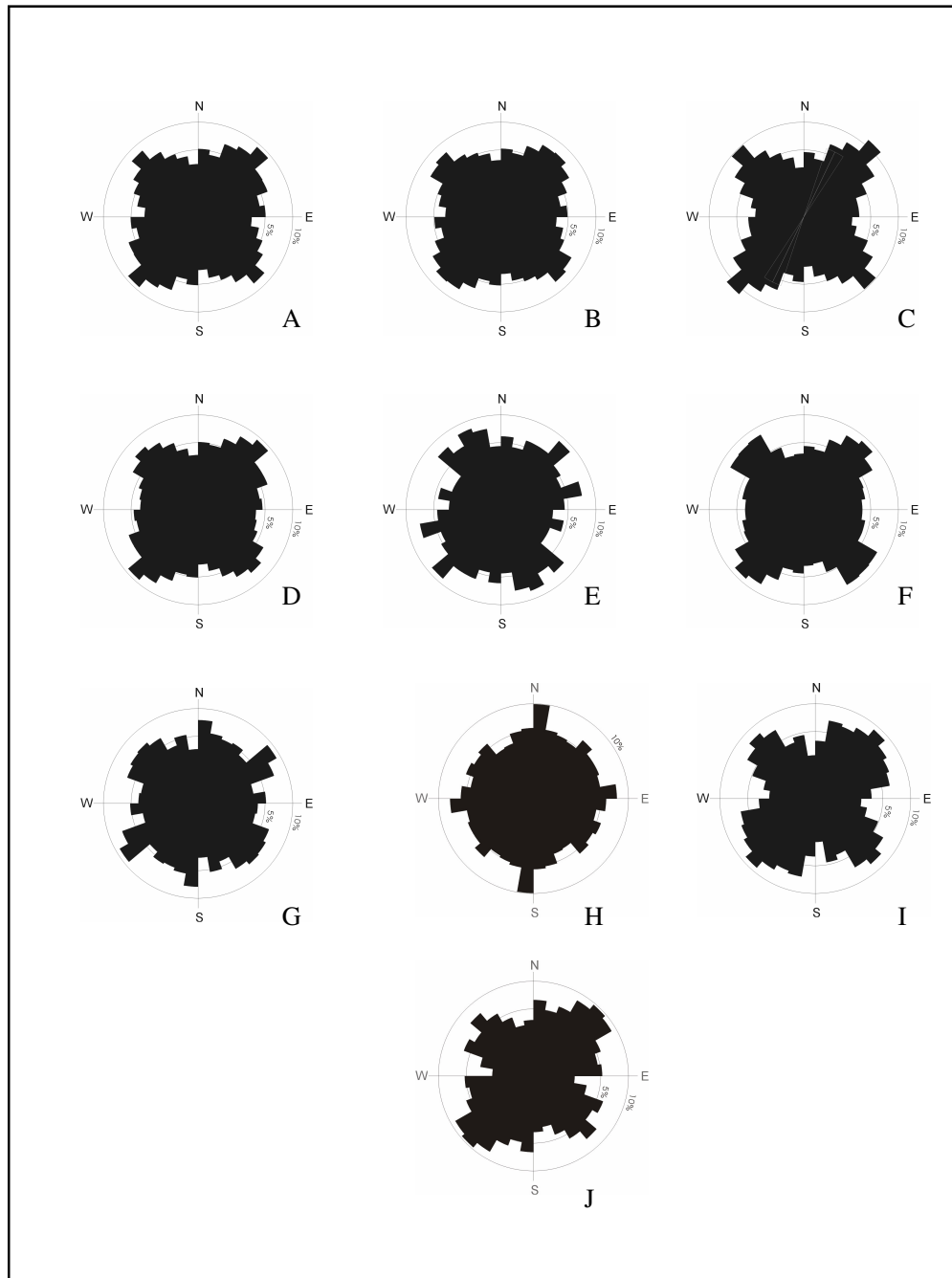


Figure 5-16. Rose diagrams for different extracted lineament maps, visual interpretations, and geological and morpholineament truth maps. All extracted lineament maps were constructed using the optimal pre and post procedures and the best H_t parameter combination ($n=30, k=4$). A: slope gradient 15% threshold, B: shaded relief 2.5% threshold, C: profile curvature map 17.5%, D: slope gradient 50k map 15% threshold, E: slope gradient SRTM map 15% threshold, F: slope gradient regional SRTM map 15% threshold, G: long-lines visual interpretation of slope gradient binary map, H: pre-thinned slope gradient map (5% threshold and $n=20, k=3$), I: regional morpholineament truth map, J: geological truth map.



Figure 5-17. Slope gradient map stretched with histogram equalization into 20 intervals and displayed with a gradual greyscale from white (lower values) to black (higher values). Extracted lineaments from this map result in the most accurate with respect to geological truth map.

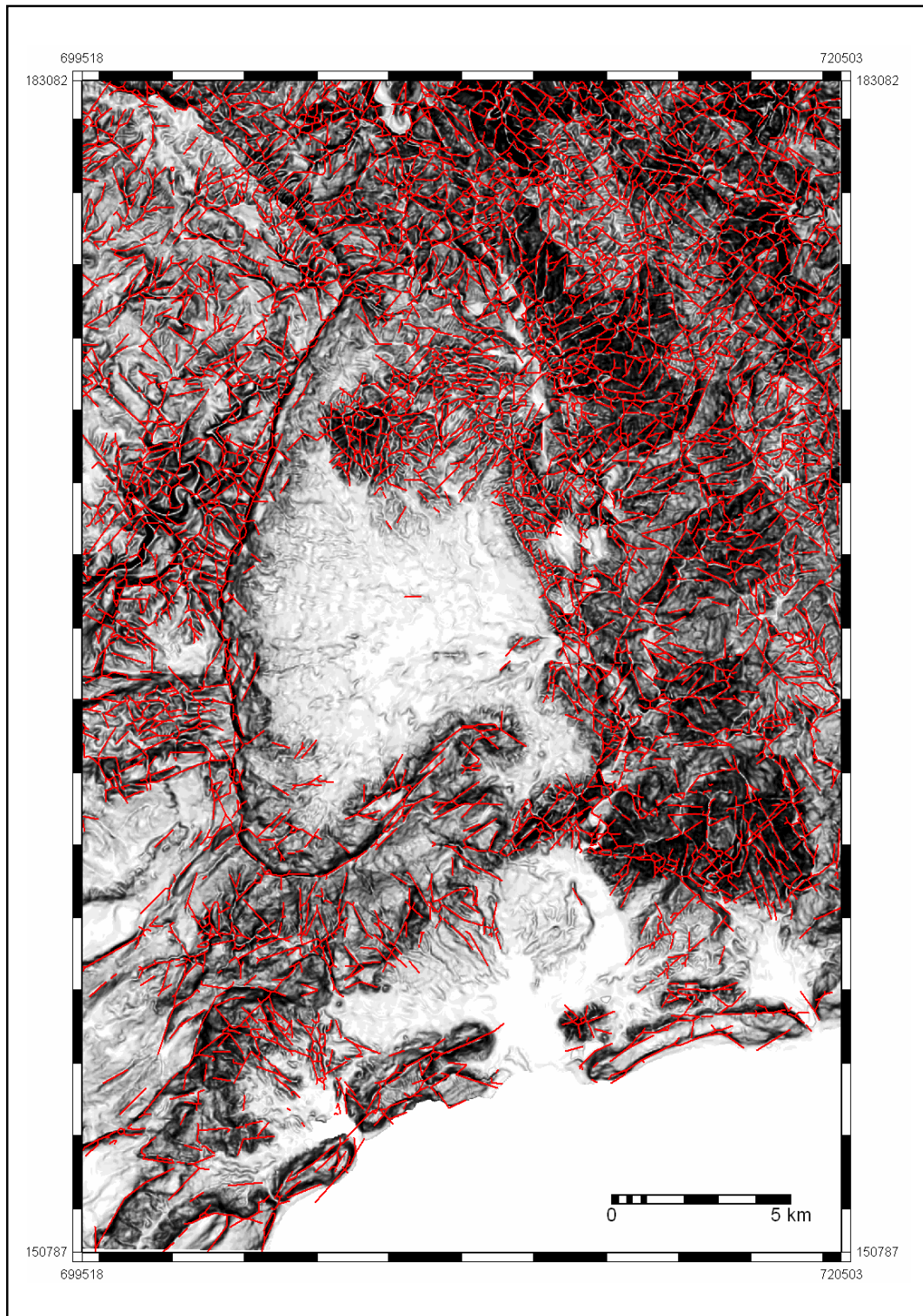


Figure 5-18. Slope gradient map (25k) stretched with histogram equalization into 20 intervals and displayed with a gradual greyscale from white (lower values) to black (higher values). The extracted lineaments with maximum accuracy overlaid the slope gradient map. Lineaments were extracted with threshold value 15% and HT parameters $n=30$ $k=4$.

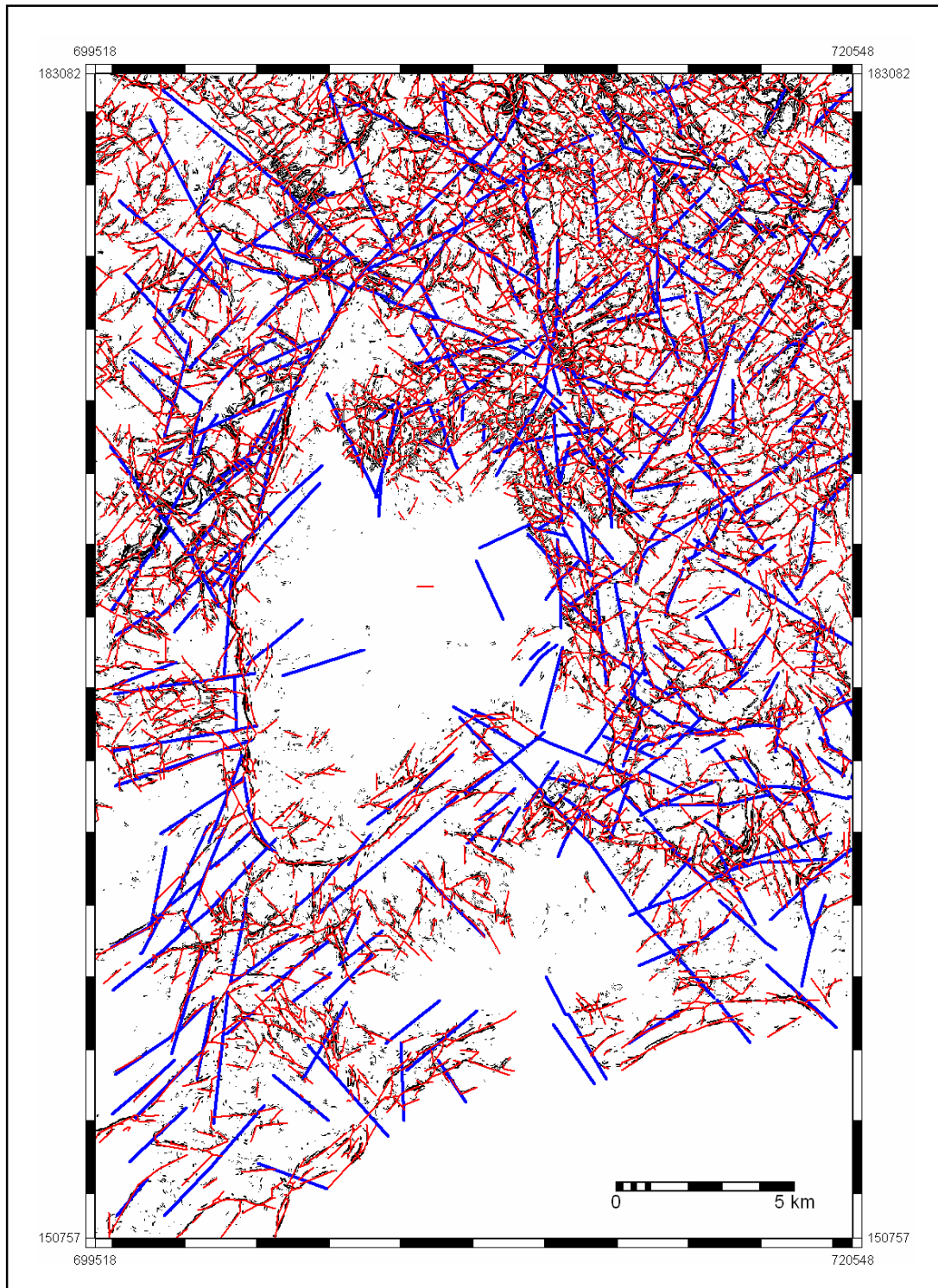


Figure 5-19. Binary slope gradient map (15%) overlain by the most accurate lineament map extracted from this image (in red). The parameters used for the extraction are 15% threshold value and HT parameters combination $n=30$ $k=4$. Geological lineaments and faults (in blue) are also shown.

5.6. Results for DEM's with larger grid sizes

To test if the obtained results at 1:25,000 scale can yield similar results on smaller scale (larger grid size) DEM's, the established procedure was applied to slope gradient maps from 1:50,000 and SRTM elevation data. Validation of results was made with the geological truth in the local study area, and with the morpholineament map for the larger SRTM regional area.

DEM at 1:50,000 scale (50k) was constructed using ANUDEM interpolation method selected in a earlier step. Summary statistics for both 1:50,000 and SRTM DEM's are shown in Figure 5-20. Compared to the 1:25,000 DEM (25k, Figure 5-1) the means, standard deviation and median are very similar for 50k. Since SRTM is not based in the same vertical datum as the contour lines, this shows slightly higher values for all the parameters except standard deviation. The three digital elevation models (25k, 50k and SRTM) show elevation histograms with different shapes; however the cumulative frequency distributions are very similar. Comparison of slope gradient statistics parameters shows that the larger the grid size the lower the maximum, mean, standard deviation and median for slope gradient map. That is expectable because a larger grid size means a higher level of generalization and that implies smoothening of all terrain parameters. The shapes for the slope gradient histograms look very similar for 25k (Figure 5-2) and 50k, but SRTM looks very different (Figure 5-21), leading to a cumulative frequency line without breaks in the curves, as it is possible to see in the other two graphs. Figure 5-22 shows the histograms for elevation and slope gradient for the regional SRTM DEM. That was used to test the extraction methodology at regional scale and also to check if local structural configuration corresponds to a regional trend.

For all these digital elevation models, lineaments were extracted using the established procedure and using the most accurate terrain parameter map (Figures 5-23 and 5-24). That is, slope gradient map enhanced with Sobel operator, threshold value 15%, HT parameters $n=30$ and $k=4$. The stated post-processing procedures differ slightly from the first stage. Because the grid sizes are larger, different parameters for R2V algorithm and length of segments to be cleaned were chosen. In this way the parameters were selected accordingly to the number of pixels established for the first stages times the grid sizes. Therefore, for 50k data the following R2V parameters were applied: maximum thickness as default (10 times pixel size = 350 m), dangle length equals to 140 m (4 times pixel size) and weed tolerance equals to 105 m (3 times pixel size). The segments shorter than 210 m (6 times grid size) were deleted. In the case of SRTM data the values for R2V were 896.67 m (10 times pixel size), 360 m (more or less 4 times grid size) and 270 m (more or less 3 times grid size). Segments shorter than 540 m (6 times pixel size) were deleted. Similar as for 25k the post-processing eliminated many short artefacts but some remain.

For the original study area both, SRTM and 50k lineaments were validated using the geological truth map. The results of accuracy assessment are shown in Table 6 (Appendix 1). With respect to the accuracy obtained for 25k, lineaments from 50k are slightly less accurate while SRTM lineaments are considerably less accurate. That was expected because larger grid sizes give less detailed topographic information than smaller grid sizes.

Rose diagram for 50k (Figure 5-16) shows a very similar shape as 25k, indicating preferential orientations NW-SE and NE-SW. SRTM rose diagram shows slightly different trends than 25k, 50k and geological truth. In SRTM rose diagram can be inferred preferential orientations in NNW-SSE, NE-SW, and ENE-WSW orientations. The regional lineaments extracted from SRTM data shows the two main trends seen at local scale (Figure 5-16). These trends are also shown in the

rose diagram of morpholineament map (Figure 5-16). The accuracies for regional lineaments compared to the latter map is however very low (6%).

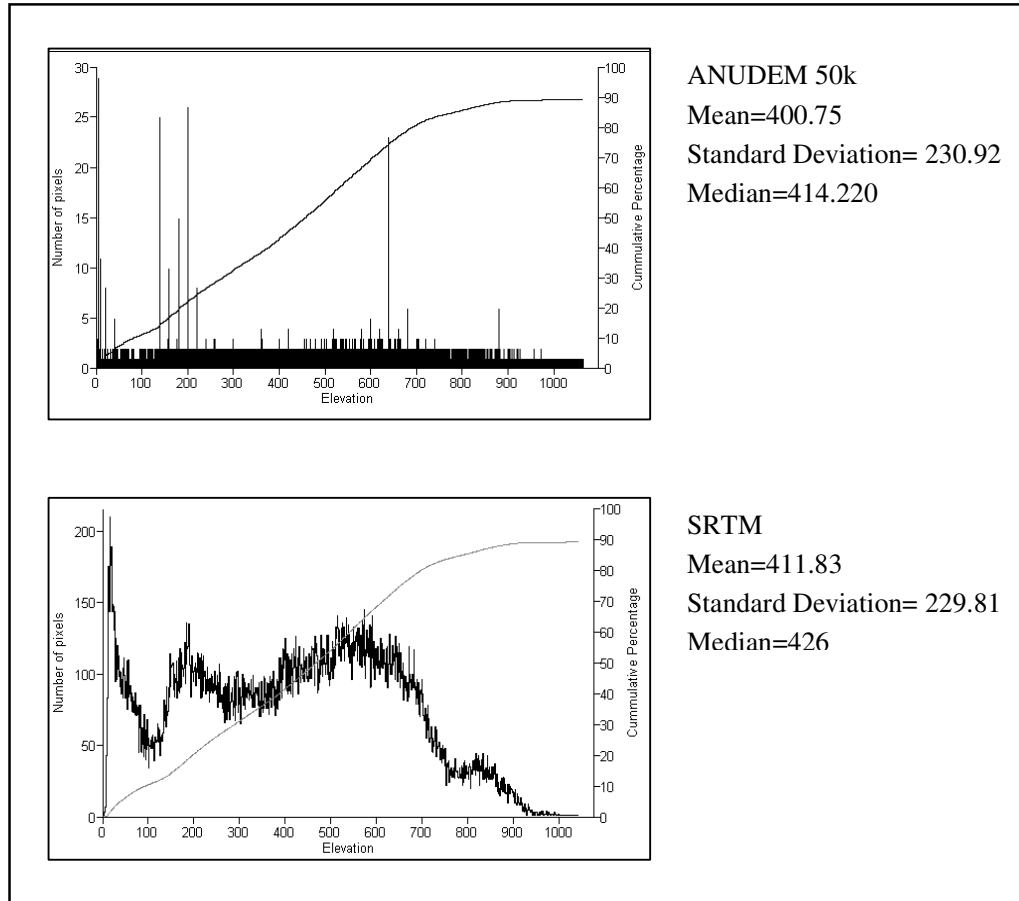


Figure 5-20. Histograms and cumulative frequency distributions (thin black line) of elevation for ANUDEM 50k (top) and SRTM (bottom) DEM's in the study area.

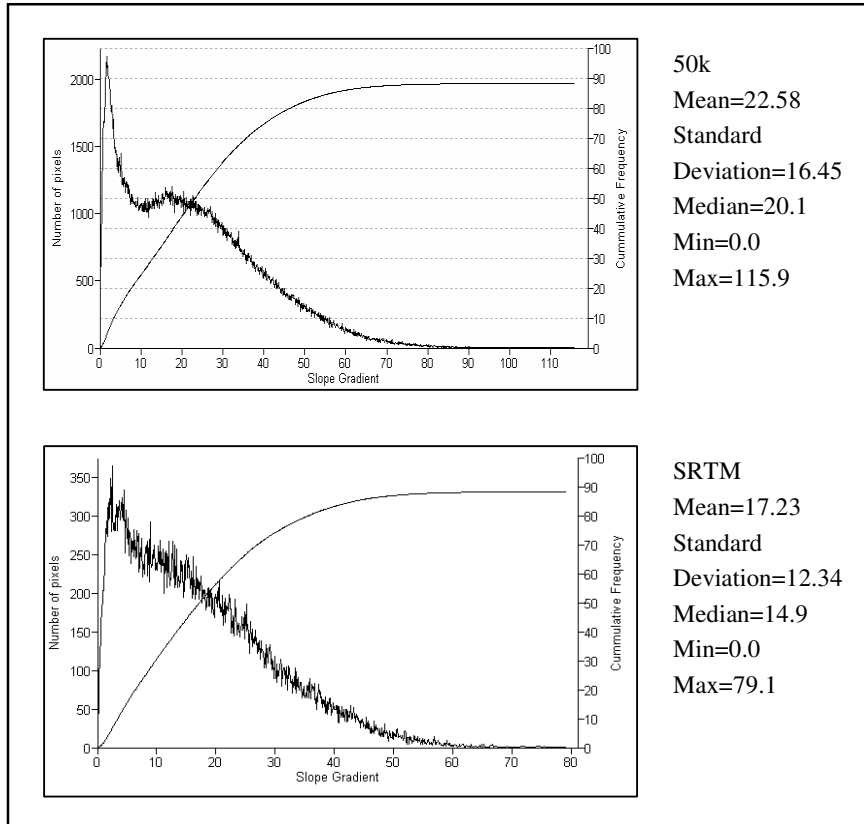


Figure 5-21. Histograms and cumulative frequency distribution (thin black line) of slope gradient for ANUDEM 50k (top) and SRTM (bottom) DEM's.

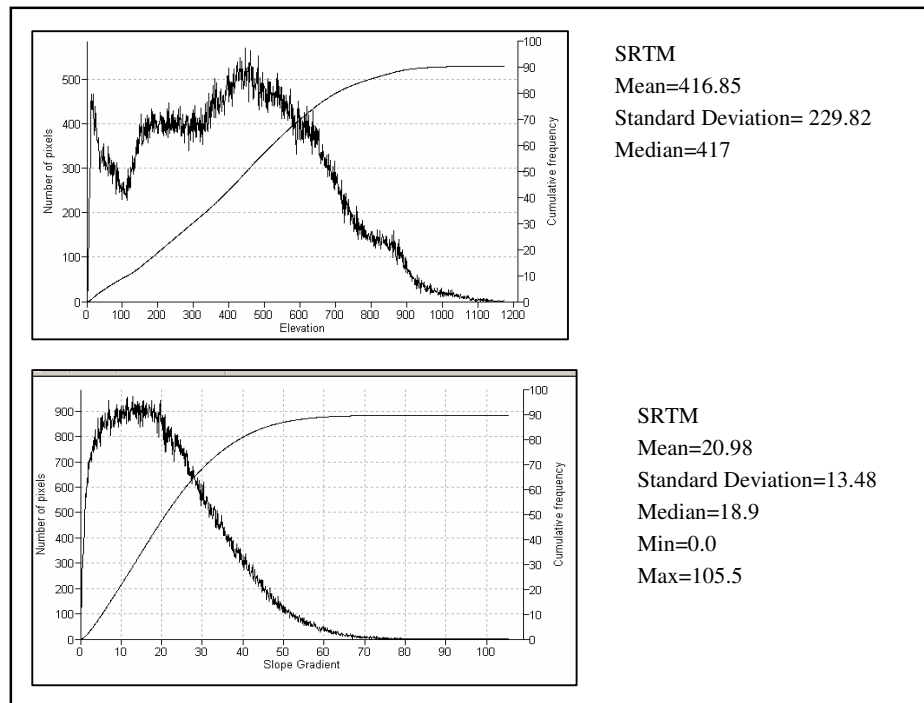


Figure 5-22. Histograms and cumulative frequency distribution (thin black line) of elevation (top) and slope gradient (bottom) for regional SRTM DEM.

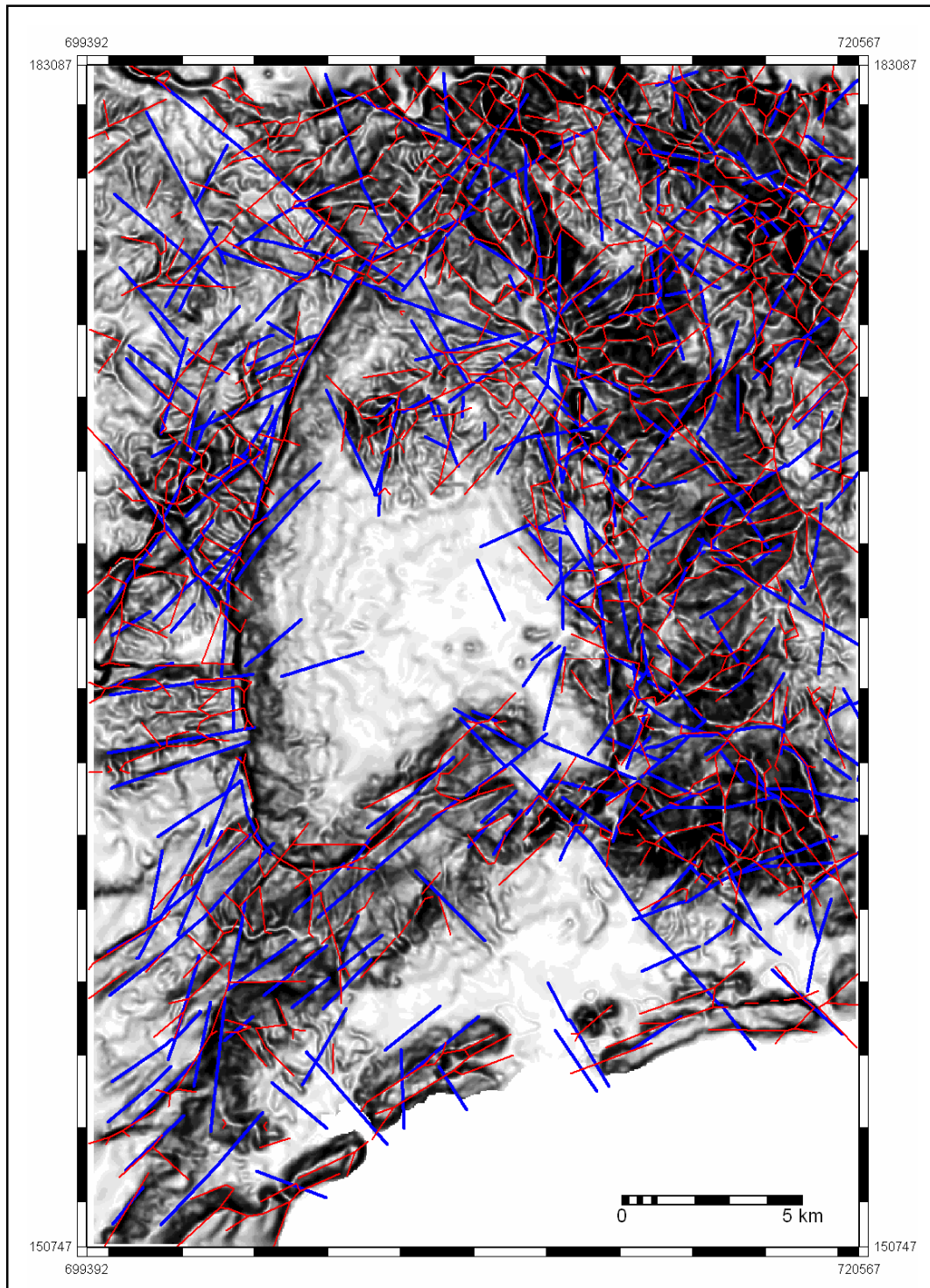


Figure 5-23. Slope gradient map (50k) stretched with histogram equalization into 20 intervals and displayed with a gradual greyscale from white (lower values) to black (higher values). The extracted lineaments with maximum accuracy overlaid the slope gradient map. Lineaments were extracted with threshold value 15% and HT parameters $n=30$ $k=4$. Geological lineaments and faults (in blue) are also shown.

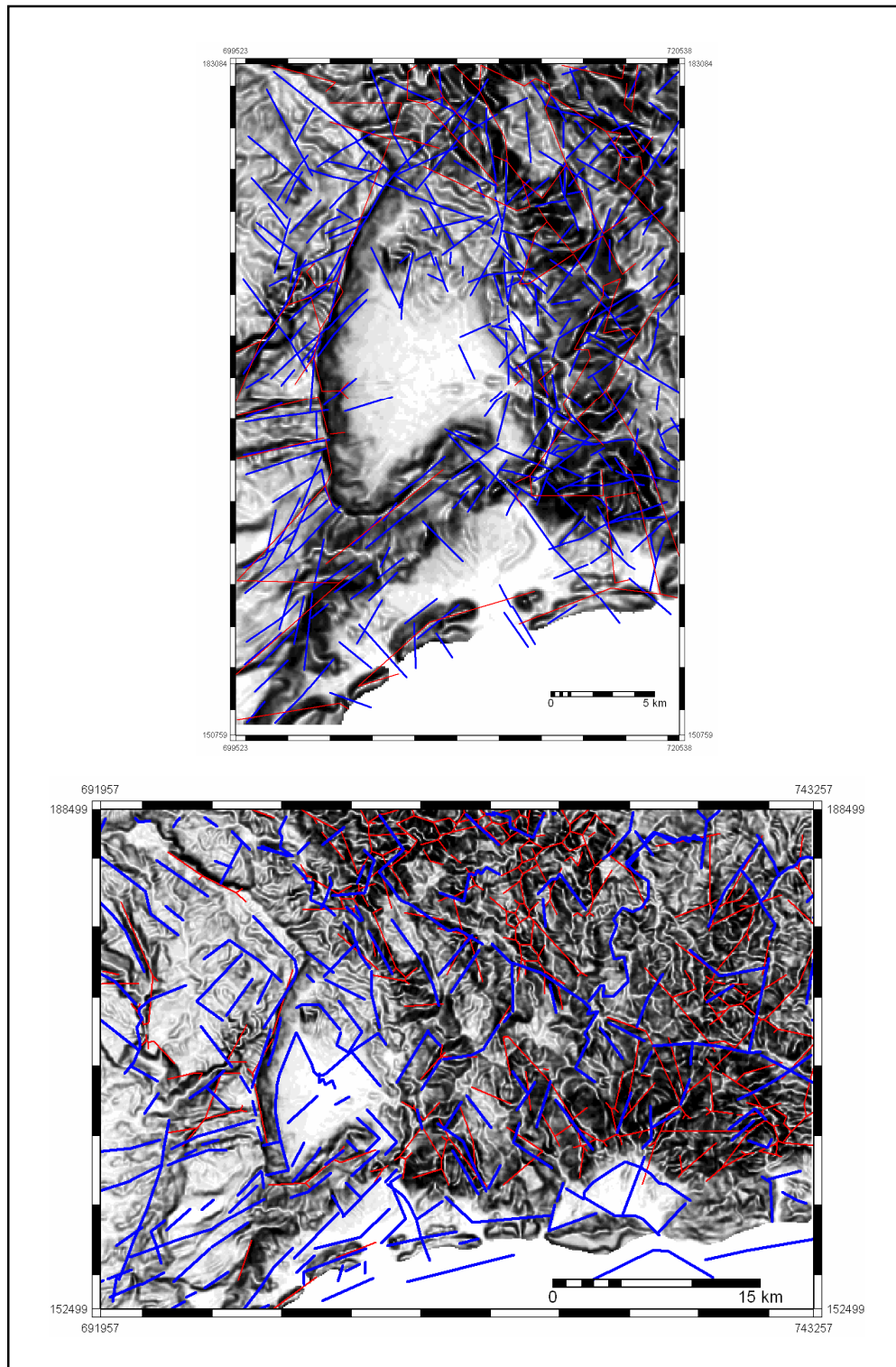


Figure 5-24. Lineaments maps (red lines) from SRTM (top) and regional SRTM (bottom) using the stated optimal procedure. Blue lines correspond to geological and morpholineament truth maps respectively. Slope gradient maps stretched with histogram equalization into 20 intervals and displayed with a gradual greyscale from white (lower values) to black (higher values) are displayed as background.

5.7. Final Discussion

ANUDEM algorithm (as implemented in ArcGIS®) was selected as the interpolation method to create the DEM's used in this research. The selection was based on the fact that this algorithm creates fewer artefacts as compared to the other tested algorithms. However, the DEM's created with ANUDEM look very smooth. This probably affects the extraction of lineaments in zones with low relief, which coincide with the recent deposits in the study area. Results are also affected by the DEM smoothing factor. The highest smoothing level was chosen in the pre-processing steps because it gives more continuous and homogeneous linear areas in the binary maps. The combination of smoother interpolation algorithm and high smoothening value might lead to a high generalization level. This way loss of lineament information, mainly in zones of low relief, is likely. This idea is supported in the fact that few lineaments were extracted in the areas of Caujerí and San Antonio valleys, where recent deposits are found. Despite of this, the established procedure was able to extract some lineaments not observed in the geological map in the latter areas.

A Sobel operator was selected for enhancement of lines in slope gradient map. While Laplace edge enhancement method gives thicker and less linear areas after threshold application, Sobel results in thinner and more linear zones. The latter method however creates some parallel lines that are extracted in the same way by the HT algorithm. Some of these areas were not joined up during the post-processing step. The elimination of these parallel lines can be solved by applying a dilate binary filter before HT application. Alternatively the number of iterations can be increased during the post-processing stage to close those lines. Apparently parallel zones correspond to abrupt changes in slope gradient in higher and bottom parts of the slope area (the *borders* in figure 5-5), while laplacian operator shows the areas between the gradient changes (the slope surface).

Since selection of smoothing value and slope gradient edge enhancement methods were based on visual assessment, it could be interesting to test how sensitive the established extraction method to changes in those parameters is.

The application of HT to binary images results in lineament maps with relatively short and parallel segment lines. The fact that some extracted lines are longer than they appear in the threshold maps is maybe related to the multi-scale method used for lines recognition. The obtained results of extraction using pre-thinned binary images are similar to those obtained by Fitton and Cox (1998) who also used a pre-thinning procedure. The best HT parameters combinations stated by these authors were not able to extract all the lineaments seen in the input binary images but the level of resemblance with these is visually acceptable. However, the pre-thinning procedure used in this study led to creation of artefacts that affect considerably the main orientation trends, and therefore pre-thinning procedure was not used to continue the research.

Post-processing steps allow a good conversion from raster to vector with elimination of some segments and creation of artefacts as side effects. The latter were deleted using a simple SQL expression to eliminate lines shorter than a given length but some remain. Moreover this cleaning step also deletes correctly extracted lines. This is due to the simple length criteria used for the cleaning. More complex GIS methods that take in account the relation of segments with other proximal segments could be developed in order to delete only the artefacts. This method could also be used to join segmented lines into long lineaments according to the distance and angle between them. Alternatively binary operations could be used to delete skeletal legs (Dong, 1997) and other thinning process could be tested in order to get better results.

The validation results show that lineaments extracted from slope gradient map match with higher accuracies the geological map of the study area than shaded relief and profile curvature maps. This result is in contradiction with some studies dealing with visual recognition of linear features from digital terrain models which have stated shaded relief maps as the best performing map (Onorati et al., 1992; Smith and Clark, 2005). Jordan *et al.* (2005) also stated shaded relief as the best base for extraction of linear tectonic features in addition to aspect map, which was not used in this research. The difference of these studies with the current one is that they used a visual interpretation approach for extraction of features while this research made use of a semi-automatic extraction of lineaments. However, shaded relief maps in this study gave accuracies only slightly lower than slope gradient map and can also be recommended as a good map for semi-automatic extraction of lineaments.

The accuracies given by the presented methodology are still too low to be considered successful. One constraint is related to the scarce capacity of lineament extraction in low relief areas. This could be improved in the case of shaded relief images by using vertical exaggeration that leads to zones of lower relief receive more contrast. The methodology is able to extract more lineaments in DTM's obtained from 1:25,000 and 1:50,000 topographic map scales than those seen in the geological map (Figures 5-19 and 5-23). However, it is not possible to state a priori if all these lineaments are false. Post-cleaning step using ancillary data as geological and geomorphologic maps, satellite images, geophysical and seismic data, as well as fieldwork surveys, could lead to define those lineaments truly related to tectonic activity.

While HT lineament extraction can create some false lines and post-processing may introduce some artefacts the whole procedure was able to delineate, in different maps, the main structural trends in the study area. The defined accuracies, however, are relatively low.

6. Conclusions

The following are the main conclusion that can be stated from the results:

- The use of DTM's and the definition of linear features based on terrain parameter values allowed the semi-automatic extraction of lineaments in the study area.
- Procedures to obtain the lineament map can be separated into 4 main stages: DEM construction from topographic contour lines and subsequent calculation of slope gradient, profile curvature and shaded relief maps; pre-processing procedures for lineament enhancement; automatic extraction of lineaments; and post-processing procedures for generalization and cleaning purposes.
- ANUDEM algorithm was selected as the interpolation method to create the DEM's used in this research because it shows fewer artefacts than the other two tested methods.
- The highest value of the selected smoothing method (Evans-Young) was chosen to carry out the study because it produces more continuous and homogeneous linear areas in the binary maps.
- Sobel operator was selected for enhancement of lines in the slope gradient map because it also gives more continuous and linear areas.
- The application of Hough Transform (HT) for extraction of lines results in lineament maps with relatively short and parallel segments. Comparison with visual interpretation of lines in input binary images gives relatively low total accuracies (28%) but the resemblance level is acceptable despite of the amount of created artefacts.
- Post-processing steps allow a good conversion from raster to vector with elimination of some segments and creation of artefacts as side effects. The processing is able to gives vector lines with high level of resemblance with input binary images and HT outputs.
- The results of validation procedure show that lineaments extracted from the slope gradient map resemble the geological map of the study area with higher accuracies than shaded relief and profile curvature maps. According to these results slope gradient map gives the best lineament map with a total accuracy of 16.35%. This was calculated from a 15 m grid size DEM (1:25,000 topographic map, 25k) using the Evans-Young method. Previous to that calculation DEM was smoothed using the method of Evans and Cox and smoothing value equal to 1. Lineaments were enhanced with a Sobel edge operator followed by a binary map construction with the highest 15% values in the cumulative frequency curve of the enhanced map. The best performing HT parameters were $n=30$ and $k=4$. Lines in the output map were generalized using a dilate filter, applied in two steps, and a medial axes extraction processing to get one-pixel thick lines. After conversion from raster to vector using ERDAS[®] *raster to vector* algorithm, lineaments were cleaned eliminating all lines shorter than 90 m.
- The accuracy obtained for lineaments extracted from 35 m grid size DEM (1:50,000 topographic map, 50k) is slightly less accurate (12%) compared to the 15 m grid size DEM (25k). While SRTM (c.a. 90 m grid size) lineament map is considerably less accurate (5.7%). The accuracy for regional SRTM lineaments compared to morpholineament map is also very low (6%).
- Although the rose diagrams for 25k extracted lineaments are not exactly the same as for the geological truth, it is possible to infer three structural trends in the study area: main orientations in

NE-SW and NW-SE, and less clear a minor N-S trending orientation. Rose diagram for 50k shows the same preferential NW-SE and NE-SW orientations while lacking a N-S trend.

- Rose diagram for SRTM shows slightly different trends than 25k, 50k and geological truth. In this rose diagram NNW-SSE, NE-SW, and ENE-WSW preferential orientations can be inferred. Nevertheless regional lineaments extracted from SRTM data show the same two main trends seen at local scale and also shown in the morpholineament rose diagram.
- Despite of the fact that accuracies are relatively low to consider the methodology completely successful; it was able to delineate the main structural trends in the study area.

7. Recommendations

In this chapter some recommendations for further investigations are delineated.

A smoothed topographic surface was used in this research and this probably leads to loss of some features. Lower levels of generalization should be tested in more detail to quantify the loss of information. This can be done choosing lower smoothing values but also using interpolation algorithms that cause less terrain smoothing. One interesting interpolation method to be tested is the triangulated irregular network. Although it requires more specific features addition (digitising of ridges, drainage network and additional spotheights) to get a good result, TIN surfaces represent sudden changes in slope gradient and aspect better than other methods. This could lead to a better automatic extraction of lineaments.

Other hill shading methodologies could be analysed using also different level of vertical exaggeration evaluating in this way the methodology sensitive to these changes. Moreover, a methodology of lineament extraction from aspect map should also be developed as this has been stated as a good terrain derivative for this task. It is also recommended to test the sensitivity of the stated procedure to changes in the algorithm to calculate the terrain parameters.

A sensitivity analysis for pre-processing procedures is recommended, focusing mainly in edge enhancement methods. Alternative thinning and pre-cleaning procedures could be also evaluated to improve the binary image presented to the HT algorithm and avoid doubled lines in the outputs. Post-processing could be also improved by developing a GIS procedure, which eliminates only the artefacts created during the medial axes extraction. In the same way, a procedure could be developed to join up separated segments based on distance and angle deviation in order to create longer lineaments and get less scattered orientation diagrams. Moreover, other circular statistic techniques could be applied to find the different populations in the multimodal lineaments distribution. This will help in the validation step allowing comparison of number of populations and their respective mean orientations.

Further GIS analysis could be implemented in order to assess the extraction accuracy of every true lineament. Through this, one could identify how well a true line was extracted in terms of length, position, and angle. Whether it was extracted with a certain displacement, angle deviation or not extracted at all.

Improvement in the way to select candidate pixels could be done by means of a knowledge-based classification. Factors to take in account would be the terrain parameter values, topographic characteristics of faults, geologic information, earthquakes and springs location, surface roughness and others.

Finally application of the extraction procedure to other study areas is necessary to test the methodology performance in different tectonic settings.

8. References

- Baas, J., 2000. EZ-ROSE: a computer program for equal-area circular histograms and statistical analysis of two dimensional vectorial data. *Computers & Geosciences*, 26: 153-166.
- Batschelet, E., 1981. Circular statistics in Biology. *Mathematics in Biology*. Academic Press Inc. (London) Ltd, London, 371 pp.
- Bergin, T., 1991. A comparison of goodness-of-fit tests for analysis of nest orientation in western Kingbirds. *The Condor*, 93: 164-171.
- Bonnet, N., 2002. An unsupervised generalized Hough transform for natural shapes. *Pattern Recognition*, 35: 1193-1196.
- Burbank, D.W. and Anderson, R.S., 2001. *Tectonic Geomorphology*. Blackwell Sciences, Inc., Malden, 274 pp.
- Burrough, P.A. and McDonnell, R.A., 1998. *Principles of geographical information systems*. Oxford University Press, Oxford, 333 pp.
- Castellanos, E., 2000. Design of a GIS-based system for landslides hazard management San Antonio del Sur, Cuba, case study. Master of Science in Applied Geomorphological Surveys Thesis, International Institute for Aerospace Survey and Earth Sciences (ITC), Enschede, 108 pp.
- Castellanos, E., 2005. Processing SRTM DEM data for national landslide hazard assessment, VI Congreso de Geología, La Habana.
- Chambers, J. and Others, 2006. R.
- Dong, P., 1997. Implementation of mathematical morphological operations for spatial data processing. *Computers & Geosciences*, 23(1): 103-107.
- ESRI, 2004. Arc Gis Desktop Help.
- Evans, I.S., 1980. An integrated system of terrain analysis and slope mapping. *Zeitschrift für Geomorphologie*, 36: 274-295.
- Evans, I.S., 1998. What do terrain statistics really mean? In: S.N. Lane, K.S. Richards and J.H. Chandler (Editors), *Landform monitoring, modelling and analysis*. John Wiley & Sons Ltd.
- Fitton, N.C. and Cox, S.J.D., 1998. Optimising the application of the Hough transform for automatic feature extraction from geoscientific images. *Computers & Geosciences*, 24(10): 933-951.
- Florinsky, I., 1998. Accuracy of local topographic variables derived from digital elevation models. *International Journal of Geographical Information Science*, 12(1): 47-61.
- Florinsky, I.V., 1996. Quantitative topographic method of fault morphology recognition. *Geomorphology*, 16(2): 103-119.
- Ganas, A., Pavlides, S. and Karastathis, V., 2005. DEM-based morphometry of range-front escarpments in Attica, central Greece, and its relation to fault slip rates. *Geomorphology*, 65(3-4): 301-319.
- García, J., Slejko, D., Alvarez, L., Peruzza, L. and Rebez, A., 2003. Seismic hazard maps for Cuba and surroundings areas. *Bulletin of the Seismological Society of America*, 93(6): 2263-2590.
- Giardini, D., 1999. The Global Seismic Hazard Assessment Program (GSHAP) - 1992/1999. *Annali di Geofisica*, 42(6): 957-974.
- Grupo de Atención Integral de la Montaña, , Cuba, 2000, 2000. In: S.N.-C. Baracoa-Puriales (Editor). *Ministerio de Ciencia, Tecnología y Medio Ambiente, La Habana*.
- Heddi, M., Eastaff, D.J. and Petch, J., 1999. Relationships between tectonic and geomorphological linear features in the Guadix-Baza basin, southern Spain. *Earth Surface Processes and Landforms*, 24(10): 931-942.
- Hengl, T., Gruber, S. and Shrestha, D., 2003. *Digital Terrain Analysis in ILWIS, Lectures notes and user guide*. International Institute for Geo-information Science and Earth Observation, Enschede.
- Hengl, T., Gruber, S. and Shrestha, D., 2004. Reduction of errors in digital terrain parameters used in soil-landscape modelling. *International Journal of Applied Earth Observation and Geoinformation*, 5: 97-112.

- Hooper, D.M., Bursik, M.I. and Webb, F.H., 2003. Application of high-resolution, interferometric DEMs to geomorphic studies of fault scarps, Fish Lake Valley, Nevada-California, USA. *Remote Sensing of Environment*, 84(2): 255-267.
- Hough, P.V.C., 1962. A method and means for recognizing complex patterns, U.S.
- ITC, 2001. ILWIS 3.0 Academic User's Guide. International Institute for Aerospace Survey and earth Sciences, Enschede.
- Jamieson, S.S.R., Sinclair, H.D., Kirstein, L.A. and Purves, R.S., 2004. Tectonic forcing of longitudinal valleys in the Himalaya: morphological analysis of the Ladakh Batholith, North India. *Geomorphology*, 58(1-4): 49-65.
- Jordan, G., 2003a. Application of digital terrain modelling and GIS methods for the morphotectonic investigation of the Kali Basin, Hungary. *Zeitschrift für Geomorphologie*, 47(2): 145-169.
- Jordan, G., 2003b. Morphometric analysis and tectonic interpretation of digital terrain data: a case study. *Earth Surface Processes and Landforms*, 28(8): 807-822.
- Jordan, G., Meijninger, B.M.L., Hinsbergen, D.J.J.v., Meulenkamp, J.E. and Dijk, P.M.v., 2005. Extraction of morphotectonic features from DEMs: Development and applications for study areas in Hungary and NW Greece. *International Journal of Applied Earth Observation and Geoinformation*, 7: 163-182.
- Keller, E.A. and Pinter, N., 1996. *Active Tectonics: Earthquakes, Uplift and Landforms*. Prentice Hall, New Jersey.
- Kienzle, S., 2004. The effect of DEM raster resolution on first order, second order and compound terrain derivatives. *Transactions in GIS*, 8(1): 83-111.
- Koike, K., Nagano, S. and Kawaba, K., 1998. Construction and analysis of interpreted fracture planes through combination of satellite-image derived lineaments and digital elevation model data. *Computers & Geosciences*, 24(6): 573-583.
- Korup, O., Schmidt, J. and McSaveney, M.J., 2005. Regional relief characteristics and denudation pattern of the western Southern Alps, New Zealand. *Geomorphology*, 71(3-4): 402-423.
- Leica Geosystems, 2003. ERDAS IMAGINE 8.7 on-line manuals.
- Low, A., 1991. *Introductory computer vision and image processing*. McGraw-Hill International Limited, Berkshire.
- Mayer, L., 1986. *Tectonic Geomorphology of escarpments and Mountain Fronts, Active Tectonics*. National Academy Press, Washington, pp. 125-135.
- Mayer, L., 2000. Application of digital elevation models to macroscale tectonic geomorphology. In: M. Summerfield (Editor), *Geomorphology and Global Tectonics*. John Wiley & Sons Ltd, Chichester, pp. 15 - 28.
- Mitas, L. and Mitasova, H., 1999. Spatial Interpolation. In: P. Longley, M.F. Goodchild, D.J. Maguire and D.W. Rhind (Editors), *Geographical Information Systems: Principles, Techniques, Management and Applications*. Wiley, pp. 481-492.
- Moore, I.D., Grayson, F. and Ladson, R., 1994. Digital terrain modelling: a review of hydrological, geomorphological and biological applications. In: K.J. Beven and I.D. Moore (Editors), *Terrain analysis and distributed modelling in hydrology. Advances in hydrological processes*. Wiley & Sons, Chichester, pp. 7 - 34.
- Muir-Wood, R., 1993. From global sismotectonics to global seismic hazard. *Annali di Geofisica*, XXXVI(3-4): 153-168.
- Murphy, W., 1993. Remote sensing of active faults: case studies from southern Italy. *Zeitschrift für Geomorphologie*, 94: 1-23.
- Núñez, K., 2000. *Geology and structural characteristics of the San Antonio del Sur area, Cuba, using data integration techniques*. Master of Science in Geology Thesis, International Institute for Aerospace Survey and Earth Sciences (ITC), Enschede, 73 pp.
- Oguchi, T., Aoki, T. and Matsuta, N., 2003. Identification of an active fault in the Japanese Alps from DEM-based hill shading. *Computers & Geosciences*, 29(7): 885-891.
- Ollier, C.D., 1981. *Tectonics and landforms. Geomorphology texts*, 6. Longman Group Limited, New York, 324 pp.

- Onorati, G., Ventura, R., Poscolieri, M., Chiarini, V. and Crucilla, U., 1992. The Digital Elevation Model of Italy for geomorphology and structural geology. *CATENA*, 19(2): 147-178.
- Panizza, M., Castaldini, D., Bollettinari, G., Carton, A. and Mantovani, F., 1987. Neotectonic research in applied geomorphological studies. *Zeitschrift für Geomorphologie*, 63: 173-211.
- Rabus, B., Eineder, M., Roth, A. and Bamler, R., 2003. The shuttle radar topography mission - a new class of digital elevation models acquired by spaceborne radar. *ISPRS Journal of Photogrammetry and Remote Sensing*, 57: 241-262.
- Ramsay, J. and Huber, M., 1987. The techniques of modern structural geology. Volume 2: folds and fractures. Academic Press Limited, London.
- Research Systems, Inc., 2005. IDL Online Help.
- Riley, C. and Moore, J.M., 1993. Digital elevation modelling in a study of the neotectonic geomorphology of the Sierra Nevada, southern Spain. *Zeitschrift für Geomorphologie*, 94: 25-39.
- Rojas-Agramonte, Y. et al., 2005. Variation of palaeostress patterns along the Oriente transform wrench corridor, Cuba: significance for Neogene-Quaternary tectonics of the Caribbean realm. *Tectonophysics*, 396(3-4): 161-180.
- Russ, J., 1999. The image processing handbook. CRC Press LLC and Springer-Verlag GmbH & Co. KG, Boca Raton, 771 pp.
- Shary, P.A., Sharaya, L.S. and Mitusov, A.V., 2002. Fundamental quantitative methods of land surface analysis. *Geoderma*, 107: 1-32.
- Skidmore, A., 1989. A comparison of techniques for calculating gradient and aspect from a gridded digital elevation model. *International Journal of Geographical Information Systems*, 3(4): 323-334.
- Slemmons, D.B. and Depolo, C.M., 1986. Evaluation of active faulting and associated hazards, Active Tectonics. Studies in geophysics. National Academy Press, Washington, pp. 45-62.
- Smith, M.J. and Clark, C.D., 2005. Methods for the visualization of digital elevation models for landform mapping. *Earth Surface Processes and Landforms*, 30(7): 885-900.
- Szynkaruk, E., Graduno-Monroy, V.H. and Bocco, G., 2004. Active fault systems and tectono-topographic configuration of the central Trans-Mexican Volcanic Belt. *Geomorphology*, 61(1-2): 111-126.
- Tchalenko, J.S., 1970. Similarities between shear zones of different magnitudes. *Geological Society of America Bulletin*, 81: 1625-1640.
- Tropical, I.d.G., 1994. Mapa de Morfolineamentos, La Habana.
- van der Werff, H.M.A., Bakker, W.H., van der Meer, F.D. and Siderius, W., Combining spectral signals and spatial patterns using multiple Hough transforms: An application for detection of natural gas seepages. *Computers & Geosciences*, In Press, Corrected Proof.
- Wang, J. and Howarth, P.J., 1990. Use of the Hough transform in automated lineament detection. *IEEE Transactions on Geoscience and Remote Sensing*, 28(4): 561-566.
- Wise, S., 1998. The effect of GIS Interpolation errors on the use of digital elevation models in geomorphology. In: S.N. Lane, K.S. Richards and J.H. Chandler (Editors), *Landform Monitoring, Modelling and Analysis*. British Geomorphological Research Group Symposia. John Wiley & Sons Ltd, Chichester, pp. 139-164.
- Wise, S., 2000. Assessing the quality for hydrological applications of digital elevation models derived from contours. *Hydrological Processes*, 14(11-12): 1909-1929.
- Woldai, T., 1995. Lithologic and structural mapping in a vegetated low - relief terrain using multiple - source remotely sensed data: a case study of the Calanas area in southwest Spain. *ITC Journal*, 1995(2): 95 - 114.
- Wood, J., 1996. The Geomorphological Characterization of Digital Elevation Models. PhD Thesis, University of Leicester.
- Zazula, J., 2005. Find Polyline Angle, pp. Visual Basic Language for ArcGIS Dektop.

9. Appendices

9.1. Appendix 1: Tables

Table 1. Number of isolated pixels in two different maps. An increasing of smoothing values leads to less noisy maps.

Map	Smoothing value	Isolated Candidate Pixels
Slope 5% Threshold	0	2927
	0.5	2343
	1	1806
Profile Curvature 5% Threshold	0	1937
	0.5	1457
	1	1140

Table 2. Total, position and length accuracy for lineaments extracted from slope gradient binary map (5% threshold value) compared to long visual interpreted lines.

HT parameters combination	Total Accuracy $\sqrt{LA * PA}$	Position Accuracy (PA) [CE / AE]	Length Accuracy (LA) [CE / TL]	Number of Lines	Length All extracted Lines [AE]	Length corrected Extracted Lines [CE]
15_0	17.40	9.06	33.43	9322	1967788	178193
15_1	20.34	11.45	36.15	7483	1683591	192692
15_2	20.15	11.50	35.33	7204	1638183	188341
15_3	21.58	12.48	37.34	6882	1595441	199042
15_4	21.52	12.59	36.79	6649	1558069	196139
20_0	20.00	11.35	35.26	7611	1656390	187932
20_1	23.11	14.45	36.95	5771	1362572	196942
20_2	23.71	15.25	36.86	5340	1288114	196483
20_3	23.56	15.56	35.68	4910	1222866	190219
20_4	23.42	15.57	35.23	4832	1206115	187815
25_0	21.21	12.96	34.73	6393	1428941	185120
25_1	24.23	17.03	34.46	4354	1078606	183713
25_2	24.88	18.25	33.93	3862	991282	180892
25_3	26.53	19.88	35.39	3583	948857	188658
25_4	25.70	19.49	33.89	3518	926745	180638
30_0	22.39	15.10	33.19	5248	1171763	176935
30_1	25.51	20.46	31.81	3265	828983	169587
30_2	26.09	22.05	30.86	2648	745941	164488
30_3	27.36	23.56	31.76	2535	718510	169308
30_4	27.59	24.40	31.19	2340	681450	166280
35_0	23.97	17.75	32.37	4302	972084	172530
35_1	26.45	24.22	28.89	2296	635808	153998
35_2	25.76	25.29	26.24	1857	553182	139875
35_3	26.50	27.26	25.76	1631	503796	137340
35_4	26.77	28.15	25.47	1548	482282	135749
Visual Interpretation				429	533059	

Table 3. Total, position and length accuracy for lineaments extracted from slope gradient binary map (5% threshold value) compared to short-detailed visual interpreted lines.

HT parameters combination	Total Accuracy	Position Accuracy (PA)	Length Accuracy (LA)	Number of Lines	Length All extracted Lines	Length corrected Extracted Lines
	$\sqrt{LA * PA}$	[CE / AE]	[CE / TL]		[AE]	[CE]
15_0	27.39	17.01	44.12	9322	1967788	334635
15_1	34.52	23.17	51.42	7483	1683591	390032
15_2	35.83	24.38	52.65	7204	1638183	399364
15_3	35.91	24.76	52.08	6882	1595441	395033
15_4	36.07	25.17	51.70	6649	1558069	392134
20_0	32.70	22.13	48.32	7611	1656390	366490
20_1	40.91	30.52	54.83	5771	1362572	415890
20_2	43.00	33.00	56.04	5340	1288114	425048
20_3	41.98	33.06	53.31	4910	1222866	404321
20_4	42.24	33.50	53.26	4832	1206115	404002
25_0	37.88	27.60	51.99	6393	1428941	394334
25_1	44.73	37.51	53.34	4354	1078606	404565
25_2	45.34	39.66	51.83	3862	991282	393126
25_3	46.18	41.29	51.65	3583	948857	391743
25_4	45.24	40.93	50.01	3518	926745	379285
30_0	40.77	32.80	50.67	5248	1171763	384322
30_1	45.45	43.48	47.52	3265	828983	360421
30_2	46.75	47.14	46.36	2648	745941	351665
30_3	45.94	47.20	44.71	2535	718510	339152
30_4	45.87	48.39	43.48	2340	681450	329771
35_0	43.52	38.44	49.26	4302	972084	373655
35_1	45.66	49.87	41.80	2296	635808	317073
35_2	43.13	50.51	36.84	1857	553182	279405
35_3	41.89	51.40	34.14	1631	503796	258962
35_4	40.97	51.38	32.67	1548	482282	247792
Visual Interpretation				1495	758483	

Table 4. Total, position and length accuracy for pre-thinned slope gradient map 5% threshold value compared to long visual interpreted lines.

HT parameters combination	Total Accuracy	Position Accuracy (PA)	Length Accuracy (LA)	Number of Lines	Length All extracted Lines	Length corrected Extracted Lines
	$\sqrt{LA * PA}$	[CE / AE]	[CE / TL]		[AE]	[CE]
15_0	19.97	12.71	31.36	5175	1315184	167182
15_1	23.37	16.82	32.47	3566	1029131	173073
15_2	23.44	17.23	31.89	3227	986271	169981
15_3	24.61	18.42	32.88	3020	951503	175290
15_4	24.94	19.23	32.34	2663	896442	172397
20_0	22.13	16.22	30.19	3031	992184	160921
20_1	24.84	21.78	28.33	1747	693135	150999.01
20_2	24.30	22.56	26.17	1439	618512	139514
20_3	25.07	25.26	24.88	1154	525033	132623.09
20_4	24.99	25.46	24.52	1109	513274	130692
25_0	22.53	18.95	26.79	2248	753401	142802
25_1	23.37	27.78	19.66	883	377280	104814
25_2	21.78	28.94	16.39	1439	302002	87390
25_3	21.65	32.64	14.36	495	234516	76546
25_4	21.47	33.31	13.83	474	221318	73729
30_0	22.76	23.79	21.77	396	487864	116042
30_1	19.67	34.58	11.19	396	172446	59637
30_2	19.18	43.14	8.52	221	105307	45434
30_3	16.44	40.18	6.72	182	89199	35842
30_4	14.67	40.90	5.26	141	68618	28065
35_0	18.91	25.33	14.12	908	297203	75273
35_1	13.65	37.45	4.98	163	70867	26537
35_2	12.16	42.22	3.50	93	44235	18676
35_3	11.03	50.40	2.41	54	25509	12856
35_4	10.83	52.54	2.23	49	22655	11902
Visual Interpretation				429	533059	

Table 5. Total, position and length accuracy for slope gradient map, shaded relief and profile curvature lineament maps using the best HT parameter combination $n=30$ $k=4$ and different threshold values. Accuracies for visual interpretation of binary maps (5% threshold) are also shown.

Map	Threshold Value	Total Accuracy	Position Accuracy (PA)	Length Accuracy (LA)	Number of Lines	Length All Extracted Lineaments	Length Correctly Extracted Lineaments
		$\sqrt{LA * PA}$	[CE/ AE]	[CE / LT]		[AE]	[CE]
Slope Gradient	2.5%	12.59	17.02	9.32	950	321340	54679
	5.0%	14.02	13.02	15.11	2340	681450	88699
	7.5%	15.78	12.04	20.68	3862	1007999	121372
	10.0%	15.67	10.48	23.42	5299	1311371	137495
	12.5%	15.84	9.63	26.04	6815	1586153	152816
	15.0%	16.35	9.41	28.41	7958	1771966	166773
	17.5%	15.21	8.40	27.53	8635	1923668	161593
	20.0%	14.73	7.88	27.53	9293	2049661	161579
	22.5%	13.96	7.42	26.26	9379	2077604	154119
	25.0%	12.87	6.76	24.52	9554	2128928	143914
Shaded Relief	0.5%	10.82	11.72	9.98	1486	499766	58576
	1.0%	13.11	10.53	16.33	3299	910218	95822
	1.5%	14.15	9.70	20.64	5029	1249357	121131
	2.0%	14.02	8.71	22.56	6355	1520448	132432
	2.5%	14.77	8.67	25.16	7418	1702622	147667
	3.0%	14.66	8.26	26.01	8223	1847424	152674
	3.5%	13.37	7.31	24.46	8854	1965160	143595
	4.0%	13.25	7.20	24.38	8935	1988179	143085
	4.5%	14.30	7.73	26.44	9020	2007838	155209
	5.0%	13.36	7.33	24.37	8494	1951987	143043
Profile Curvature	2.5%	7.27	10.24	5.17	747	296169	30331
	5.0%	9.57	8.81	10.40	2280	692569	61029
	7.5%	10.94	8.35	14.33	3769	1008093	84132
	10.0%	10.45	7.05	15.50	5204	1290826	90966
	12.5%	11.04	6.76	18.02	6563	1563919	105768
	15.0%	11.14	6.42	19.32	7684	1765826	113396
	17.5%	12.05	6.61	21.99	8687	1952679	129050
	20.0%	10.88	5.87	20.15	9019	2014681	118286
	22.5%	11.32	5.98	21.42	9402	2101316	125721
	25.0%	11.07	5.87	20.86	9307	2084714	122429
Detailed Visual Interpretation	5%	12.68	13.29	12.07	429	533059	185972
Long-lines Visual Interpretation	5%	16.50	16.57	16.42	443	581457	221294
Geological Truth					748	586961	

Table 6. Total, position and length accuracy for slope gradient map from 50k, SRTM and regional SRTM using the HT parameter combination $n=30$ $k=4$ and the optimal threshold value 15%. Accuracy values in relation to geological truth and morpholineaments maps.

Map	Total Accuracy	Position Accuracy (PA)	Length Accuracy (LA)	Number of Lines	Length All Extracted Lineaments	Length Correctly Extracted Lineaments
	$\sqrt{LA * PA}$	[CE/ AE]	[CE / LT]		[AE]	[CE]
Slope Gradient 50k	12.12	10.52	13.96	1477	778910	81958
Slope Gradient SRTM	5.75	8.80	3.76	134	250743	22062
Geological Truth	-	-	-	748	586961	-
Slope Gradient SRTM regional	5.97533	5.53	6.46	602	829144	45836
Morpholineaments	-	-	-	432	709660	-

Table 7. Rao's Test for extracted lineament maps, geological and morpholineaments truth maps.

Map	Test Statistic	Level 0.01 critical value	null hypothesis of uniformity
Slope Gradient 25k	351.8573	138.84	Reject
Slope Gradient thinned 25k	320.442	138.84	Reject
Profile curvature 25k	352.5406	138.84	Reject
Shaded relief 25k	351.2645	138.84	Reject
Slope Gradient 50k	316.371	138.84	Reject
Slope Gradient SRTM	208.5224	148.84	Reject
Slope Gradient SRTM regional	252.2093	138.84	Reject
Geological truth	281.0695	140.09	Reject
Morpholineaments	230.8333	142.54	Reject

9.2. Appendix 2: Scripts

9.2.1. Evans and Young method for terrain derivative calculation

```
Script Name: Evans_Young.isl
//script by T. Hengl (last modified: Apr/2003)
//Modified by M. Arenas (last modified: Jan/2006)
//input maps: %1.mpr. - DEM, %2 - smoothing parameter s[0,1]
//all filters in 3x3 window environment
//Evans-Young method formulas, explained in detail by Shary et al. (2002)

//smooth the DEM before extracting derivatives

DEM_s.mpr{ dom=value.dom;vr=0.00:5000.00:0.01 }=%2*(%1#[1]+%1#[2]+%1#[3]+%1#[4]+%1#[6]
+%1#[7]+%1#[8]+%1#[9])/9+(1-8*%2/9)*%1#[5]
calc DEM_s.mpr

dx.mpr{ dom=value.dom;vr=-500.0000:500.0000:0.0001 }=( DEM_s#[3]+ DEM_s#[6]+ DEM_s#[9]-
DEM_s#[1]- DEM_s#[4]- DEM_s#[7])/(6*pixsize( DEM_s))

dy.mpr{ dom=value.dom;vr=-500.0000:500.0000:0.0001 }=( DEM_s#[1]+ DEM_s#[2]+ DEM_s#[3]-
DEM_s#[7]- DEM_s#[8]- DEM_s#[9])/(6*pixsize( DEM_s))

//derive second-order derivates and smooth them to get a more generalized picture

d2x_tmp.mpr{ dom=value.dom;vr=-
50.00000:50.00000:0.00001 }=(DEM_s#[1]+DEM_s#[3]+DEM_s#[4]+DEM_s#[6]+DEM_s#[7]+DE
M_s#[9]-2*(DEM_s#[2]+DEM_s#[5]+DEM_s#[8]))/(3*pixsize(DEM_s)^2)

d2x=MapFilter(d2x_tmp, avg3x3)

d2y_tmp.mpr{ dom=value.dom;vr=-
50.00000:50.00000:0.00001 }=(DEM_s#[1]+DEM_s#[2]+DEM_s#[3]+DEM_s#[7]+DEM_s#[8]+DE
M_s#[9]-2*(DEM_s#[4]+DEM_s#[5]+DEM_s#[6]))/(3*pixsize(DEM_s)^2)

d2y=MapFilter(d2y_tmp, avg3x3)

dxy_tmp.mpr{ dom=value.dom;vr=-50.00000:50.00000:0.00001 }=(DEM_s#[3]-DEM_s#[7]-
DEM_s#[1]+DEM_s#[9])/(4*pixsize(DEM_s)^2)

dxy=MapFilter(dxy_tmp, avg3x3)

//slope gradient
```

```
SL_%2.mpr{ dom=value.dom;vr=0.0:5000.0:0.1 }:=100*sqrt(dx^2+dy^2)

//aspect map 0-360

ASP_%2.mpr{ dom=value.dom;vr=0:360:1 }=raddeg(atan2(dx,dy)+pi)

//plan, profile and mean curvatures
//curvature values are multiplied by 100 for easier interpretation (radians/100 m)

PLANC_%2.mpr{ dom=value.dom;vr=-50.000:50.000:0.001 }:=-(dy^2*d2x-
2*dx*dy*dxy+dx^2*d2y)/((dx^2+dy^2)*(1+dx^2+dy^2)^0.5)*100

PROFC_%2.mpr{ dom=value.dom;vr=-50.000:50.000:0.001 }:=-(
(dx^2*d2x+2*dx*dy*dxy+dy^2*d2y)/((dx^2+dy^2)*(1+dx^2+dy^2)^1.5)*100

//MEANC.mpr{ dom=value.dom;vr=-50.000:50.000:0.001 }:=-(1+dy^2)*d2x-
2*dx*dy*dxy+(1+dx^2)*d2y)/(2*(1+dx^2+dy^2)^1.5)*100

calc SL_%2.mpr
calc ASP_%2.mpr
calc PLANC_%2.mpr
calc PROFC_%2.mpr

//set description

setdescr SL_%2.mpr Slope in %
setdescr ASP_%2.mpr Aspect (0,360)
setdescr PLANC_%2.mpr Horizontal or plan curvature in 100rad/m
setdescr PROFC_%2.mpr Vertical or profile curvature in 100rad/m

//delete all temporary files

del ?????_tmp.mpr -force
del d??_tmp.mpr -force
del dxy.mpr -force
del d?.mpr -force
del d2?.mpr -force
del DEM_s.mpr -force
```

9.2.2. Method for construction of shaded relief binary maps for lineament extraction

Script Name: Shadow_Process.isl

//script by M. Arenas (last modified: Nov/2005)

//Processing for extraction of lineaments from shaded relief maps illuminated from 8 direction and using gradient filters perpendicular to each direction illumination.

//Parameters: %1: smoothed DEM, %2: threshold value for binary map creation

//Shadow and perpendicular derivative from North illumination

shN.mpr{ dom=value;vr=-1000000.0:1000000.0:0.1 } := MapFilter(%1,ShadowN)

calc shN.mpr

shdN.mpr{ dom=value;vr=-1000000.0:1000000.0:0.1 } := MapFilter(shN,DFDY)

calc shdN.mpr

//Shadow and perpendicular derivative from South illumination

shS.mpr{ dom=value;vr=-1000000.0:1000000.0:0.1 } := MapFilter(%1,ShadowS)

calc shS.mpr

shdS.mpr{ dom=value;vr=-1000000.0:1000000.0:0.1 } := MapFilter(shS,DFDY)

calc shdS.mpr

//Shadow and perpendicular derivative from West illumination

shW.mpr{ dom=value;vr=-1000000.0:1000000.0:0.1 } := MapFilter(%1,ShadowW)

calc shW.mpr

shdW.mpr{ dom=value;vr=-1000000.0:1000000.0:0.1 } := MapFilter(shW,DFDX)

calc shdW.mpr

//Shadow and perpendicular derivative from East illumination

shE.mpr{ dom=value;vr=-1000000.0:1000000.0:0.1 } := MapFilter(%1,ShadowE)

calc shE.mpr

shdE.mpr{ dom=value;vr=-1000000.0:1000000.0:0.1 } := MapFilter(shE,DFDX)

calc shdE.mpr

//Shadow and perpendicular derivative from North-East illumination

shNE.mpr{ dom=value;vr=-1000000.0:1000000.0:0.1 } := MapFilter(%1,ShadowNE)

calc shNE.mpr

shdNE.mpr{ dom=value;vr=-1000000.0:1000000.0:0.1 } := MapFilter(shNE,DFDUP)

calc shdNE.mpr

//Shadow and perpendicular derivative from South-West illumination

```
shSW.mpr{ dom=value;vr=-1000000.0:1000000.0:0.1 } := MapFilter(%1,ShadowSW)
calc shSW.mpr
shdSW.mpr{ dom=value;vr=-1000000.0:1000000.0:0.1 } := MapFilter(shSW,DFDUP)
calc shdSW.mpr

//Shadow and perpendicular derivative from North-West illumination

shNW.mpr{ dom=value;vr=-1000000.0:1000000.0:0.1 } := MapFilter(%1,SHADOW)
calc shNW.mpr
shdNW.mpr{ dom=value;vr=-1000000.0:1000000.0:0.1 } := MapFilter(shNW,DFDDN)
calc shdNW.mpr

//Shadow and perpendicular derivative from South-East illumination

shSE.mpr{ dom=value;vr=-1000000.0:1000000.0:0.1 } := MapFilter(%1,ShadowSE)
calc shSE.mpr
shdSE.mpr{ dom=value;vr=-1000000.0:1000000.0:0.1 } := MapFilter(shSE,DFDDN)
calc shdSE.mpr

//Thresholding maps using %2 value

run ThreShadow.isl shdN %2
run ThreShadow.isl shdS %2
run ThreShadow.isl shdNE %2
run ThreShadow.isl shdNW %2
run ThreShadow.isl shdE %2
run ThreShadow.isl shdW %2
run ThreShadow.isl shdSE %2
run ThreShadow.isl shdSW %2

calc TshdN.mpr
calc TshdS.mpr
calc TshdW.mpr
calc TshdE.mpr
calc TshdNW.mpr
calc TshdNE.mpr
calc TshdSW.mpr
calc TshdSE.mpr

//Eliminate undefined values (ocean)

N.mpr:=IFUNDEF(TshdN,0)
calc N.mpr
S.mpr:=IFUNDEF(TshdS,0)
```

```
calc S.mpr
W.mpr:=IFUNDEF(TshdW,0)
calc W.mpr
E.mpr:=IFUNDEF(TshdE,0)
calc E.mpr
NES.mpr:=IFUNDEF(TshdNE,0)
calc NE.mpr
NW.mpr:=IFUNDEF(TshdNW,0)
calc NW.mpr
SE.mpr:=IFUNDEF(TshdSE,0)
calc SE.mpr
SW.mpr:=IFUNDEF(TshdSW,0)
calc SW.mpr

//Calculate Final map

Shadow_%2.mpr:= IFF((N+S+W+E+NES+NW+SE+SW)>=1,1,0)
calc Shadow_%2.mpr

//Delete temporary files

del Tshd?.mpr -force
del Tshd??.mpr -force
del sh?.mpr -force
del sh??.mpr -force
del Shadows.mpr -force
del ?.mpr -force
del ???.mpr -force
```

9.2.3. Threshold method for enhanced shaded relief maps

```
Script Name: ThreShadow.isl
//script by M. Arenas (last modified: Nov/2005) with the help of B. van Leeuwen
//Processing to threshold enhanced shaded relief map %1 according to the %2 threshold value

//1. Create a cross map and table from input map

Cross = TableCross(%1, %1, Cross)
calc Cross.tbt

//2. Create a cumulative column in the table: cumcol = cum(NPix)

opentbl Cross.tbt

Tabcalc Cross.tbt cumcol=cum(NPix)
```

```
calc Cross.tbt.cumcol
```

```
//3. Convert the column to percentages: cumcolpct = cumcol/max(cumcol)*100
```

```
Tabcalc Cross.tbt cumcolpct = cumcol/max(cumcol)*100
```

```
calc Cross.tbt.cumcolpct
```

```
closetbl Cross.tbt
```

```
//4. Create an attribute map based on the new column
```

```
CrossAtrib = MapAttribute(Cross, Cross.cumcolpct)
```

```
//5. Thresholding for the highest %2 enhanced values
```

```
T%1.mpr{ dom=value.dom;vr=-0:1:1 }:=IFF(CrossAtrib>=(100-(%2)),1,0)
```

```
calc T%1.mpr
```

```
//deleting temporary files
```

```
del Cross.* -force
```

```
del CrossAtrib.mpr -force
```

9.2.4. Threshold method for profile curvature maps

```
Script Name: Thresh_Curvature.isl
```

```
//script by M. Arenas (last modified: Nov/2005) with the help of B. van Leeuwen
```

```
//Process to threshold a profile curvature map %1 according to the %2 threshold value
```

```
//1. Create a cross map and table from %1 input map
```

```
Cross = TableCross(%1, %1, Cross)
```

```
calc Cross.tbt
```

```
//2. Create a cumulative column in the table: cumcol = cum(NPix)
```

```
opentbl Cross.tbt
```

```
Tabcalc Cross.tbt cumcol=cum(NPix)
```

```
calc Cross.tbt.cumcol
```

```
//3. Convert the column to percentages: cumcolpct = cumcol/max(cumcol)*100
```

```
Tabcalc Cross.tbt cumcolpct = cumcol/max(cumcol)*100
```

```
calc Cross.tbt.cumcolpct
```

```
closetbl Cross.tbt
```

//4. Create an attribute map based on the new column

```
CrossAtrib.mpr:= MapAttribute(Cross, Cross.cumcolpct)
```

//5. Thresholding for the highest and lowest profile curvature values (half of input, Threshold value=%2/2)

```
kv_%2.mpr:=IFUNDEF(CrossAtrib,0,IFF((CrossAtrib>=(100-  
(%2/2)))OR(CrossAtrib<=(%2/2)),1,0))
```

```
calc kv_%2.mpr
```

//Delete temporary files

```
del Cross.* -force
```

```
del CrossAtrib.mpr -force
```

```
del Thresh.* -force
```

9.2.5. Sobel enhancement and threshold method for slope gradient maps

Script Name: Slope_sobel_process.isl

//script by M. Arenas (last modified: Oct/2005)

//script to enhance lineaments and construct binary image from slope gradient maps using Sobel operator

//Input parameters: %1.mpr-Slope gradient map; %2-threshold value

//Calculate Sobel edge map using dfdx and dfdy filters

```
dx.mpr:=MapFilter(%1,dfdx)
```

```
calc dx.mpr -force
```

```
dy.mpr:=MapFilter(%1,dfdy)
```

```
calc dy.mpr -force
```

```
%1sob.mpr:=SQRT(dx^2+dy^2)
```

```
calc %1sob.mpr
```

//Tresholding edge map using the highest %2 values

```
run ThreshPercentage.isl %1sob %2
```

```
calc %1sob_%2.mpr -force
```

//Delete temporary files

```
del dx.mpr -force
```

```
del dy.mpr -force
del %1sob.mpr -force
```

9.2.6. Laplacian enhancement and threshold method for slope gradient maps

```
Script Name: Slope_Laplace_process.isl
//script by M. Arenas (last modified: Oct/2005)
//script to enhance lineaments and construct binary image from slope gradient maps using laplacian
operator
//Input parameters: %1.mpr -Slope gradient map; %2-threshold value

//Calculate Laplace edge map using edgesenh filter

%1Lp.mpr{ dom=value.dom;vr=-10000.0000:10000.0000:0.1 }:=MapFilter(%1,edgesenh)
calc %1Lp.mpr

//Thresholding edge map using the highest %2 values

run ThreshPercentage.isl %1Lp %2
calc %1Lp_%2.mpr -force

//Delete temporary maps

del %1Lp.mpr -force
```

9.2.7. General threshold method used with slope gradient maps

```
Script Name: ThreshPercentage.isl
//script by M. Arenas (last modified: Oct/2005) with the help of B. van Leeuwen
//General process to threshold a map %1 according to the %2 highest threshold value

//1. Create a cross map and table from input map

Cross = TableCross(%1, %1, Cross)
calc Cross.tbt

//2. Create a cumulative column in the table: cumcol = cum(NPix)

opentbl Cross.tbt

Tabcalc Cross.tbt cumcol=cum(NPix)
calc Cross.tbt.cumcol

//3. Convert the column to percentages: cumcolpct = cumcol/max(cumcol)*100
```



```
Tabcalc Cross.tbt cumcolpct = cumcol/max(cumcol)*100  
calc Cross.tbt.cumcolpct
```

```
closetbl Cross.tbt
```

```
//4. Create an attribute map based on the new column
```

```
CrossAtrib:= MapAttribute(Cross, Cross.cumcolpct)
```

```
//5. Thresholding for the highest values
```

```
Thresh.mpr{ dom=value.dom;vr=-0:1:1 }:=IFF((CrossAtrib>=(100-%2)),1,0)  
calc Thresh.mpr
```

```
//Operation to eliminate undefined values (ocean)
```

```
%1_%2.mpr{ dom=value.dom;vr=-0:1:1 }:=IFUNDEF(Thresh,0)  
calc %1_%2.mpr
```

```
//delete temporary files
```

```
del Cross.* -force  
del CrossAtrib.mpr -force  
del Thresh.* -force
```

9.2.8. Post-processing steps for HT output lineament maps

```
Script Name: Post_process.isl
```

```
//script by M. Arenas (last modified: Jan/2006)
```

```
//Closing and medial axes extraction for Hough Transform output lineament maps
```

```
//Input parameters: %1- HT output lines map, %2-Edge domain, %3-original georeference
```

```
//dilate filter for closing
```

```
a.mpr=MapFilter(%1,dilate8)  
calc a.mpr  
b.mpr=MapFilter(a,dilate8)  
calc b.mpr
```

```
%1_D.mpr:=IFF(b=TRUE,1,0)  
calc %1_D.mpr
```

```
//Medial axes extraction
```

```
run Medial_axes.isl %1_D %2 %3
```

//Export to ERDAS imagine format for raster to vector conversion

export imagine(%1_D_x.mpr,%1_D_x,GeoGateway)

//Delete temporary files

del ?.mpr -force

9.2.9. Method for extraction of medial axes

Script Name: Medial_axes.isl

//script by M. Arenas (last modified: Jan/2006)

//based on a script written by T. Hengl (last modified: Apr/2003)

//Extraction of medial axes to get connected one-pixel thick lines

//Input parameters: %1- input map, %2-Edge domain, %3-original georeference

//Dilate Input map

Dil.mpr:=MapFilter(%1,dilate8)

calc Dil.mpr

//Edge map

Edge_1.mpr:=Dil-%1

calc Edge_1.mpr

//Change domain for distance calculation

changedom Edge_1.mpr %2

Edge_2.mpr{ dom=%2 }:=IFF(Edge_1="No edge",?,"Edge")

calc Edge_2.mpr

//Calculate distance map

Distance.mpr:=MapDistance(Edge_2)

calc Distance.mpr

//Calculate medial axes

%1_x:=IFF((nbcnt(Distance>Distance#)>4)AND(%1=1),1,0)

calc %1_x

//Change georeference to original DEM georeference

```
setgrf %1_x %3 -force
```

```
//Delete temporary files
```

```
del Edge_*.mpr -force  
del Distance.mpr -force  
del Dil.mpr -force
```

9.2.10. Method for importing lineament into ILWIS and calculations for rose diagrams construction

```
Script Name: Import_rose.isl
```

```
//script by M. Arenas (last modified: Jan/2006)
```

```
//Script for importing lineament maps from shapefiles to ILWIS format and posterior calculations for construction of rose diagrams
```

```
//Input parameters: %1- vector map to be imported, %2-original coordinate system
```

```
//Import shapefile via Geogateway
```

```
import shape(%1.shp, %1)
```

```
//open %1.mps -force
```

```
setcsy %1.mps %2
```

```
//Calculate histogram for segment maps
```

```
%1:= TableHistogramSeg(%1.mps)  
calc %1.hss
```

```
//Calculate direction histogram
```

```
%1Dir := TableSegDir(%1)  
calc %1Dir.tbt
```

```
//Calculation for rose diagram construction
```

```
opentbl %1Dir.tbt
```

```
//Change angles to north orientation
```

```
Tabcalc %1Dir.tbt Direction_new{vr=0:179:1.0} = iff(direction <= 90, 90-direction, 270-direction)  
calc %1Dir.tbt.Direction_new
```

//Classified segments in intervals of 5 degrees and aggregation for cumulative frequency per interval

```
Tabcalc %1Dir.tbt FiveDegree { dom = FiveDegree.dom } = iff(%k<178,round(%k/5)*5, 0)
calc %1Dir.tbt.FiveDegree
```

```
Tabcalc %1Dir.tbt FiveDegSum = ColumnAggregateSum(nrlines, FiveDegree,1)
calc %1Dir.tbt.FiveDegSum
```

//Classified segments in intervals of 10 degrees and aggregation sum of number of lines for cumulative frequency per interval

```
Tabcalc %1Dir.tbt TenDegree { dom =TenDegree.dom } = iff(%k<178,round(%k/10)*10, 0)
calc %1Dir.tbt.TenDegree
Tabcalc %1Dir.tbt TenDegSum = ColumnAggregateSum(nrlines, TenDegree,1)
calc %1Dir.tbt.TenDegSum
```

//Calculation of square root of line relative frequency

```
Tabcalc %1Dir.tbt SqrNrlines=SQRT(Nrlines)
calc %1Dir.tbt.SqrNrlines
```

//Aggregation sum of square root of number of lines for cumulative frequency per interval. This ensure petals of equal area in rose diagrams

```
Tabcalc %1Dir.tbt FiveDegSum2 = ColumnAggregateSum(SqrNrLines, FiveDegree,1)
calc %1Dir.tbt.FiveDegSum2
```

```
Tabcalc %1Dir.tbt TenDegSum2= ColumnAggregateSum(SqrNrlines, TenDegree,1)
calc %1Dir.tbt.TenDegSum2
```

```
closetbl %1Dir.tbt
```

9.2.11. Method for selection of correctly extracted lineaments

Script Name: Correct_lines_MapAttribute.isl

//script by M. Arenas (last modified: Jan/2006)

//Calculation of differences in angle within the buffer

//Lines with deviation less than 15 degrees will be consider in length accuracy and noise factor calculation

//Input parameters: %1- table from imported intersected line map (truth buffer and extracted line map)

```
opentbl %1.tbt
```

```
Tabcalc %1.tbt Geoangle_2=IFF(GEOANGLE<=179,GEOANGLE,SQRT((GEOANGLE-180)^2))
calc %1Dir.tbt.Geoangle_2
```

```
Tabcalc %1.tbt Geoangle1_2=IFF(GEOANGLE_1<=179,GEOANGLE_1,SQRT((GEOANGLE_1-180)^2))
calc %1Dir.tbt.Geoangle1_2
```

```
Tabcalc %1.tbt Diff_Angle{vr=0:180:1.0}:=IFF(((Geoangle_2>165)AND(Geoangle1_2<15)),
(Geoangle1_2-(Geoangle_2-180)),(IFF(((Geoangle_2<15)AND(Geoangle1_2>165)),(Geoangle_2-
(Geoangle1_2-180)), SQRT((Geoangle_2-Geoangle1_2)^2))))
calc %1Dir.tbt.Diff_Angle
```

```
Tabcalc %1.tbt Diff_angle_15:=iff(Diff_Angle<=15,Diff_Angle,?)
calc %1Dir.tbt.Diff_angle_15
```

```
closetbl %1Dir.tbt
```

```
//Creating the attribute map
```

```
%1_15:= SegmentMapAttribute(%1, %1.Diff_angle_15)
calc %1_15.mps
```

9.2.12. Converter TIFF to RW Format for Hough Transform Calculation

```
#!/bin/bash
#
# Simple script around hough
# converts input image (tiff) to raw pgm
# applies HT, and converts back to tiff
#
# vdwerff@itc.nl, october 2005

if [ $# -le 3 ]; then
  echo "USAGE: hough.sh <filename>"
  echo "  -h <cutoff>          (Hough Transform)"
  echo "  -k <normalisation_factor>"
  echo "  -g <size>           (Automatic Gain Control)"
  echo "  -t                  (thin)"
  echo "  -b <threshold>      (threshold)"
  echo "  -r                  (if thresholding, invert image"
  echo
  exit 0
fi

if [ ! -e $1 ]; then
  echo "ERROR: file $1 not found"
  exit 1
else
```

```
FN=`basename $1 .tif`
fi

echo " Converting $FN.tif $FN.pgm..."
convert $FN.tif $FN.pgm
echo " Converting $FN.pgm $FN.raw..."
convert $FN.pgm $FN.raw

echo " Applying Hough transform..."
/home/arenas08286/bin/hough -i $FN.raw -o $FN-out.pgm $2 $3 $4 $5 $6 $7 $8 $9

echo " Converting $FN-out.pgm $FN-out.tif..."
convert $FN-out.pgm $FN-out.tif

echo " Removing temporary files..."
rm *.pgm
rm *.raw

echo " Done."
exit 0
```